Characterisation of the yeast Nfs1/Isd11 cysteine desulphurase complex

Thesis presented in partial fulfilment of the requirements for the degree of Doctor of Philosophy (PhD)

Kerem Terali

School of Biological and Chemical Sciences
Queen Mary, University of London

December 2010

Declaration

I hereby certify that this Thesis, which is approximately 23,000 words in length, has been composed by me, that it is the record of the work conducted by me and that it has not been submitted in any previous application for a post-graduate degree. I confirm that I have made full acknowledgement of the work and/or ideas of any other people who are cited in this thesis or who have contributed to it.

....

Date **Name**

.....

Signature

Abstract

Small inorganic assemblies of alternating ferrous/ferric iron and sulphide ions, so-called iron–sulphur (Fe–S) clusters, are probably nature's most ancient prosthetic groups. These multipurpose reactive centres are biosynthesised by dedicated Fe–S cluster assembly proteins which are conserved in the mitochondria of all eukaryotes. One of the early actors in Fe–S cluster biosynthesis is a cysteine desulphurase, Nfs1, which catalyses the release of elemental sulphur from cysteine and plays a key role in its transfer to a molecular scaffold. Recent work has discovered that these reactions require the involvement of a small adaptor protein, Isd11. Isd11 belongs to the LYR family of proteins and helps stabilise Nfs1 upon binding. In this Thesis, heterologous production of soluble yeast Nfs1 on its own as well as in complex with yeast Isd11 in *E. coli* is presented. In the absence of Nfs1, Isd11 aggregated in the form of inclusion bodies from which the *in vitro* recovery of soluble protein could not be achieved. Both Nfs1 and the Nfs1/Isd11 complex were shown to be active, reflecting the correct fold of Nfs1. Biophysical approaches were used to provide new insights into the stoichiometry and structure of the Nfs1/Isd11 complex.

Table of contents

Acknowledgements.....**11**

List of tables.....**12**

List of figures.....**13**

Abbreviations.....**16**

1 Introduction.....**18**

1.1 Background and objectives.....18

1.2 Thesis structure.....18

1.3 Biological (protein-bound) Fe–S clusters.....19

1.3.1 Structural aspects of Fe–S clusters.....20

1.3.2 Functional aspects of Fe–S clusters.....21

1.4 Formation of Fe–S clusters in eukaryotes.....23

1.4.1 Yeast as a model eukaryote.....23

1.4.2 Components of the Fe–S cluster assembly machinery.....24

1.4.3 Mechanisms of Fe–S cluster assembly.....27

1.5 Human diseases associated with Fe–S cluster assembly.....30

1.6 Nfs1: the NifS-like cysteine desulphurase of eukaryotes.....31

1.6.1 Related structures.....33

1.6.2 Reaction mechanism.....35

1.6.3 Other reactions.....37

1.7 Isd11: the ISC assembly desulphurase-interacting protein.....37

1.8 Nfs1/Isd11: the functional desulphurase complex.....39

1.9 Summary.....40

1.10 Aims.....40

2 Materials and methods.....42

2.1 PCR amplification of genes.....42

2.1.1 Materials.....43

2.1.2 Reaction mixture.....44

2.1.3 Thermal cycling conditions.....45

2.1.4 Agarose gel electrophoresis and gel-purification of PCR products.....45

2.2 Directional cloning of PCR products.....46

2.2.1 Materials.....47

2.2.2 Double digestion and clean-up of DNA.....48

2.2.3 Sticky-end ligation.....49

2.2.4 Transforming a general subcloning host.....50

2.2.5 Plasmid preparation.....50

2.2.6 Custom DNA sequencing.....51

2.3 Heterologous production of proteins.....53

2.3.1 Materials.....53

2.3.2 Transforming a gene expression host.....54

2.3.3 Cell growth.....55

2.3.4 IPTG induction.....55

2.3.5 Harvest and storage.....56

2.3.6 Preparing glycerol stocks of cells.....56

2.4 Purification of His_6-tagged proteins.....56

2.4.1 Materials.....57

2.4.2 Cell lysis and clarification of lysate.....59

2.4.3 Immobilised metal affinity chromatography.....59

2.4.4 Concentrating/buffer-exchanging proteins by centrifugal ultrafiltration.....60

2.4.5 Size-exclusion chromatography.....61

2.4.6 SDS–polyacrylamide gel electrophoresis of proteins.....62

2.5 Protein refolding.....62

2.5.1 Materials.....63

2.5.2 Isolation and solubilisation of inclusion bodies.....64

2.5.3 In vitro *refolding strategies*.....64

2.6 Analytical ultracentrifugation.....65

2.6.1 Sample.....66

2.6.2 Procedure.....66

2.7 Quantitative Western blotting.....66

2.7.1 Materials.....67

2.7.2 SDS–PAGE.....68

2.7.3 Semi-dry electroblotting.....68

2.7.4 Blocking.....69

2.7.5 Primary-antibody incubation.....69

2.7.6 Secondary-antibody incubation.....70

2.7.7 Colour detection, analysis and interpretation.....70

2.8 Quantitative amino acid analysis.....70

2.8.1 Sample.....71

2.8.2 Procedure.....71

2.9 UV-visible absorbance spectrophotometry.....71

2.9.1 Materials.....72

2.9.2 Spectrophotometric determination of protein concentration..72

2.9.3 Obtaining substrate binding spectra.....73

2.10 Fluorescence spectrophotometry.....74

2.10.1 Materials.....74

2.10.2 Data collection.....75

2.11 Far-UV circular dichroism spectroscopy.....75

2.11.1 Materials.....76

2.11.2 Data collection.....76

2.11.3 Data analysis and interpretation.....77

2.12 Homology modelling.....77

2.12.1 Template selection.....*78*

2.12.2 Target–template alignment.....*78*

2.12.3 Model building and inspection.....*78*

2.13 Protein crystallisation screening.....78

2.13.1 Materials.....*79*

2.13.2 Sample preparation.....*80*

2.13.3 Screening strategies.....*80*

3 *In silico* analysis and production of yeast Isd11.....**82**

3.1 Bioinformatic studies suggest that Isd11 is a eukaryote-specific mitochondrial protein with a high α-helical propensity.....82

3.2 The DNA fragment encoding the predicted mature form of Isd11 can be overexpressed in the *E. coli* system.....85

3.3 Recombinantly produced Isd11 is deposited as inclusion bodies in the cytoplasm of host cells.....87

3.4 Denatured Isd11 cannot be readily refolded *in vitro* into its native state.....88

3.5 Summary.....89

4 Production and characterisation of yeast Nfs1.....**90**

4.1 Bioinformatic studies of Nfs1 assist in the development of new experimental strategies.....90

4.2 Yeast Nfs1 constructs can be successfully overexpressed in *E. coli*.....91

4.3 Recombinantly produced Nfs1 is a soluble protein with a bright yellow colour attributable to PLP.....93

4.4 Size-exclusion chromatography indicates that recombinant Nfs1 exists as a homodimer in solution.....97

4.5 UV-visible absorbance spectrophotometry confirms the presence of PLP and shows that recombinant Nfs1 is active towards L-cysteine..98

4.6 Far-UV CD spectroscopy reveals that recombinant Nfs1 has an extensive α-helical content.....101

4.7 Homology modelling provides insights into the structural organisation of Nfs1 and the integrity of its active site.....103

4.8 Summary.....106

5 Production of the yeast Nfs1/Isd11 protein complex and studies of the Nfs1–Isd11 interaction.....107

5.1 Co-expression of the two target DNA fragments in *E. coli* allows formation of the Nfs1/Isd11 protein complex.....107

5.2 Size-exclusion chromatography estimates that the Nfs1/Isd11 complex has a native mass nearly twice that of the Nfs1 homodimer.....110

5.3 UV-visible absorbance spectrophotometry reveals that recombinantly produced Nfs1/Isd11 retains its activity towards L-cysteine and that Isd11 helps stabilise Nfs1 during and/or after the catalytic desulphuration of L-cysteine.....110

5.4 Quantitative amino acid analysis of Nfs1/Isd11 suggests that Nfs1 interacts with Isd11 in a 1:1 ratio.....113

5.5 Analytical ultracentrifugation suggests that Nfs1 and Isd11 associate to form the $(Nfs1/Isd11)_3$ heterohexamer.....115

5.6 Intrinsic tryptophan fluorescence measurements indicate a conformational change in Nfs1 upon Isd11 binding.....118

5.7 Far-UV CD spectroscopy supports the earlier indication that Nfs1 undergoes a conformational rearrangement upon complex formation.....120

5.8 Summary.....122

6 Conclusion and future prospects.....**124**

References.....**130**

Appendix.....**139**

Acknowledgements

This PhD Thesis is based on three years of research funded by the Queen Mary, University of London Research Studentship. My time at QM was truly incredible. Of course, I have to thank several people who, in some way, contributed to this Thesis.

First of all, I am extremely grateful to Prof Richard Pickersgill for the supervision that supervisors do not normally have time for! He was always kind and helpful towards me, even when I was exhausted, difficult or pessimistic. Also, he provided some very useful feedback to improve the quality of this document.

Next, many thanks are due to Dr Mark van der Giezen with whom I started conducting my experiments. Although he is kilometres away from QM now, he proof-read this document and helped me further refine it.

Dr Rebecca Beavil helped me with the analytical ultracentrifugation studies, while Dr Robin Maytum and Dr John Viles shared their expertise in the field of molecular/structural biology. Mr Mustafa Batıbeniz helped me draw the mitochondrion figure in Chapter 1. I am particularly thankful to these people.

Special thanks are due to my lab mates, members of the Pickersgill and Viles groups. I will certainly miss our conversations of everything and, sometimes, nothing!

Last but not least, I owe a lot to my family for the support and encouragement they have given me since I started my PhD.

List of tables

1.1 Compilation of Fe–S proteins involved in various functions in yeast.....22

1.2 Compilation of central components involved in Fe–S protein biogenesis in yeast.....26

2.1 Gene-specific oligonucleotide primers used in this study.....43

2.2 PCR mixture.....45

2.3 Thermal cycling conditions.....45

2.4 Restriction enzymes used for the cloning of PCR products into corresponding expression vectors.....48

2.5 Double-digest conditions.....49

2.6 Sticky-end ligation reaction mixture.....49

2.7 Names and concentrations of antibiotics used for the selection of expression vectors.....50

2.8 Induction conditions for the expression constructs used in this study.....56

4.1 Calculated fractions of the regular secondary structural features of Nfs1Δ1–34.....103

5.1 Quantitative amino acid analysis of Nfs1/Isd11.....114

List of figures

1.1 Chemical structures and names of the most commonly encountered Fe–S clusters.....21

1.2 Working model of Fe–S cluster assembly in yeast.....29

1.3 Ribbon structure of *E. coli* IscS homodimer (PDB entry 3LVM), seen looking down the two-fold axis.....34

1.4 Proposed mechanism for the cysteine desulphuration reaction catalysed by NifS-like enzymes.....36

2.1 Representative constructs used in this study.....52

3.1 Multiple alignment of deduced amino acid sequences of Isd11 proteins from taxonomically diverse organisms.....83

3.2 Predictive analysis of the primary sequence of yeast Isd11 based on bioinformatic tools.....84

3.3 Top-scoring (energy rank = 1) *ab initio* model of yeast Isd11.....85

3.4 Agarose gel electrophoretic analysis of PCR-amplified *isd11*Δ1–30.....86

3.5 SDS–polyacrylamide gel electrophoretic analysis of Isd11Δ1–10 overproduced on an analytical scale.....87

3.6 SDS–polyacrylamide gel electrophoretic analysis of Isd11Δ1–10 produced on a preparative scale and purified by affinity chromatography under denaturing conditions.....88

4.1 Alignment of deduced amino acid sequences of *E. coli* (Ec) IscS and *S. cerevisiae* (Sc) Nfs1.....90

4.2 Agarose gel electrophoretic analysis of PCR-amplified (A) *nfs1*Δ1–102 and (B) *nfs1*Δ1–294.....92

4.3 Sample of Nfs1Δ1–34 captured on a HisTrap HP affinity column.....94

4.4 Elution profiles of (A) and Nfs1Δ1–34 and (B) Nfs1Δ1–98 from the HiPrep Sephacryl S-200 HR size-exclusion column.....95

4.5 SDS–polyacrylamide gel electrophoretic analysis of (A) Nfs1Δ1–34 and (B) Nfs1Δ1–34, both produced on a preparative scale and purified by subsequent steps of affinity and size-exclusion chromatographies.....97

4.6 UV-visible absorbance spectrum of Nfs1Δ1–34.....99

4.7 Time-dependent spectral analysis of L-cysteine binding to Nfs1Δ1–34.....100

4.8 Far-UV CD spectrum of Nfs1Δ1–34.....102

4.9 Modelled overall structure of Nfs1Δ1–98.....104

4.10 Cartoon representation of the active site of Nfs1Δ1–98, with PLP and the PLP-binding residues shown in stick representation.....105

5.1 Elution profile of the Nfs1/Isd11 complex from the HiPrep Sephacryl S-200 size-exclusion column.....108

5.2 SDS-PAGE analysis of the purified and concentrated Nfs1/Isd11 complex, showing the dissociated subunits Nfs1 and Isd11.....109

5.3 UV-visible absorbance spectrum of Nfs1/Isd11.....111

5.4 Time-dependent spectral analysis of L-cysteine binding to Nfs1/Isd11.....112

5.5 Sedimentation equilibrium profile at 280 nm, and the corresponding residuals, for the Nfs1/Isd11 complex run at 8,500 rpm.....116

5.6 Sedimentation equilibrium profile at 280 nm, and the corresponding residuals, for the Nfs1/Isd11 complex run at 8,500 rpm.....117

5.7 Comparison of the emission spectra of Nfs1 and the Nfs1/Isd11 complex...119

5.8 Comparison of the far-UV CD spectra of Nfs1 and Nfs1/Isd11.....121

5.9 Alignment of deduced amino acid sequences of selenocysteine lyase (SCL) and the predicted mature form (Smíd *et al.*, 2006) of cysteine desulphurase (Nfs1) both from *T. brucei*.....128

Abbreviations

ABC	ATP-binding cassette
ATP	Adenosine 5′-triphosphate
Bicine	N,N-Bis(2-hydroxyethyl)glycine
DNA	Deoxyribonucleic acid
dNTPs	Deoxynucleoside triphosphates
DTT	Dithiothreitol
EDTA	Ethylenediaminetetraacetic acid
HEPES	4-(2-hydroxyethyl)-1-piperazineethanesulfonic acid
IgG	Immunoglobulin G
IPTG	Isopropyl-β-D-thiogalactopyranoside
LB	Luria–Bertani
NADH	Nicotinamide adenine dinucleotide (reduced form)
PDB	Protein Data Bank
PEG	Poly(ethylene glycol)
PVDF	Poly(vinylidene fluoride)
RNA	Ribonucleic acid
rpm	Revolutions per minute
SDS	Sodium dodecyl sulphate
SOC	Super optimal broth (SOB) with catabolite repression

Tris	Tris(hydroxymethyl)aminomethane
tRNA	Transfer RNA
UV	Ultraviolet

Chapter 1: Introduction

1.1 Background and motivation

Iron–sulphur (Fe–S) clusters, which are small inorganic assemblies of iron and sulphur, are among the most ubiquitous co-factors used by many biological systems in a number of reactions. These multipurpose structures were originally discovered in the early 1960s as reactive centres in electron-transfer proteins engaged in such crucial biological processes as respiration and photosynthesis. Since then, they have been reported in all living organisms, from bacteria to mammals. Organisms assemble Fe–S clusters using dedicated systems, each consisting of several to many proteins. Interestingly, it is only over the last two decades that these proteins involved in the assembly of Fe–S clusters have begun to be documented. Some of the Fe–S cluster assembly proteins have been shown to cause disease in humans. Apparently, recent discoveries in the field of Fe–S cluster assembly present inspiring challenges for a broad range of researchers, including molecular and structural biologists.

1.2 Thesis structure

The main body of this Thesis begins with an introductory section focusing on the structures and functions of biological, or protein-bound, Fe–S clusters. This section provides insight into the emergence of Fe–S clusters as co-factors of many proteins and explains their structural and functional versatility, using examples. The next section features the proteins and mechanisms involved in the assembly of Fe–S clusters in a eukaryotic cell, with particular emphasis on yeast. This section is followed by a brief section outlining five human diseases that have been linked to

defects (mutations) in the genes encoding the Fe–S cluster assembly proteins. The next three sections of Chapter 1 detail the eukaryotic cysteine desulphurase Nfs1, its functional binding partner Isd11 and their specific complex Nfs1/Isd11, respectively. The indispensable Nfs1/Isd11 cysteine desulphurase complex of the Fe–S cluster assembly apparatus, which has not been studied in depth before, is the primary subject of this PhD Thesis. Chapter 3 includes the heterologous production and bioinformatic investigation of yeast Isd11. Chapter 4 specifies the heterologous production, biophysical characterisation and comparative modelling of yeast Nfs1. Chapter 5 is dedicated to the heterologous production and biophysical characterisation of the yeast Nfs1/Isd11 protein complex and the measurements of the Nfs1–Isd11 interaction by spectroscopic means. Chapter 2 describes the materials and methods used in the experimental work, and Chapter 6 concludes with a discussion of what was achieved and what were the major bottlenecks in this project. Chapter 6 also offers suggestions on novel and testable strategies for future experiments.

1.3 Biological (protein-bound) Fe–S clusters

Since the appearance of the first organisms on Earth, cyclic transformations of the primary biogenic elements (carbon, hydrogen, nitrogen, oxygen, phosphorus, and sulphur) have been pivotal events that support life. Cycles involving the oxidation and reduction of these elements provide organisms with usable energy and the building blocks of cellular structures. In today's life forms, enzymes bearing Fe–S clusters are usually involved in these transformations. It is therefore likely that Fe–S clusters are among the earliest co-factors available for enzyme catalysis, holding a

mirror to naturally occurring chemical transformations in the primordial world with a highly reductive atmosphere (Rees & Howard, 2003).

1.3.1 Structural aspects of Fe–S clusters

Most frequently, protein-bound Fe–S clusters arise in nature as rhombic, [2Fe–2S], or cubic, [4Fe–4S], types in which iron ions are co-ordinated by thiolate sulphur of cysteinyl residues of the apoprotein and bridged to each other by inorganic sulphide ions (Figure 1.1). While iron can adopt oxidation states of $Fe^{2+}$and Fe^{3+}, sulphur is invariably present in the S^{2-} oxidation state. A relatively rare type, [3Fe–4S], is formed via the loss of one iron atom from one corner of the [4Fe–4S] cluster (Figure 1.1). The [3Fe–4S] cluster serves as a building block for the assembly of more complex clusters (Beinert, 2000).

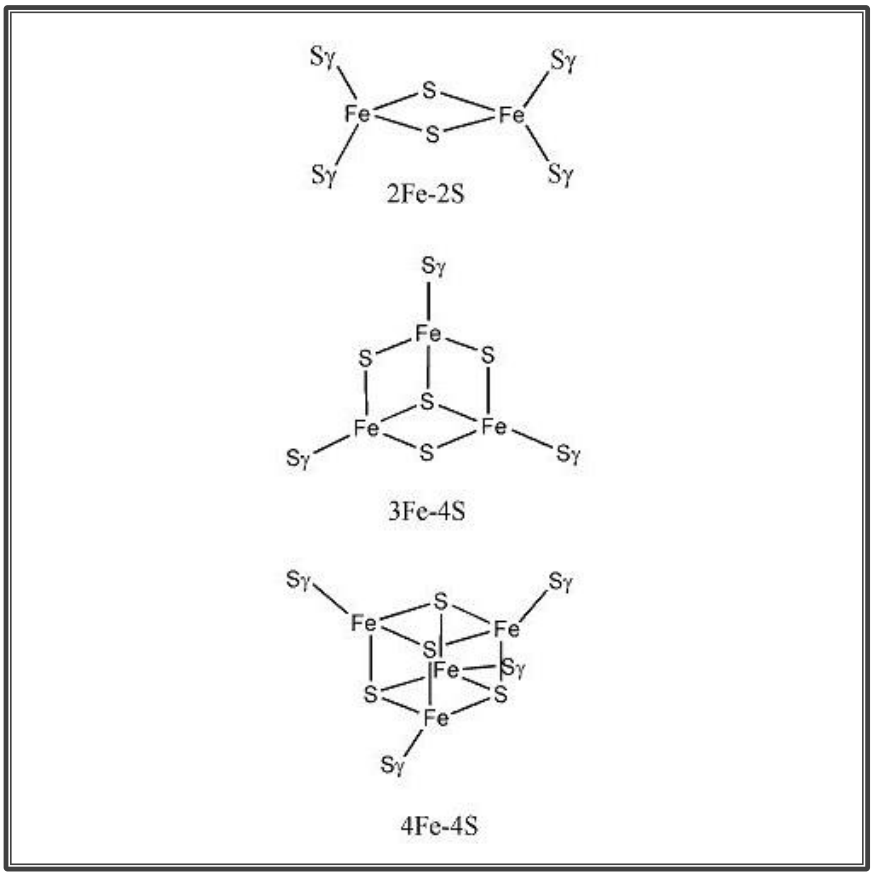

Figure 1.1 Chemical structures and names of the most commonly encountered Fe–S clusters. The simplest [2Fe–2S] cluster consists of two iron ions bridged by two sulphide ions and co-ordinated by four cysteinyl ligands (in [2Fe–2S] ferredoxins) or by two cysteines and two histidines (in Rieske proteins). The [3Fe–4S] centre, which features one iron ion less than the more common [4Fe–4S] cluster, consists of three sulphide ions that bridge two iron ions each, while the fourth sulphide bridges three iron ions. The common [4Fe–4S] motif features four iron ions and four sulphide ions placed at the vertices of a cubane-type structure. These centres are typically further co-ordinated by cysteinyl ligands. Sγ in the structural formulae represents the sulphur atom of a cysteinyl residue in the peptide backbone co-ordinating the Fe–S cluster. This figure was prepared using ChemDraw (http://www.cambridgesoft.com/).

1.3.2 Functional aspects of Fe–S clusters

The structural versatility and chemical reactivity of Fe–S clusters have allowed for their selection as co-factors for many proteins, enabling these proteins to gain novel functions. It is therefore not surprising that proteins harbouring Fe–S cores (termed Fe–S proteins) are present in all organisms and play crucial roles in several cellular processes including electron transfer, biosynthesis, central metabolism, regulation of

gene expression, RNA modification, and DNA repair and replication (see reviews by Lill *et al.*, 2006; Lill & Mühlenhoff, 2008; Sheftel *et al.*, 2010). To date, about 20 different Fe–S proteins with a range of cellular functions have been discovered in yeast (Table 1.1).

Table 1.1 Compilation of Fe–S proteins involved in various functions in yeast.

Protein	Name	Cluster(s) present	Function
Sdh2	Complex II	[2Fe–2S], [3Fe–4S], [4Fe–4S]	Component of the respiratory (electron transport) chain
Rip1	Complex III	[2Fe–2S] (Rieske-type)	Component of the respiratory (electron transport) chain
Yah1	Ferredoxin	[2Fe–2S]	Provides electrons for mitochondrial Fe–S cluster assembly
Lip5	Lipoate synthase	[4Fe–4S], [4Fe–4S]	Lipoic acid biosynthesis
Bio2	Biotin synthase	[2Fe–2S], [4Fe–4S]	Biotin biosynthesis
Lys4	Homoaconitase	[4Fe–4S]	Lysine biosynthesis
Ilv3	Dihydroxy-acid dehydratase	[4Fe–4S]	Branched-chain amino acid biosynthesis
Leu1	Isopropylmalate isomerase	[4Fe–4S]	Leucine biosynthesis
Glt1	Glutamate dehydrogenase	[4Fe–4S]	Glutamate biosynthesis
Ecm17	Sulphite reductase	[4Fe–4S]	Methionine biosynthesis
Aco1	Aconitase	[4Fe–4S]	Tricarboxylic acid (TCA) cycle
Nbp35	Nucleotide-binding protein 35	[4Fe–4S], [4Fe–4S]	Cytosolic Fe–S cluster assembly
Nar1	Nuclear architecture-related protein 1	Complex-type	Cytosolic Fe–S cluster assembly
Rli1	RNase L inhibitor protein 1	[4Fe–4S], [4Fe–4S]	Translation initiation; ribosome assembly
Elp3	Elongator complex protein 3	[4Fe–4S]	Transcription elongation; tRNA modification
Tyw1	tRNA wybutosine-synthesising protein 1	[4Fe–4S]	tRNA modification
Ntg2	DNA glycosylase	[4Fe–4S]	DNA damage repair
Rad3	DNA helicase	[4Fe–4S]	DNA damage repair
Pri2	DNA primase large subunit	[4Fe–4S]	DNA replication

1.4 Formation of Fe–S clusters in eukaryotes

Although Fe–S clusters are simply composed of ferrous (Fe^{2+}) and/or ferric (Fe^{3+}) iron and inorganic sulphide (S^{2-}) ions, their *in vivo* assembly and onward delivery to recipient apoproteins is notably complex. In eukaryotes, a proteinaceous **i**ron–**s**ulphur **c**luster (ISC) assembly machinery, which is conserved from yeast to man, is responsible for the assembly process. Components of the eukaryotic ISC system are derived from their prokaryotic counterparts and originally arrived with the endosymbiont that gave rise to the mitochondrion. The eukaryotic ISC system is still primarily, or exclusively, localised in mitochondria.

1.4.1 Yeast as a model eukaryote

The yeasts, which are unicellular ascomycetes or 'sac fungi', are considered to be one of the best organisms for the study of eukaryotic biology because the basic mechanisms of DNA replication, gene expression, cell division, and metabolism are largely conserved between yeasts and higher eukaryotes including mammals. Baker's yeast (*Saccharomyces cerevisiae*) was the first eukaryote whose genome (approximately 6,000 genes distributed throughout 16 chromosomes) was completely sequenced (Goffeau *et al.*, 1996). It was also the first organism for which a whole-proteome microarray was developed (Zhu *et al.*, 2001). Among other features that make *S. cerevisiae* a model eukaryote for biological research are its GRAS (Generally Recognised As Safe) status, ease of cultivation, and rapid growth.

In addition to whole-proteome studies, comprehensive proteomic analyses of different subcellular compartments, such as mitochondria, were also undertaken in *S. cerevisiae* (Sickmann *et al.*, 2003; Reinders *et al.*, 2006). Yeast mitochondria contain

approximately 1,000 different proteins, most of which are encoded by nuclear genes. Surprisingly, only a few percent of mitochondrial proteins of known function are strictly essential for cell viability. These proteins are primarily involved in three processes: Fe–S cluster assembly (see **Section 1.4.2**), protein folding or protein translocation. Complete characterisation of the yeast mitochondrial proteome and functional assignment of mitochondrial proteins, with particular emphasis on those being essential for cell viability, will provide insights into the role of mitochondria in health and disease.

1.4.2 Components of the Fe–S cluster assembly machinery

Prokaryotic Fe–S cluster biogenesis has been extensively studied in the nitrogen-fixing bacterium *Azotobacter vinelandii*, the common intestinal bacterium *Escherichia coli* and the plant pathogen *Erwinia chrysanthemi*. Genetic and biochemical studies have identified three distinct systems by which bacteria build Fe–S clusters: the NIF (**ni**trogen **f**ixation) system, for the specific maturation of nitrogenase; the ISC (**i**ron–**s**ulphur **c**luster) system, for the general maturation of Fe–S proteins; and the SUF (**s**ulphur **u**tilisation **f**actor) system, for the maturation of Fe–S proteins under conditions of oxidative stress and iron deprivation. The evolutionary maintenance of these dedicated Fe–S cluster biogenesis systems addresses the change from a reductive to an oxidative environment, the latter supporting neither the formation nor the stability of Fe–S clusters (see reviews by Johnson *et al.*, 2005a; Fontecave & Ollagnier-de-Choudens, 2008; Py & Barras, 2010).

Two of the three prokaryotic Fe–S cluster biogenesis systems, the ISC and SUF systems, have been inherited by eukaryotes. At present, homologues of major

components of the ISC assembly machinery are maintained in mitochondria, and homologues of the major components of the relatively oxygen-stable SUF machinery are maintained in plastids (Lill & Mühlenhoff, 2008). Strikingly, the intestinal parasite *Entamoeba histolytica* (Ali *et al.*, 2004; van der Giezen *et al.*, 2004) and the free-living amoeba *Mastigamoeba balamuthi* (Gill *et al.*, 2007) do not possess the ISC system; they rather use the non-redundant NIF system, which has been acquired by lateral gene transfer from ε-proteobacteria, for the biogenesis of nascent Fe–S clusters. This thesis will focus exclusively on Fe–S cluster assembly in non-plant eukaryotes, featuring yeast as a model organism.

Eukaryotes possess Fe–S proteins in diverse subcellular compartments. Mitochondrial Fe–S proteins are formed by the involvement of the ISC assembly machinery, and cytosolic/nuclear Fe–S proteins are formed by the involvement of both the ISC assembly machinery and the **c**ytosolic **i**ron–sulphur cluster **a**ssembly (CIA) machinery. Like components of the ISC assembly machinery, components of the CIA machinery are also essential for cell viability in yeast. CIA proteins reside in the cytosol and can only build cytosolic/nuclear Fe–S proteins in the presence of a sulphurous precursor molecule exported from the mitochondrial matrix to the cytosol (see reviews by Lill & Mühlenhoff, 2008; Lill, 2009; Sheftel *et al.*, 2010). Genetic and biochemical studies in yeast have shown that up to 20 different proteins participate in this highly co-operative biosynthetic process (Table 1.2).

Table 1.2 Compilation of central components involved in Fe–S protein biogenesis in yeast.

Protein	Full name	Proposed function	Cellular location
Nfs1	NifS-like protein 1	Cysteine desulphurase; provides sulphur for Fe–S cluster assembly	Mitochondrial matrix, nucleus
Isd11	Iron–sulphur cluster assembly desulphurase-interacting protein	Serves as an adaptor and stabiliser of Nfs1	Mitochondrial matrix
Isu1, Isu2	IscU-like proteins 1 and 2	Serve as molecular scaffolds for Fe–S cluster assembly	Mitochondrial matrix
Nfu1	NifU-like protein 1	May serve as an alternative scaffold	Mitochondrial matrix
Yfh1	Yeast frataxin homologue 1	Provides iron for Fe–S cluster assembly	Mitochondrial matrix
Yah1	Yeast adrenodoxin homologue 1	Provides electrons for the reduction of sulphur to sulphide	Mitochondrial matrix
Arh1	Adrenodoxin reductase homologue 1	Provides electrons for the reduction of sulphur to sulphide	Mitochondrial matrix
Ssq1	Stress-seventy Q protein 1	ATP-dependent chaperone; facilitates Fe–S cluster delivery to recipient apoproteins	Mitochondrial matrix
Jac1	J-type accessory chaperone 1	Co-chaperone; stimulates the ATPase function of Ssq1	Mitochondrial matrix
Mge1	Mitochondrial GrpE homologue 1	Exchanges Ssq1-bound ADP for ATP to initiate a new cycle	Mitochondrial matrix
Grx5	Glutaredoxin 5	Facilitates Fe–S cluster delivery to recipient apoproteins	Mitochondrial matrix
Atm1	Mitochondrial ABC transporter protein 1	Exports a sulphurous precursor molecule to the cytosol	Mitochondrial inner membrane
Erv1	Essential-for-respiration-and-vegetative-growth protein 1	Sulphydryl oxidase; facilitates the export of the precursor molecule	Mitochondrial intermembrane space
Cfd1	Cytosolic Fe–S cluster-deficient protein 1	Serves as a molecular scaffold for Fe–S cluster assembly	Cytosol
Nbp35	Nucleotide-binding protein 35	Serves as a molecular scaffold for Fe–S cluster assembly	Cytosol
Nar1	Nuclear architecture-related protein 1	Facilitates Fe–S cluster delivery to recipient apoproteins	Cytosol
Cia1	Cytosolic iron–sulphur cluster assembly protein 1	Facilitates Fe–S cluster delivery to recipient apoproteins	Cytosol

Another significant finding from genetic and biochemical investigations is that Fe–S cluster biogenesis is required for the maintenance of mitochondrial iron homeostasis. Yeast strains that are depleted of Fe–S cluster biogenesis proteins (e.g. Nfs1, Isd11, Isu1, Isu2, Yfh1, Yah1, Nfu1, Ssq1, and Jac1) exhibit marked iron accumulation in their mitochondria. Mitochondrial iron overload is also a characteristic of a subset of human diseases which are linked to Fe–S cluster formation (Rouault & Tong, 2008).

1.4.3 Mechanisms of Fe–S cluster assembly

It has been known for decades that Fe–S clusters can be synthesised *in vitro* starting with an iron source (Fe^{2+}) and elemental sulphur (S^0) (reviewed by Beinert *et al.*, 1997). The low solubility of iron and high toxicity of free Fe^{2+}, Fe^{3+} and S^{2-} ions within the cell, however, have caused organisms to develop salient mechanisms which promote: (i) the donation of iron and sulphur in a non-toxic form; (ii) the *de novo* assembly of Fe–S clusters on molecular scaffolds; and (iii) the delivery of pre-assembled clusters from scaffolds to target apoproteins.

Functioning of the ISC assembly, ISC export and CIA machineries is central to the formation of nascent Fe–S clusters as well as their transfer to recipient apoproteins (Figure 1.2). An early crucial reaction in mitochondrial Fe–S cluster assembly is the release of sulphur from L-cysteine to yield L-alanine. This reaction is catalysed by a two-protein desulphurase complex comprising a pyridoxal-5′-phosphate (PLP)-dependent cysteine desulphurase, Nfs1, and its 11-kDa functional partner, Isd11. Nfs1-bound sulphur is then donated to a pair of scaffold proteins, Isu1 and Isu2, that provide a chemically and structurally favourable platform for *de novo* Fe–S cluster biosynthesis. (Given the fact that *isu2* originates from a recent duplication of *isu1* and that Isu2 is functionally redundant with Isu1, only Isu1 will be mentioned in the

following text.) The transfer of sulphur to the site of Fe–S cluster biosynthesis is aided by the transient binding of Nfs1 to Isu1. Electrons, which are required for the reduction of S^0 to S^{2-}, are provided by a short electron-transport chain consisting of Arh1 (yeast ferredoxin reductase) and Yah1 (yeast ferredoxin). The flow of electrons is likely to be coupled to the oxidation of NADH. Fe^{2+}, which is pre-imported from the cytosol to the mitochondrial matrix in a membrane-potential-dependent manner, is donated to Isu1 by Yfh (yeast frataxin). The liberation and subsequent trafficking of the Isu1-bound Fe–S cluster (either [2Fe–2S] or [4Fe–4S]) is facilitated by a mitochondrial monothiol glutaredoxin, Grx5, and a dedicated chaperone system consisting of Ssq1, Jac1 and Mge1. The chaperone system relies on ATP hydrolysis for the transfer of the pre-assembled Fe–S cluster to mitochondrial apoproteins. Extramitochondrial Fe–S cluster assembly is connected to mitochondrial Fe–S cluster assembly via an uncharacterised precursor. A sulphurous compound (which may be the pre-assembled Fe–S cluster itself or a modified form of sulphur) is exported from the mitochondrial matrix to the cytosol by the action of an ABC-type transporter of the mitochondrial inner membrane, Atm1. The export reaction is further facilitated by a sulphydryl oxidase, Erv1, localised to the mitochondrial intermembrane space. In the cytosol, a transiently bound Fe–S cluster is formed on a two-protein scaffold complex comprising P-loop NTPases, Cfd1 and Nbp35. The pre-formed Fe–S cluster is then transferred to cytosolic/nuclear apoproteins in a reaction involving Nar1 and Cia1 (see reviews by Lill & Mühlenhoff, 2008; Lill, 2009; Sheftel *et al.*, 2010).

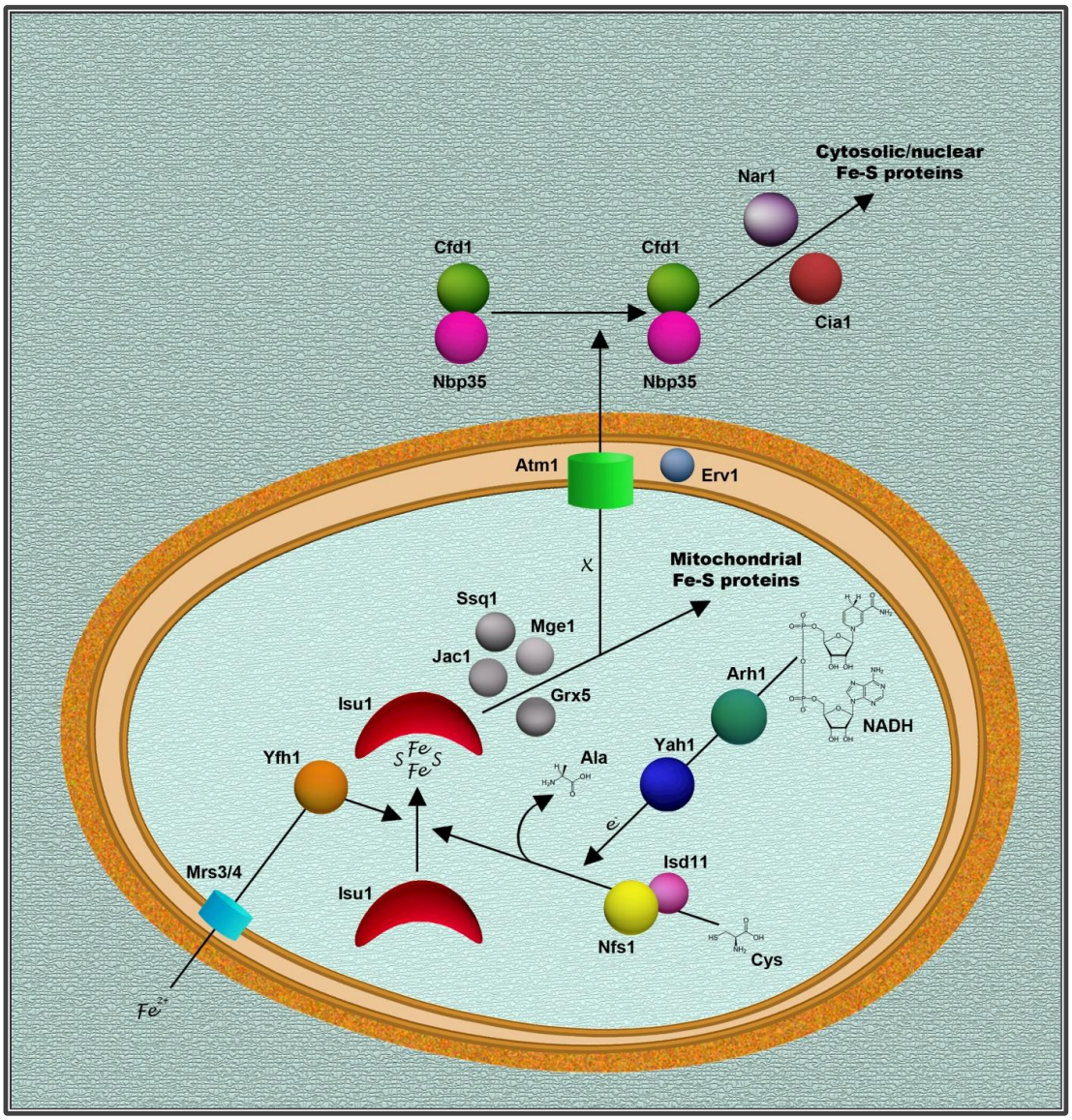

Figure 1.2 Working model of Fe–S cluster assembly in yeast. In the mitochondrion, the Nfs1/Isd11 cysteine desulphurase complex mobilises elemental sulphur required for cluster formation. A nascent Fe–S cluster is assembled on the Isu1 scaffold protein, with ferrous iron imported from the cytosol by mitoferrins (Mrs3/4) and delivered to Isu1 by Yfh1. A short electron transfer chain, which involves NADH, Arh1 and Yah1, provides electrons for the reduction of elemental sulphur to sulphide. A chaperone system, which consists of Ssq1–ATP, Jac1 and Mge1, transfers the pre-assembled cluster from Isu1 to a mitochondrial apoprotein. Grx5 also participates in this transfer reaction. The ISC export machinery, which is comprised of Atm1 and Erv1, exports a precursor molecule (X) produced by the ISC assembly machinery to the cytosol. The CIA machinery depends on this molecule to lead the maturation of cytosolic/nuclear Fe–S proteins. A transient cluster is formed on the Cfd1/Nbp35 scaffold complex and subsequently transferred from Cfd1/Nbp35 to recipient apoproteins by Nar1 and Cia1.

1.5 Human diseases associated with Fe–S cluster assembly

Several human disorders have been linked to defects in the essential process of Fe–S cluster biogenesis. Mutations in certain Fe–S cluster assembly genes either cause a loss of function of the corresponding proteins or result in diminished protein amounts. For instance, GAA triplet repeat expansion in the first intron of the *FXN* gene (which encodes frataxin) is the most frequent mutation encountered in Friedreich's ataxia (FRDA), an autosomal recessive neurodegenerative disease. FRDA is the most common manifestation of hereditary ataxia in humans and occurs due to a functional deficiency in frataxin. In FRDA patients, sensory neurons and cardiac myocytes are adversely affected. The diseased cells are known to exhibit deficiencies in the mitochondrial Fe–S proteins aconitase and complex I–III and sequester iron in mitochondria. The very characteristic of iron as an outstanding biological catalyst also results in the generation of highly toxic hydroxyl radicals via the Fenton reaction, reflecting the double-edged role of this metal in the cell. Other diseases associated with Fe–S cluster assembly are: ISCU-deficient myopathy with exercise intolerance, appearing in skeletal and cardiac myocytes; GLRX5-deficient microcytic anaemia, appearing in developing red blood cells; ABCB7-deficient XLSA/A (X-linked sideroblastic anaemia with ataxia), appearing in developing red blood cells and cerebellar neurons; and GFER-deficient myopathy with combined respiratory-chain deficiency, appearing in skeletal myocytes. (ABCB7 is the human Atm1 orthologue; GFER is the human Erv1 orthologue.) On the basis of the fact that defects in a ubiquitous biosynthetic pathway are responsible for diverse disease presentations in different tissues ranging from nerve to muscle to blood, it is likely that mutations in several other Fe–S cluster assembly genes may account for diseases

of which the definite etiology has not been elucidated yet (see reviews by Rouault & Tong, 2008; Sheftel & Rill, 2009; Sheftel *et al.*, 2010; Ye & Rouault, 2010).

1.6 Nfs1: the NifS-like cysteine desulphurase of eukaryotes

Nfs1 is a pyridoxal-5′-phosphate (PLP)-dependent cysteine desulphurase belonging to the class V aminotransferase family of proteins (Pfam entry PF00266). The corresponding open reading frame (YCL017c) was first discovered when the entire DNA sequence of *S. cerevisiae* chromosome III was determined (Oliver *et al.*, 1992). The gene product was named Nfs1 for bearing a certain degree of sequence identity to NifS of nitrogen-fixing bacteria.

Only some time after the identification of a NifS-like protein in a eukaryote did researchers reveal that NifS from *A. vinelandii* was a PLP-containing homodimer and catalysed the conversion of L-cysteine into L-alanine, sequestering the released sulphur atom in the form of a protein-bound persulphide on a conserved cysteine residue (Zheng *et al.*, 1993; Zheng *et al.*, 1994). The same mechanism was subsequently described for IscS, another NifS-like protein, from *E. coli* (Flint, 1996). The ability of NifS-like proteins to mobilise sulphur as well as their presence in other organisms than nitrogen-fixing bacteria raised the possibility that NifS-like proteins might play a global role in Fe–S cluster biosynthesis. Now, it is known that all organisms encode NifS-like proteins (termed NifS, IscS, CsdA, or SufS in prokaryotes, depending on the operon in which they reside; termed Nfs1 in eukaryotes). Nfs1 shows the highest degree of similarity to IscS, which has a general housekeeping role in the formation of Fe–S clusters. NifS is responsible only for the maturation of the Fe–S protein nitrogenase and cannot replace IscS in *A. vinelandii* (Johnson *et al.*, 2005b). An exceptional group of eukaryotes with regard to the

housekeeping nature of the ISC system seem to be Amoebozoa, which possess the elements of the NIF system (Ali *et al.*, 2004; van der Giezen *et al.*, 2004; Gill *et al.*, 2007). This blurs the clear separation between these systems and provides evidence for their interchangeability.

Some organisms, such as *E. coli*, possess multiple NifS-like proteins (IscS, CsdA and SufS), whereas the yeast and human genomes encode only a single NifS-like protein (Nfs1/NFS1). Yeast Nfs1 was demonstrated to be an essential Fe–S cluster assembly protein localising to mitochondria (Kispal *et al.*, 1999; Li *et al.*, 1999; Mühlenhoff *et al.*, 2004). However, identification of a potential nuclear localisation signal sequence, RRRPR, in the predicted mature form of yeast Nfs1 raised the possibility that the protein might also present in a different subcellular location (Nakai *et al.*, 2001). Recent work provided direct evidence that yeast Nfs1 was found at very low levels in the nucleus and that the mitochondrial and nuclear isoforms of Nfs1 were derived from a single translation product (Naamati *et al.*, 2009). Although human NFS1 was also shown to localise to different subcellular compartments (mitochondria, cytosol and nucleus), this distribution was claimed to occur via alternative translation initiation (Land & Rouault, 1998). The existence of distinct isoforms within the cell may reflect the involvement of Nfs1 in general sulphur trafficking as well as Fe–S cluster formation (see **Section 1.6.3**).

In addition to its pivotal role in the mobilisation and trafficking of sulphur, Nfs1 was also shown to exert regulatory effects on cellular iron metabolism (Li *et al.*, 1999). These effects, resulting from lowered Nfs1 amounts, include the up-regulation of cellular iron uptake and occurrence of mitochondrial iron overload.

1.6.1 Related structures

NifS from the hypertermophilic bacterium *Thermotaga maritima* was the first NifS-like protein of which the crystal structure was reported to a resolution of 2.0 Å (Kaiser *et al.*, 2000). *T. maritima* NifS (PDB entry 1ECX) is a dimer of two identical subunits, each of which is divided into a small and a large domain. The active site lies close to the surface near the dimer interface and harbours the PLP co-factor attached to a conserved lysine (Lys203) at the base of a pocket. The catalytic cysteine (Cys324) resides in the middle of a 12-residue-long highly flexible loop. Stacking on top of PLP is a conserved histidine (His99) which is proposed to serve as an acid/base catalyst during the reaction.

The crystal structure of *T. maritima* NifS was followed by the crystal structure of IscS from *E. coli* to a resolution of 2.1 Å (Cupp-Vickery et al., 2003). Despite the fact that *E. coli* IscS shows only 39% sequence identity with *T. maritima* NifS, the overall topology of *E. coli* IscS (PDB entry 1P3W) is virtually the same as that of *T. maritima* NifS, with nearly identical secondary structural elements (Figure 1.3). In *E. coli* IscS, however, the peptide loop accommodating the catalytic cysteine (Cys328) is ordered to a certain extent. *E. coli* IscS exhibits a significant degree of similarity to NifS-like enzymes from higher organisms (56% sequence identity with yeast Nfs1; 59% sequence identity with human NFS1), providing a good model for eukaryotic cysteine desulphurases.

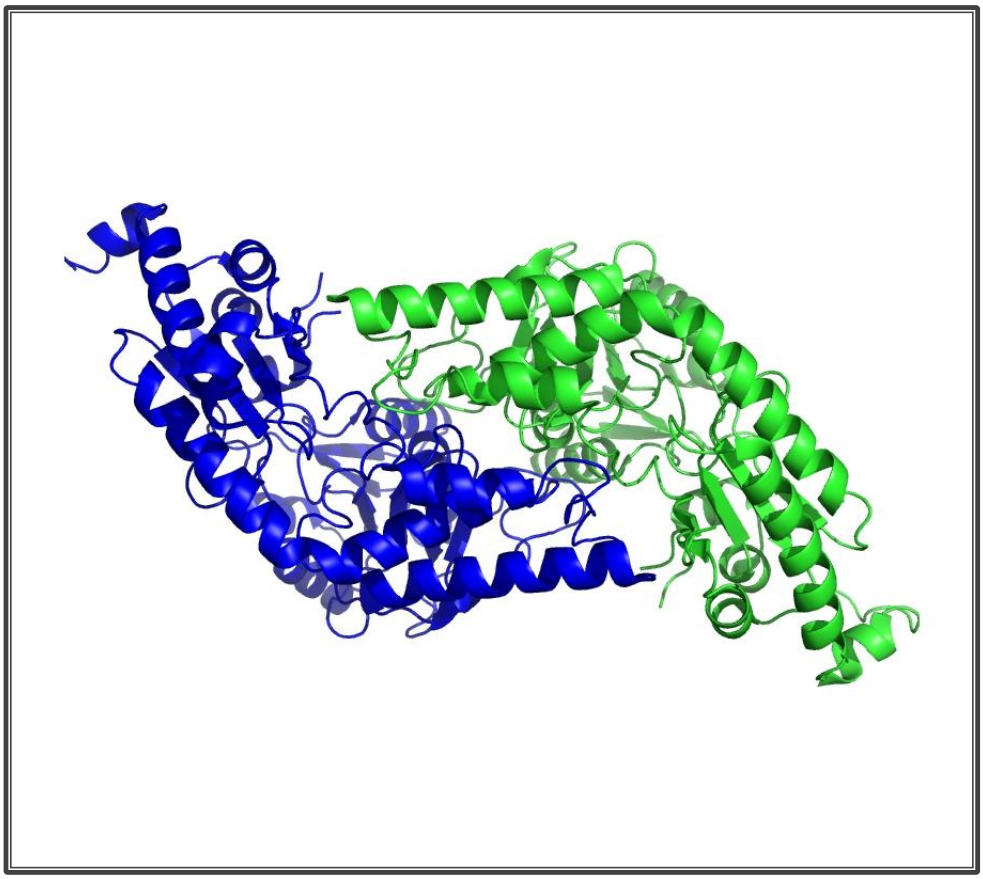

Figure 1.3 Ribbon structure of *E. coli* IscS homodimer (PDB entry 3LVM), seen looking down the two-fold axis. A greater portion of the peptide backbone adopts an α-helical conformation. The two subunits are shown in blue and green. This figure was generated using PyMOL (http://www.pymol.org).

In another success story, crystal structures of *E. coli* IscS bound to the sulphur-acceptor proteins TusA and IscU (PDB entries 3LVJ, 3LVK and 3LVL) disclosed distinct docking sites for the different binding partners, all accepting sulphur from the same catalytic residue (Shi *et al.*, 2010). Structures of the IscS/TusA and IscS/IscU complexes showed that the sulphur-accepting proteins TusA and IscU approach Cys328 from different directions, implying that the conformational plasticity of the long loop accommodating this active-site cysteinyl residue is crucial for IscS to effectively deliver its sulphur cargo to multiple recipient proteins.

1.6.2 Reaction mechanism

Dean and co-workers were the first to characterise the mechanism for the desulphuration of L-cysteine catalysed by a NifS-like enzyme (Zheng *et al.*, 1994). Because the catalytic activity of *A. vinelandii* NifS was greatly sensitive to thiol-alkylating agents, a reactive cysteinyl residue was proposed to be engaged in catalysis. They also suggested that the Fe–S cluster assembly process was driven by a NifS-bound cysteinyl persulphide intermediate, which could be formed through nucleophilic attack by the catalytic cysteinyl thiolate on the L-cysteine–PLP adduct.

In the light of crystal structures available for *A. vinelandii* NifS and *E. coli* IscS, it is now known that NifS-like enzymes are composed of two identical subunits, each harbouring a PLP molecule covalently attached to a conserved active-site lysinyl residue by an imine linkage (internal aldimine) in the resting state (Kaiser *et al.*, 2000; Cupp-Vickery *et al.*, 2003). The catalytic cycle is initiated upon binding of the amino acid substrate, L-cysteine, to form a Michaelis complex. A conserved histidinyl resiude, which is positioned directly on top of the PLP co-factor, is believed to deprotonate the α-amino group of L-cysteine. The deprotonated substrate performs a nucleophilic attack on C4′ of PLP, releasing the ε-amino group of lysine and forming a new imine bond with PLP (external aldimine). The external aldimine is formed via the intermediacy of a transient *geminal*-diamine. The active-site lysinyl residue abstracts the C^{α} proton of the substrate to yield a substrate–PLP quinonoid adduct. Reprotonation of the quinonoid intermediate results in a substrate–PLP ketimine adduct, on which the reactive cysteine thiolate performs a nucleophilic attack to cleave the C–S bond and form the enzyme-bound cysteinyl persulphide intermediate (Cys–S–SH) and an enamine derivative of L–alanine (Figure 1.4).

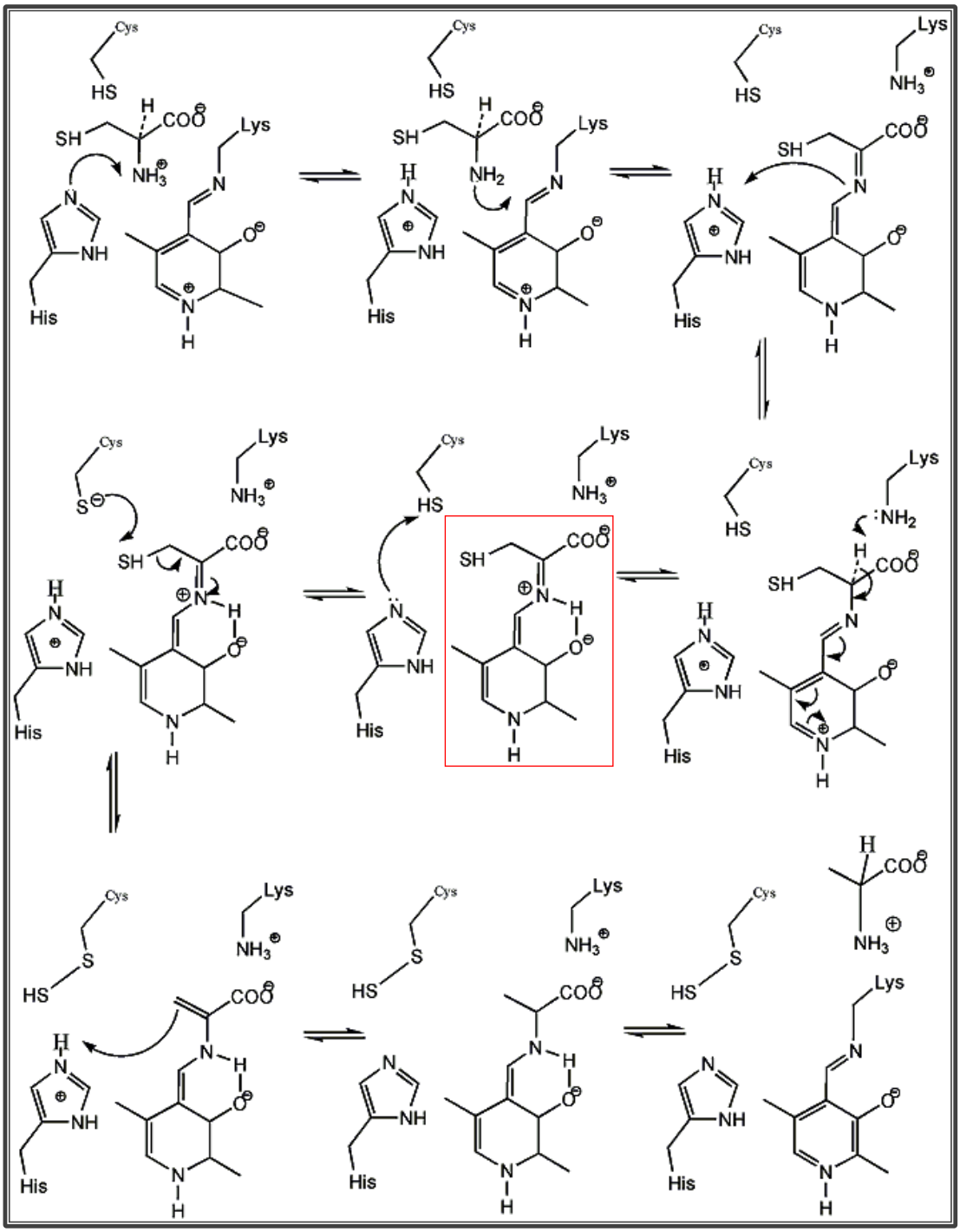

Figure 1.4 Proposed mechanism for the cysteine desulphuration reaction catalysed by NifS-like enzymes. The reaction simply involves formation of an L-cysteine–PLP ketimine adduct, with subsequent nucleophilic attack by the thiolate anion of the active-site cysteinyl residue on the sulphur atom of the PLP-activated cysteine substrate. An enzyme-bound persulphide intermediate is eventually generated, forming the basis of sulphur transfer to recipient proteins (e.g., U-type scaffold proteins, as in the case of Fe–S cluster assembly). The L-cysteine–PLP ketimine adduct is shown in a red rectangular box. This figure was prepared using ChemDraw (http://www.cambridgesoft.com/).

1.6.3 Other reactions

To date, numerous reports have documented the role of IscS in Fe–S cluster assembly. IscS interacts with IscU, which is the primary scaffold for the biosynthesis of the [2Fe–2S] and [4Fe–4S] clusters, to deliver sulphur. In fact, this versatile enzyme can interact with several other acceptor proteins (e.g., ThiI, TusA and MoaD/MoeB) through a broad docking surface centred on Cys328, transferring sulphur to different metabolic pathways including the biosynthesis of thiamine and biotin, thiolation of tRNAs, and biosynthesis of the molybdenum co-factor (Moco) (Shi *et al.*, 2010).

In analogy with the bacterial system, yeast Nfs1 (Nakai *et al.*, 2004) and *Trypanosoma brucei* Nfs1 (Paris *et al.*, 2010) were shown to be involved in the post-transcriptional thio-modification of both mitochondrial and cytosolic tRNAs *in vivo*. What is more, the cytosolic isoform of human NFS1 was demonstrated to act as a sulphur donor for Moco formation *in vitro*, bearing functional resemblance to its bacterial orthologue (Marelja *et al.*, 2008).

1.7 Isd11: the ISC assembly desulphurase-interacting protein

Until recently, Nfs1 was thought to catalyse sulphur transfer to the Isu1 scaffold protein by itself. This, however, was disproved by two independent groups of workers who reported that *S. cerevisiae* Nfs1 required binding of a small (11 kDa) protein called Isd11 to fulfil its regular function (Adam *et al.*, 2006; Wiedemann *et al.*, 2006). They found that Isd11 was an essential protein of the mitochondrial matrix, loosely associated with the mitochondrial inner membrane. Although isolated Nfs1 exhibited enzymatic activity as a cysteine desulphurase and released

sulphide from cysteine *in vitro*, the Nfs1/Isd11 complex (which was estimated to be 190 ± 10 kDa in size) is the active sulphur donor *in vivo*. Isd11, therefore, was suggested to act as a stabiliser of Nfs1. Further studies revealed that Isd11 transiently bound to the proposed iron donor Yfh1 (frataxin) both *in vitro* and *in vivo*, suggesting that the interaction of frataxin with the Nfs1/Isu1 scaffold complex was mediated by Isd11 (Shan *et al.*, 2007; Li *et al.*, 2009).

Isd11 belongs to the LYR family of proteins (Pfam entry PF05347), which is named for the presence of a conserved leucine–tyrosine–arginine tripeptide motif near the N-terminus. The corresponding open reading frame (YER048w-a) resides on yeast chromosome V. Comparative analysis of sequenced genomes uncovered that Isd11 was exclusive to eukaryotes including mitosomal and hydrogenosomal lineages (Richards & van der Giezen, 2006). The absence of Isd11 in currently available prokaryotic genomes directly implies that Isd11 is a eukaryotic supplement to the bacterium-derived ISC assembly apparatus. In fact, mitosomal localisation and functionality of the Nfs1/Isd11 complex from the microsporidians *Encephalitozoon cuniculi* and *Trachipleistophora hominis* was verified experimentally (Goldberg *et al.*, 2008). Direct evidence regarding the localisation and metabolic function of microsporidian Fe–S cluster assembly proteins indicates an essential role for the mitosome in the biosynthesis of Fe–S proteins.

Unlike yeast Isd11, which could not be detected in the cytosol and nucleus of yeast cells, endogenous ISD11 was shown to be targeted to both the mitochondrial and nuclear compartments in human cells (Shi *et al.*, 2009). Given its co-localisation and tight association with Nfs1, one would expect Isd11 to be essential for tRNA thiolation. Very recently, Isd11 from *Trypanosoma brucei* was demonstrated to be

indispensable for the thiolation of cytosolic and mitochondrial tRNAs (Paris *et al.*, 2010).

In addition to their central role in Fe–S cluster assembly, both Isd11 and ISD11 also seem to be responsible for the regulation of normal cellular iron levels (Adam *et al.*, 2006; Shi *et al.*, 2009). This makes ISD11 a potential candidate protein for disease pathology.

1.8 Nfs1/Isd11: the functional desulphurase complex

As mentioned previously in **Section 1.4.3**, the biosynthesis of nascent Fe–S clusters on Isu1 critically depends on the action of the mitochondrial Nfs1/Isd11 cysteine desulphurase complex. Native Nfs1/Isd11 is estimated to be about 190 kDa in size, with no clue as to its subunit stoichiometry (Adam *et al.*, 2006). Although Nfs1 is a well-known ISC-assembly protein, its 11-kDa binding partner Isd11 is a recently identified member of the same subset of proteins and its exact function remains to be characterised.

The presence of mitochondrial-type proteins, such as the ISC-assembly proteins, and residual organelles corresponding to mitochondria in microsporidia and other supposedly amitochondriates falsifies the central prediction of the 'Archezoa' hypothesis (which simply states that organisms such as *Giardia* sp., *Trichomonas* sp., and microsporidia have arisen before the establishment of the mitochondrion in the eukaryotic lineage). The evolution of the Nfs1/Isd11 protein complex among eukaryal groups stands for a latter-day evidence for the universality of mitochondria in formerly unknown manifestations. Furthermore, the eukaryotic invention of Isd11 as a functional partner to Nfs1 directly indicates a single shared α-proteobacterial

endosymbiotic origin for today's eukaryotes (Richards & van der Giezen, 2006). This places α-proteobacterial endosymbiosis before the last common ancestor of all eukaryotes in the evolutionary chronology.

1.9 Summary

Small inorganic constructs of alternating ferrous/ferric iron and sulphide ions, so-called Fe–S clusters, are probably nature's most ancient prosthetic groups. In eukaryotes, these multipurpose reactive centres are assembled by a proteinaceous machinery known as the ISC assembly machinery. The ISC assembly machinery is primarily localised in mitochondria, establishing the essential role of this organelle in Fe–S cluster assembly and providing new insights into human diseases linked to impaired Fe–S cluster formation and mitochondrial iron overload. High conservation of the ISC assembly machinery in prokaryotes, as well as in eukaryotes, reflects its aboriginal and indispensable function and serves as an effective means of tracing endosymbiotic evolutionary history. The Nfs1/Isd11 cysteine desulphurase complex, which allows for the mobilisation of organic sulphur, is one of the central components of the eukaryotic ISC assembly machinery. A thorough characterisation of Nfs1/Isd11 should prove useful for a better understanding of the molecular mechanisms underlying Fe–S cluster assembly, or intracellular sulphur trafficking in general, and associated processes.

1.10 Aims

This study aims to produce and characterise a key component, named the Nfs1/Isd11 cysteine desulphurase complex, of the eukaryotic Fe–S cluster assembly system, using advanced laboratory techniques. The architecture of the Nfs1/Isd11 protein

complex and the specific interaction between its constituent subunits are the main issues to be addressed here.

Chapter 2: Materials and methods

2.1 PCR amplification of genes

The polymerase chain reaction (PCR) relies on the general principle of primer-directed DNA synthesis by DNA polymerases. It expands this process in a cyclical series of reactions as the DNA polymerase involved is thermostable and withstands repeated cycles of denaturing temperature. Each cycle of PCR comprises steps for template denaturation, primer annealing and primer extension. The reaction is automated; a thermal cycler is used to programme the temperatures and times for a given PCR application. In the present study, *S. cerevisiae* genomic DNA was used as a template for the PCR amplification of the target genes *nfs1* and *isd11* with gene-specific primers and the *PfuUltra* II Fusion HS DNA Polymerase.

Primer design is the key to the generation of DNA fragments of desired length and with tailored ends. Given that Nfs1 and Isd11 localise to the mitochondrion, they are expected to carry an N-terminal mitochondrial signal sequence, which directs the proteins to the organelle. Since mature proteins lack this internal targeting information, it is essential to remove the portion of nucleotides encoding the signal sequence before the cloning step. In addition to this, it is also crucial to incorporate specific restriction sites at both ends of the PCR product, allowing it to be cloned into a vector with compatible sites. MitoProt (http://ihg2.helmholtz-muenchen.de/ihg/mitoprot.html) predicted that the first 34 amino acid residues of Nfs1 (which corresponds to the first 102 nucleotides of *nfs1*) as well as the first 10 amino acid residues of Isd11 (which corresponds to the first 30 nucleotides of *isd11*) represent the mitochondrial signal sequence. Therefore, PCR primers were designed

in accordance with the MitoProt results as well as the vector preferences (Table 2.1). Primer synthesis was achieved externally by Eurofins MWG Operon.

Table 2.1 Gene-specific oligonucleotide primers used in this study. (Uppercase letters: complementary sequence; lowercase letters: newly introduced sequence; yellow highlight: *Nde*I restriction site; bright green highlight: *BamH*I restriction site; turquoise highlight: *Xho*I restriction site; pink highlight: *Not*I restriction site; underlined letters: hexahistidine-tag-coding sequence)

Primer set (5′→3′)	Amplification product	Translation product
Forward: aga aga cat atg TCC CCT CCT GCA GCA GGC GTG AAG TTA GAC G **Reverse:** tct tct gga tcc TCA ATG ACC TGA CCA TTT GAT GGA GTT TAA G	*nfs1*Δ1–102	Nfs1Δ1–34
Forward: aga aga cat atg CAG GTG TTG TCT TTA TAC AAG G **Reverse:** tct tct gga tcc TTA GTG TTT TCT TCC TTG CAA TGG	*isd11*Δ1–30	Isd11Δ1–10
Forward: aga aga cat atg CCC ATA TAT CTT GAC ATG CAA GCC ACT ACA CC **Reverse:** tct tct gga tcc TCA ATG ACC TGA CCA TTT GAT GGA GTT TAA G	*nfs1*Δ1–294	Nfs1Δ1–98
Forward: aga aga cat atg cat cac cat cac cat cac TCC CCT CCT GCA GCA GGC GTG AAG TTA GAC G **Reverse:** tct tct ctc gag TCA ATG ACC TGA CCA TTT GAT GGA GTT TAA G	*nfs1*Δ1–102	Nfs1Δ1–34
Forward: aga aga gga tcc g CAG GTG TTG TCT TTA TAC AAG G **Reverse:** tct tct gcg gcc gc TTA GTG TTT TCT TCC TTG CAA TGG	*isd11*Δ1–30	Isd11Δ1–10

2.1.1 Materials

Reagents

- *PfuUltra* II Fusion HS DNA Polymerase and 10× *PfuUltra* II Reaction Buffer (both Stratagene)
- ‘Long Range’ dNTP-Mix, each dNTP at 10 mM (Bioline)
- Gene-specific oligonucleotide primers (see Table 2.1 for details)

- *S. cerevisiae* genomic DNA, at 100 ng μl^{-1}
- peqGOLD Universal Agarose (Peqlab)
- 1× Tris–acetate–EDTA (TAE) buffer: 40 mM Tris, 20 mM acetic acid, 1 mM EDTA
- Ethidium bromide solution, at 10 mg ml^{-1} (Fisher Scientific)
- 5× DNA Loading Buffer (Bioline)
- DNA HyperLadder I (Bioline)
- QIAprep Gel Extraction Kit (Qiagen)

Equipment and instruments

- Agarose gel electrophoresis apparatus
- Thermal cycler
- Microcentrifuge

2.1.2 Reaction mixture

The PCR reagents were mixed in appropriate amounts in thin-walled PCR tubes that were kept on ice throughout the preparation period (Table 2.2).

Table 2.2 PCR mixture.

Reagent	Amount
PfuUltra II Reaction Buffer (10×)	5 µl
'Long Range' dNTP-Mix (10 mM each dNTP)	2 µl
S. cerevisiae genomic DNA (100 ng μl^{-1})	1 µl
Forward primer (10 µM)	1 µl
Reverse primer (10 µM)	1 µl
Distilled water	39 µl
PfuUltra II Fusion HS DNA Polymerase	1 µl
Total reaction volume	**50 µl**

2.1.3 Thermal cycling conditions

Thermal cycler was programmed using the recommended cycling parameters for the *PfuUltra* II Fusion HS DNA Polymerase (Table 2.3). 'Hot lid' option was chosen in order to prevent evaporation.

Table 2.3 Thermal cycling conditions. ([a]: optimised for the target *isd11*Δ1–30; [b]: optimised for the targets *nfs1*Δ1–102 and *nfs1*Δ1–294)

Segment	No. of cycles	Temperature	Duration
1	1	95 °C	2 min
2	30	95 °C	20 s
		60 °C	20 s
		72 °C	15 s[a] or 1 min 15 s[b]
3	1	72 °C	3 min
4	1	4 °C	∞

2.1.4 Agarose gel electrophoresis and gel-purification of PCR products

The principle of agarose gel electrophoresis is the separation of DNA molecules according to conformation and size by their movement through a defined-percentage

agarose gel under the influence of an electric field. Here, agarose gel electrophoresis of DNA was used to assess the success of the amplification reaction as well as to isolate the PCR product from the reaction mixture.

A 1% (w/v) horizontal agarose gel, supplemented with 0.5 µl ethidium bromide per 100 ml gel, was prepared. 50 µl of PCR mixture was mixed with 12.5 µl of 5× agarose gel loading dye, and the resulting sample was loaded in roughly equal amounts to multiple wells of the agarose gel submerged in 1× TAE buffer. The gel was run at 75 V until the tracking dye migrated about one third of the gel. The bands corresponding to the PCR product to be cloned were excised on a UV illuminator using a clean scalpel. The resulting pieces of agarose containing the PCR product were treated with the QIAquick Gel Extraction Kit according to the manufacturer's instructions. The clean PCR product was eluted in 50 µl of Qiagen's elution buffer. The purified PCR product was either stored at -20 °C or directly used in subsequent cloning reactions.

2.2 Directional cloning of PCR products

Gene cloning is the process of constructing and propagating recombinant DNA molecules. The activity of commercially available enzymes (restriction endonucleases and the T4 DNA ligase) to manipulate DNA is central to gene cloning. The PCR product and the vector are cut in a double-digest experiment with the same pair of restriction endonucleases to yield cohesive ends for ligation. Covalent linkage of pieces of DNA and formation of closed circular DNA permit subsequent transformation reactions to occur efficiently. Transformation is simply the introduction of recombinant plasmid DNA constructs into host cells that are rendered competent to enable effective uptake of plasmids.

2.2.1 Materials

Reagents

- Expression vectors: pET-14b, pET-3a and pCDFDuet-1 (all Novagen)
- Restriction endonucleases: *Nde*I, *BamH*I, *Xho*I and *Not*I (all New England Biolabs)
- 10× reaction buffers: NEBuffer 3 and NEBuffer 4 (both New England Biolabs)
- Bovine serum albumin, at 10 mg ml^{-1} (New England Biolabs)
- DNA Ligation Kit (Takara)
- α-Select Chemically Competent Cells (Bioline)
- SOC medium: 2% (w/v) tryptone, 0.5% (w/v) yeast extract, 0.4% (w/v) glucose, 10 mM NaCl, 2.5 mM KCl, 10 mM $MgCl_2$, 10 mM $MgSO_4$
- LB broth, Lennox: 1% (w/v) tryptone, 0.5% (w/v) yeast extract, 10 mM NaCl
- LB–agar, Lennox: 1% (w/v) tryptone, 0.5% (w/v) yeast extract, 10 mM NaCl, 1.5% (w/v) agar
- Selective antibiotics: ampicillin and streptomycin (both Sigma-Aldrich)
- QIAquick Spin Miniprep Kit (Qiagen)
- DNA sequencing primer: ACYCDuetUP1 Primer (Novagen)

Equipment and instruments

- Temperature-controlled water bath
- Temperature-controlled incubator

- Temperature-controlled shaking incubator
- Microcentrifuge

2.2.2 Double digestion and clean-up of DNA

The insert was prepared by double digesting the PCR product with appropriate restriction endonucleases. Each corresponding vector (see **Appendix** for details) was also double digested with the same set of restriction endonucleases (Table 2.4). New England Biolabs' Double Digest Calculator programme (http://www.neb.com/nebecomm/DoubleDigestCalculator.asp) was used to determine the double-digest conditions (Table 2.5).

Table 2.4 Restriction enzymes used for the cloning of PCR products into corresponding expression vectors.

PCR product	Vector	Enzyme set
*nfs1*Δ1–102	pET-14b	*Nde*I–*BamH*I
*isd11*Δ1–30	pET-14b	*Nde*I–*BamH*I
*isd11*Δ1–30	pET-3a	*Nde*I–*BamH*I
*nfs1*Δ1–292	pET-14b	*Nde*I–*BamH*I
*nfs1*Δ1–102	pCDFDuet-1 (MCS2)	*Nde*I–*Xho*I
*isd11*Δ1–30	pCDFDuet-1 (MCS1)	*BamH*I–*Not*I

Table 2.5 Double-digest conditions. ([c]: optimised for the *BamH*I/*Not*I and *Nde*I/*BamH*I digests; [d]: optimised for the *Nde*I/*Xho*I digest)

Reagent	Amount
Vector or PCR product (400 ng μl^{-1})	10 µl
NEBuffer 3[c] or 4[d] (10×)	10 µl
Bovine serum albumin (10 mg ml^{-1})	1 µl
Distilled water	77 µl
Restriction endonuclease #1 (10/20 U μl^{-1})	1 µl
Restriction endonuclease #2 (10/20 U μl^{-1})	1 µl
Total reaction volume	**100 µl**

Each reaction was incubated for 4 h at 37 °C. After the incubation period, both the insert and the vector were purified using the specified reagents from the QIAquick Gel Extraction Kit. 30 µl of Qiagen's elution buffer was used to elute digested DNA. The purified digestion product was either stored at -20 °C or directly used in subsequent ligation reactions.

2.2.3 Sticky-end ligation

Ligation of the insert into the vector was performed using Takara's DNA Ligation Kit, which involves an optimised buffer system and T4 DNA Ligase. The standard protocol was employed for the sticky-end ligation (Table 2.6).

Table 2.6 Sticky-end ligation reaction mixture.

Reagent	Amount
Vector DNA	2 µl
Insert DNA	8 µl
Ligation Mix	10 µl
Total reaction volume	**20 µl**

Each reaction was incubated for 30 min at 16 °C. Following ligation, the reaction mixture was either stored at 4 °C or directly used in subsequent transformation reactions.

2.2.4 Transforming a general subcloning host

5 µl of the ligation reaction was used to transform 50 µl of *E. coli* α-Select Chemically Competent Cells according to the manufacturer's instructions. The suggested transformation protocol basically involves a 40-s heat-shock treatment at 42°C. Transformants were selected for growth by plating the cells on LB–agar supplemented with the appropriate antibiotic for the chosen vector (Table 2.7). The plates were incubated overnight (16–18 h) at 37 °C. The competent cells provide *rec*A1 and *end*A1 markers to minimise recombination and enhance the quality of the construct (see **Appendix** for details).

Table 2.7 Names and concentrations of antibiotics used for the selection of expression vectors

Vector	Selective antibiotic	Antibiotic concentration
pET-14b	Ampicillin	100 µg ml^{-1}
pET-3a	Ampicillin	100 µg ml^{-1}
pCDFDuet-1	Streptomycin	50 µg ml^{-1}

2.2.5 Plasmid preparation

Following overnight incubation at 37 °C, several colonies were picked and each was used to inoculate 5 ml of LB containing the appropriate antibiotic. The cultures were allowed to grow overnight at 37 °C. Plasmid DNA was isolated from the cultures using the QIAquick Spin Miniprep Kit according to the manufacturer's instructions.

50 µl of Qiagen's elution buffer was used to elute DNA. This isolation protocol yields plasmid at a concentration of about 400 ng μl^{-1}.

2.2.6 Custom DNA sequencing

Bacterial clones were verified for each target via DNA sequencing achieved externally by Eurofins MWG Operon. pET-14b- and pET-3a-based constructs were sequenced using the T7 Promoter Primer and the T7 Terminator Primer (both provided by Eurofins MWG Operon), whereas pCDFDuet-1-based constructs were sequenced using the ACYCDuetUP1 Primer and the T7 Terminator Primer. The verified plasmids were designated as pKT1 (pET-14b-based construct encoding His_6-tagged Isd11Δ1–10), pKT2 (pET-14-based construct encoding His_6-tagged Nfs1Δ1–34), pKT3 (pET-14b-based construct encoding His_6-Nfs1Δ1–98), pKT4 (pCDFDuet-1-based construct simultaneously encoding His_6-tagged Nfs1Δ1–34 and His_6-tagged Isd11Δ1–10), and pKT5 (pET-3a-based construct encoding tag-free Isd11Δ1–10) (Figure 2.1).

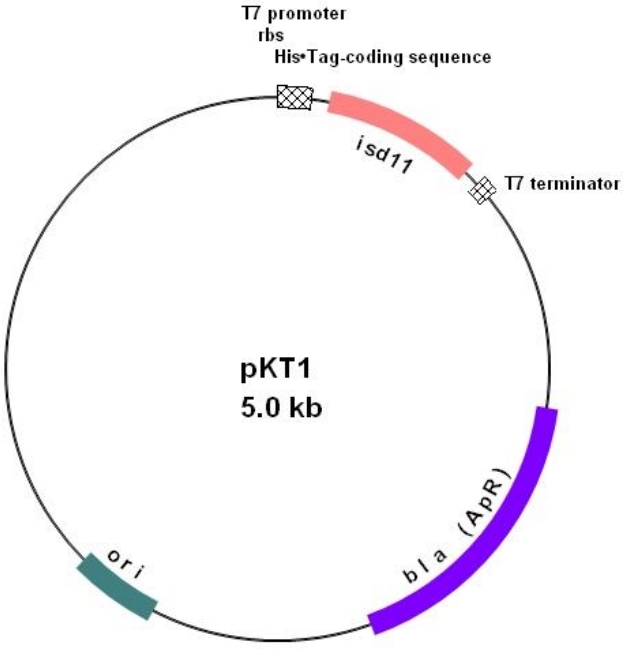

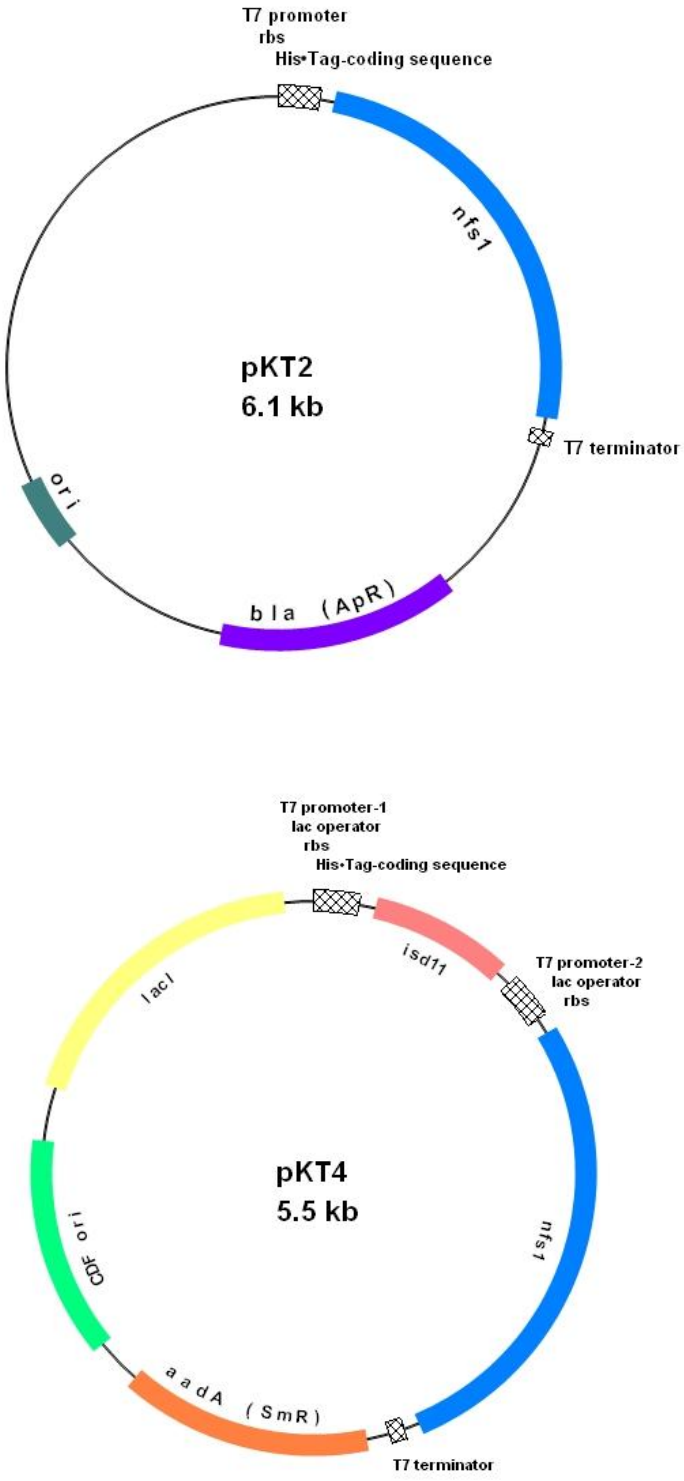

Figure 2.1 Representative constructs used in this study. rbs: ribosome-binding site; *bla* (Ap^R): ampicillin resistance gene; *ori*: pBR322 origin; *lacI*: *lac* repressor gene; *aadA* (Sm^R): streptomycin resistance gene; CDF *ori*: CloDF13 origin.

1.3 Heterologous production of proteins

One of the most useful applications of recombinant DNA technology is heterologous protein production, which consists of the directed synthesis of large amounts of foreign proteins in a host cell such as bacteria or yeast. By far, the most favoured host for the heterologous production of proteins is *E. coli*. The production is achieved using a T7 RNA polymerase promoter system. The expression vector (e.g., pET) contains a phage T7 RNA polymerase promoter and an *E. coli* ribosome-binding site (RBS), followed by the AUG start codon, a multiple cloning site (MCS), and, finally, a T7 transcription terminator. Expression is achieved in a special *E. coli* strain, a λDE3 lysogen, which produces the T7 RNA polymerase upon induction with IPTG, a non-metabolisable synthetic analogue of lactose. The enzyme is highly selective and efficient, only transcribing from the T7 promoter. The activity of the T7 promoter may be modulated by a regulatory sequence, such as that from the *E. coli lac* operon. Some vectors, such as the Duet vectors, feature two MCSs each of which is preceded by a T7 promoter, a *lac* operator, and an RBS. They allow for the co-expression and subsequent complexation of interacting proteins with each other *in vivo*.

2.3.1 Materials

Reagents

- Competent cells: RosettaBlue(DE3)pLysS and RosettaBlue(DE3) (both Novagen)
- Construct DNA: pKT1, pKT2, pKT3, pKT4, and pKT5 (see **Section 2.2.6** for details)

- SOC medium (see **Section 2.2.1** for details)
- LB–agar, Lennox (see **Section 2.2.1** for details)
- Selective antibiotics: ampicillin, streptomycin and chloramphenicol (all Sigma-Aldrich)
- LB broth, Lennox (see **Section 2.2.1** for details)
- IPTG (Fisher Scientific)
- Non-detergent sulfobetaine (NDSB) 201 (Sigma-Aldrich)
- Pyridoxine HCl (Fluka) and pyridoxal-5′-phosphate (PLP) monohydrate (Acros Organics)
- Lysis buffer, ice-cold: 50 mM KH_2PO_4, 300 mM NaCl, 5 mM 2-mercaptoethanol, 20 mM imidazole, 50 μM PLP, 0.125 mM NDSB-201, 10% (v/v) glycerol (pH 7.0)

Equipment and instruments

- Temperature-controlled water bath
- Temperature-controlled incubator
- Temperature-controlled shaking incubator
- Microcentrifuge
- Preparative centrifuge

2.3.2 Transforming a gene expression host

1 μl of purified plasmid DNA was used to transform 20 μl of RosettaBlue competent cells according to the manufacturer's instructions. The suggested transformation

protocol basically involves a 30-s heat-shock treatment at 42 °C. Transformants were selected for growth by plating the cells on LB–agar supplemented with chloramphenicol (34 μg ml^{-1}) and the appropriate antibiotic for the plasmid used (i.e., either ampicillin or streptomycin). The plates were incubated overnight (16–18 h) at 37 °C.

2.3.3 Cell growth

A single colony from a fresh plate was used to inoculate 20 ml of LB broth containing 0.5% (w/v) glucose and the appropriate antibiotics. The cells were allowed to grow overnight (16–18 h) at 30 °C with shaking. The starter culture was then diluted 1:25 into 500 ml of pre-warmed (37 °C) LB broth supplemented with 50 μM pyridoxine HCl and the appropriate antibiotics. (The expression was scaled up using multiple colonies and repeating the steps above.) The expression culture was incubated at 37 °C with shaking until A_{600} reached 0.6–0.8. 10 μl of the culture (which represents non-induced total cell protein fraction) was removed for analysis by SDS–polyacrylamide gel electrophoresis (SDS–PAGE).

2.3.4 IPTG induction

Gene expression was induced by adding IPTG to the remaining culture, which was then incubated for an additional period of time at a pre-determined temperature (Table 2.8). 10 μl of the culture (which represents induced total cell protein fraction) was removed for analysis by SDS–PAGE. 10 μl of the 2× polyacrylamide gel loading buffer was added to both of the 10-μl aliquots of fractions (non-induced and induced), and the samples were heated to 95 °C for 10 min. Proteins were analysed using standard SDS–PAGE methods to determine expression levels by Coomassie staining (see **Section 2.4.6** for details).

Table 2.8 Induction conditions for the expression constructs used in this study. (*c*: IPTG concentration; *t*: incubation period; *T*: incubation temperature)

Plasmid	Host strain	*c* (mM)	*t* (h)	*T* (°C)
pKT1	RosettaBlue(DE3)pLysS	0.4	2	37
pKT2	RosettaBlue(DE3)pLysS	0.4	14	25
pKT3	RosettaBlue(DE3)pLysS	0.4	14	25
pKT4	RosettaBlue(DE3)	1	14	25

2.3.5 Harvest and storage

The culture was chilled on ice for several minutes, and the cells were collected by centrifuging at 4,000 rpm for 15 min at 4 °C. The resulting supernatant was discarded, and the cell pellet was resuspended in 10 ml of ice-cold lysis buffer. Resuspended cells were frozen at -80 °C.

2.3.6 Preparing glycerol stocks of cells

5 ml of LB broth containing the appropriate antibiotics and 0.5% (w/v) glucose was inoculated with an isolated colony from a fresh plate. The cells were incubated with vigorous shaking (250 rpm) at 30 °C overnight. 0.1 ml of sterile 80% (v/v) glycerol was added to 0.9 ml of the culture, and the mixture was mixed well by vortexing. These glycerol–cell stocks were flash-frozen in liquid nitrogen and stored at -80 °C.

2.4 Purification of His_6-tagged proteins

A crucial step for studying individual proteins is the isolation of the protein of interest. Fusing non-disruptive tags in-frame to either terminus of the expression product is the preferred method for purifying the protein in a rapid manner. To date, hexahistidine (His_6) moiety is the most popular tag because of its small size and high

affinity for Ni^{2+} ions, even under denaturing conditions. The His_6 moiety can also be used as an epitope tag for which commercial monoclonal antibodies are available.

2.4.1 Materials

Reagents

- Lysozyme from chicken egg white (Fluka)
- DNase I (Roche Applied Science)
- cOmplete, Mini, EDTA-free Protease Inhibitor Cocktail Tablets (Roche Applied Science)
- Ni^{2+}-charged HisTrap HP column, 5 ml (GE Healthcare)
- Native immobilised metal affinity chromatography (IMAC) binding/wash buffer: 50 mM KH_2PO_4, 300 mM NaCl, 5 mM 2-mercaptoethanol, 20 mM imidazole, 10 μM PLP, 0.125 mM NDSB-201 (pH 7.0)
- Native IMAC elution buffer: 50 mM KH_2PO_4, 300 mM NaCl, 5 mM 2-mercaptoethanol, 500 mM imidazole, 10 μM PLP, 0.125 mM NDSB-201 (pH 7.0)
- Denaturing IMAC binding/wash buffer: 50 mM KH_2PO_4, 300 mM NaCl, 5 mM 2-mercaptoethanol, 8 M urea, 20 mM imidazole, 10 μM PLP, 0.125 mM NDSB-201 (pH 7.0)
- Denaturing IMAC elution buffer: 50 mM KH_2PO_4, 300 mM NaCl, 5 mM 2-mercaptoethanol, 8 M urea, 500 mM imidazole, 10 μM PLP, 0.125 mM NDSB-201 (pH 7.0)
- HiPrep Sephacryl S-200 HR column, 120 ml (GE Healthcare)

- Size-exclusion chromatography (SEC) equilibration/elution buffer: 20 mM HEPES, 200 mM NaCl, 1 mM DTT, 1 mM EDTA, 5% (v/v) glycerol (pH 7.0)
- 2× polyacrylamide gel loading buffer: 125 mM Tris–HCl (pH 6.8), 4% (w/v) SDS, 40% (v/v) glycerol, 0.1% (w/v) bromophenol blue, 5% (v/v) 2-mercaptoethanol
- SeeBlue Plus2 Pre-Stained Standard (Invitrogen)
- Pre-cast 4–20% Tris–HEPES LongLife iGels (NuSep)
- 1× SDS–PAGE running buffer: 100 mM Tris, 100 mM HEPES, 0.1% (w/v) SDS (pH 8.0)
- Staining solution: 30% (v/v) methanol, 10% (v/v) acetic acid, 0.1% (w/v) Coomassie Brilliant Blue R-250
- Destaining solution: 30% (v/v) methanol, 10% (v/v) acetic acid

Equipment and instruments

- Sonicator
- Microcentrifuge
- Refrigerated bench centrifuge
- Refrigerated preparative centrifuge
- Peristaltic pump
- ÄKTA FPLC System (GE Healthcare)
- Vivaspin 20 centrifugal concentrators (Sartorius Stedim)
- SDS–PAGE apparatus

2.4.2 Cell lysis and clarification of lysate

Resuspended cells were thawed using cold (4 °C) water. Following the addition of lysozyme at a final concentration of 1 mg ml^{-1}, DNase I at a final concentration of 5 μg ml^{-1} and protease inhibitors excluding EDTA, the suspension was incubated at 4 °C for 30 min. (No exogenous lysozyme was used for the lysis of the RosettaBlue(DE3)pLysS host strain, which constitutively expresses T7 lysozyme.) For further disruption, the cells were subjected to sonication on ice. The process involved six 10-s bursts at 40–50% duty with 10-s cooling periods between each burst. The cell debris (and inclusion bodies, if any) was sedimented by centrifuging at 15,000 rpm for 30 min at 4 °C. The supernatant (which represents soluble cytoplasmic fraction) was transferred into a fresh, pre-chilled tube, and 10 μl of it was maintained for analysis by SDS–PAGE.

2.4.3 Immobilised metal affinity chromatography

Affinity chromatography takes advantage of a specific intrinsic or extrinsic feature of the target protein to isolate it from other (i.e., contaminating) proteins in the sample. Immobilised metal affinity chromatography (IMAC) is a special form of affinity chromatography in which an immobilised metal ion is used to selectively retain proteins by forming a coordinate bond with a given chemical group. Chelating Sepharose, when charged with Ni^{2+} ions, selectively adsorbs proteins if complex-forming amino acid residues, particularly histidine, are exposed on the protein surface. For the large-scale purification of soluble His_6-tagged proteins, pre-packed columns can be used with a syringe, a peristaltic pump or a liquid chromatography system. These columns also allow for the purification of insoluble His_6-tagged

proteins from inclusion bodies when denaturing conditions are applied. His_6-tagged proteins can be readily desorbed with buffers supplemented with imidazole.

To purify the soluble yeast Nfs1 protein from *E. coli* proteins under native conditions, cleared lysate (approximately 10 ml) was loaded with the aid of a peristaltic pump onto a 5-ml HisTrap HP affinity column pre-equilibrated with the native IMAC binding/wash buffer. The column was washed with 10 column volumes of the same buffer, and the target protein was eluted with 3 column volumes of the native IMAC elution buffer. The pump was operated at 4 °C at a constant flow rate of 5 ml min^{-1}.

To purify the urea-solubilised yeast Isd11 protein (see **Section 2.5.2** for details) from *E. coli* proteins under denaturing conditions, solubilised inclusion body fraction (approximately 2.5 ml) was loaded with the aid of a peristaltic pump onto a 5-ml HisTrap HP affinity column pre-equilibrated with the denaturing IMAC binding/wash buffer. The column was washed with 10 column volumes of the same buffer, and the target protein was eluted with 3 column volumes of the denaturing IMAC elution buffer. The pump was operated at room temperature at a constant flow rate of 5 ml min^{-1}.

2.4.4 Concentrating/buffer-exchanging proteins by centrifugal ultrafiltration

To concentrate the protein of interest, the most appropriate molecular weight cut-off (MWCO) should be selected. Solutions of Nfs1Δ1–34, Nfs1Δ1–98 and the Nfs1Δ1–34/Isd11Δ1–10 complex were all applied to Vivaspin 20 10,000 MWCO concentrators. Solutions of urea-solubilised Isd11Δ1–10 and refolded Isd11Δ1–10 were applied to Vivaspin 20 3,000 MWCO concentrators. Assembled concentrators were centrifuged at speeds recommended by the manufacturer until the desired

protein concentration was reached. The protein sample was recovered from the bottom of the concentrate pocket with a pipette.

Buffer-exchange was also achieved using the corresponding 10,000 and 3,000 MWCO concentrators. Once the sample was concentrated to the desired level, the filtrate container was emptied and the concentrator was refilled with an appropriate buffer. The sample was concentrated three more times with this new buffer.

2.4.5 Size-exclusion chromatography

Size-exclusion chromatography (SEC) is a straightforward and reliable technique for separating proteins according to size as they pass through a porous medium. It can also be used to determine the relative molecular mass (M_r) of proteins by comparing an elution volume parameter, such as K_{av} of the protein of interest, with the values acquired for several known calibration standards. K_{av} is calculated from the equation

$$K_{av} = \frac{V_e - V_o}{V_t - V_o}$$

where V_e is the volume in which the standard protein elutes, V_o is the column void volume, and V_t is the total bed volume.

The IMAC eluate fractions containing Nfs1Δ1–34, Nfs1Δ1–98 or the Nfs1Δ1–34/Isd11Δ1–10 complex were concentrated to 5 ml using Vivaspin centrifugal filter devices (see **Section 2.4.4** for details), cleared by microcentrifuging at maximum speed for 10 min, and loaded onto a 120-ml HiPrep Sephacryl S-200 HR column pre-equilibrated with the SEC equilibration/elution buffer. The column was washed with 1 column volume of the same buffer, and the SEC eluate fractions were collected in 5-ml aliquots. SEC was performed on the ÄKTA FPLC system at

4 °C at a constant flow rate of 0.5 ml min^{-1}. The SEC peak protein fractions were pooled, concentrated to 2 mg ml^{-1} using Vivaspin devices, and stored at 4 °C. Protein analysis was achieved by SDS–PAGE.

2.4.6 SDS–polyacrylamide gel electrophoresis of proteins

SDS–polyacrylamide gel electrophoresis (SDS–PAGE) is a technique employed to analyse and fractionate small amounts of protein. It makes use of SDS to solubilise proteins by coating them with a uniform negative charge. SDS treatment greatly reduces differences in both charge and conformation between proteins, making size the major determinant of electrophoretic mobility. This is the basis for employing SDS–PAGE to estimate the molecular weight of the protein of interest with reference to the electrophoretic mobility of standard proteins on the same gel.

10 µl of each protein sample was mixed with an equal volume of 2× polyacrylamide gel loading buffer. The samples were solubilised by heating for 5 min at 95 °C and clarified by centrifuging at 13,000 rpm for 1 min. 10–20 µl of the supernatant was applied per well onto a pre-cast 4–20% Tris–HEPES gel, and the gel was run in the SDS–PAGE running buffer at 150 V until the dye front reached the bottom of the gel. The gel was stained overnight in the staining solution and destained in the destaining solution. Distilled water containing 5% (v/v) glycerol was used to store the gel.

2.5 Protein refolding

The expression of foreign genes at high levels in *E. coli* frequently results in the formation of cytoplasmic granules or inclusion bodies composed of insoluble aggregates of the produced protein. The advantage of using inclusion bodies is that

the protein can be readily purified from inclusion bodies with high level of purity. The challenge is recovery of the active protein, which is achieved by solubilisation of isolated inclusion bodies with water-soluble chaotropic agents such as guanidine hydrochloride or urea followed by protein refolding by removal of the denaturant via dilution and buffer exchange by dialysis, diafiltration, or chromatography.

2.5.1 Materials

Reagents

- Ni^{2+}-charged HisTrap HP column, 5 ml (GE Healthcare)
- Native IMAC binding/wash buffer (see **Section 2.4.1** for details)
- Native IMAC elution buffer (see **Section 2.4.1** for details)
- Stabil-P.A.C (Expedeon)
- Solubilisation buffer: 50 mM KH_2PO_4, 300 mM NaCl, 15 mM 2-mercaptoethanol, 8 M urea, 0.125 mM NDSB-201 (pH 7.0)
- Refolding buffer 1: 50 mM KH_2PO_4, 300 mM NaCl, 5 mM 2-mercaptoethanol, 0.3 mg ml^{-1} NV10 (pH 7.0)
- Refolding buffer 2: 50 mM KH_2PO_4, 300 mM NaCl, 5 mM 2-mercaptoethanol, 1 M NDSB-201, equimass Nfs1Δ1–34 (pH 7.0)

Equipment and instruments

- Refrigerated preparative centrifuge
- Refrigerated bench centrifuge
- ÄKTA FPLC System (GE Healthcare)

- Vivaspin 20 centrifugal concentrators (Sartorius Stedim)

2.5.2 Isolation and solubilisation of inclusion bodies

The pellet containing insoluble Isd11Δ1–10 deposits (inclusion bodies) was washed twice in 10 ml of the native IMAC binding/wash buffer to remove loosely attached *E. coli* proteins and lipids. Inclusion bodies were collected by centrifuging at 15,000 rpm for 30 min at 4 °C. Air-dried inclusion bodies were solubilised in 2.5 ml of the solubilisation buffer for 30 min at room temperature. A brief sonication treatment could further facilitate the solubilisation process. Following clarification by centrifuging at 15,000 rpm for 30 min at 4 °C, the supernatant containing solubilised Isd11 was transferred to a clean tube by pouring, avoiding cell debris.

2.5.3 *In vitro* refolding strategies

On-column protein refolding method makes use of the His_6 tag to achieve rapid renaturation and purification. Solubilised Isd11 was immobilised on a 5-ml HisTrap HP column connected to the ÄKTA FPLC system. Gradual refolding of the bound protein was performed using a linear urea gradient from 8 M to 0 M (which is created by mixing the solubilisation and the native IMAC binding/wash buffers) at 0.5 ml min^{-1}. Elution of the refolded protein (if any) was carried out with 5 column volumes of the elution buffer.

Rapid dilution involves the denatured protein being delivered in a very short time to a refolding buffer, rapidly lowering the concentrations of both the protein and the denaturant. In this method, 2.5 ml of solubilised Isd11 was added to 200 ml of the refolding buffer 1 under vigorous stirring, and the protein was allowed to refold overnight at room temperature. The resulting precipitation was clarified by

centrifuging at 4,000 rpm for 30 min at 4 °C, and the sample was concentrated using Vivaspin 20 3,000 MWCO centrifugal filter devices. Pulsed dilution involves the solubilised inclusion bodies being delivered in a dropwise fashion to the refolding buffer, ensuring that the concentrations of partially folded intermediates are kept low at any instant. In this approach, 250 µl of solubilised Isd11 was added to 200 ml of the refolding buffer 2 under vigorous stirring, and the protein was allowed to refold for 30 min at 4 °C. This was repeated until the protein sample is all diluted (about 10 times). Following the removal of precipitates by centrifugation, the sample was concentrated using Vivaspin 20 centrifugal filter devices (3,000 MWCO).

2.6 Analytical ultracentrifugation

Analytical ultracentrifugation (AUC) basically involves the application of a centrifugal force, the real-time observation of the resulting macromolecular spatial redistribution, and first-principle-based quantitative analysis of the data. One of the most frequently encountered applications of AUC is the determination of relative molecular mass of proteins or multiprotein complexes. Sedimentation-equilibrium AUC approach utilises rotor speeds of approximately 7,000–8,000 rpm and establishes a balance between sedimentation under the influence of centrifugal force and diffusion of material in the opposite direction. As a result, a point is reached where there is no net migration of solute throughout the length of the analytical cell. The molecular weight can then be calculated from the concentration gradient of the solute set up from the equation

$$M_{\mathrm{r}} = \frac{2RT\ln(c_2/c_1)}{\omega^2(1-\bar{v}\rho)(r_2^2 - r_1^2)}$$

where R is the molar gas constant, T is the absolute temperature in K, ω is the angular velocity in radian s^{-1}, $\bar{v}$ is the partial specific volume of the solute, ρ is the density of the solvent in g cm^{-3}, and c_2 and c_1 are the concentrations of solute at distances r_2 and r_1, respectively, from the centre of rotation.

The analytical centrifuge bears close resemblance to a conventional preparative centrifuge that is equipped with an optical system (e.g., a UV-visible absorbance spectrophotometer) for the observation of the protein distribution in real time during the centrifugation.

2.6.1 Sample

A fresh preparation of Nfs1/Isd11 in the SEC equilibration/elution buffer was used as sample for the sedimentation equilibrium study.

2.6.2 Procedure

The protein sample was submitted to my colleague Dr Rebecca Beavil at King's College London. The experiment was conducted at three different rotor speeds (7,000 rpm, 8,500 rpm and 10,000 rpm) at 4 °C in an Optima XL-A analytical ultracentrifuge (Beckman Coulter) carrying a standard rotor. AUC parameters (ρ, $\bar{v}_{Nfs1}$, $\bar{v}_{Isd11}$) were computed using the SEDNTERP program (http://www.rasmb.bbri.org/software/). Computed molecular mass of each subunit was entered manually. Data were fitted using SigmaPlot.

2.7 Quantitative Western blotting

Measurements of the relative amounts of different proteins in a sample can be achieved by blotting separated proteins from the polyacrylamide gel on to a

membrane (i.e., Western blotting) and visualising this blot by several means, including the commonly used chemiluminescence and visible fluorescence detection methods. A third, and more accurate, detection method makes use of the near-infrared fluorescence for quantitative analysis. In this method, secondary antibodies are labelled with IRDye infrared dyes, and IRDye signals are detected by the Odyssey Infrared Imaging System over a broad linear dynamic range.

2.7.1 Materials

Reagents

- Purified Nfs1/Isd11 protein complex
- 2× polyacrylamide gel loading buffer (see **Section 2.4.1** for details)
- SeeBlue Plus2 Pre-Stained Standard (Invitrogen)
- Pre-cast 4–20% Tris–HEPES LongLife iGels (NuSep)
- 1× SDS–PAGE running buffer (see **Section 2.4.1** for details)
- Hybond-P PVDF Membrane (GE Healthcare)
- Filter paper (GE Healthcare)
- Antibodies: His·Tag Monoclonal Antibody, mouse IgG_1 (Novagen) and IRDye800-conjugated Antibody, anti-mouse IgG (Li-Cor)
- Transfer buffer, ice-cold: 25 mM Tris, 25 mM Bicine, 10% (v/v) methanol
- Phosphate-buffered saline (PBS): 10 mM Na–K phosphate buffer, 2.7 mM KCl, 137 mM NaCl (pH 7.4)
- Blocking buffer: 3% (w/v) BSA in PBS

- Wash buffer: 0.1% (v/v) Tween-20 in PBS
- Primary-antibody solution: His·Tag Monoclonal Antibody (0.1 μg ml^{-1}) in PBS containing 0.25% (w/v) BSA and 1% (v/v) Tween-20
- Secondary-antibody solution: IRDye800-conjugated Antibody (0.01 μg ml^{-1}) in PBS containing 1% (v/v) Tween-20, 0.25% (w/v) BSA and 0.01% (w/v) SDS

Equipment and instruments

- SDS–PAGE apparatus
- Microcentrifuge
- Electroblotting apparatus
- Mini rocking shaker
- Odyssey Infrared Imaging System (Li-Cor)

2.7.2 SDS–PAGE

His_6-tagged subunits of the Nfs1/Isd11 protein complex were separated using SDS–PAGE as described in **Section 2.4.6**. Different from a typical SDS–PAGE experiment, only 3 μl of the protein standard was loaded onto the gel, and the Coomassie staining was omitted.

2.7.3 Semi-dry electroblotting

A sheet of PVDF membrane was cut to size and pre-wetted in absolute methanol for 10 s, followed by a wash in distilled water for 5 min. The membrane, the gel and the filter paper were all soaked in the transfer buffer for 15 min. The electroblotting cassette was assembled as follows:

Cathode (-)

Extra-thick filter paper

SDS–polyacrylamide gel

PVDF membrane

Extra-thick filter paper

Anode (+)

The proteins were transferred for 30 min at 20 V. Following transfer, the membrane was removed from the cassette and rinsed briefly with PBS. The membrane/blot was allowed to dry overnight.

2.7.4 Blocking

The membrane was pre-wetted in absolute methanol for 10 s, rinsed with distilled water and wetted in PBS for 5 min. Non-specific binding sites on the membrane were blocked by incubating the membrane with the blocking buffer for 1 h at room temperature with gentle shaking. The blocking buffer was decanted and the membrane was rinsed briefly with the wash buffer.

2.7.5 Primary-antibody incubation

The wash buffer was decanted and the primary-antibody solution was added. The blot was incubated with primary antibodies overnight at 4 °C with gentle shaking. The primary-antibody solution was decanted, and the membrane was washed 4 times, each for 5 min, in excess wash buffer.

2.7.6 Secondary-antibody incubation

The wash buffer was decanted and the secondary-antibody solution was added. The membrane was incubated with secondary antibodies for 1 h at room temperature with gentle shaking. The incubation was carried out in the dark. Following the secondary-antibody incubation, the membrane was washed 4 times, each for 5 min, in excess wash buffer.

2.7.7 Colour detection, analysis and interpretation

The blot was rinsed with PBS to remove residual Tween-20 and directly scanned on the Odyssey Infrared Imaging System in the 800-nm fluorescence channel. Visible bands were sized and quantified using the Odyssey Software. Sizing and quantification data were stored in a data file for further analysis and presentation.

2.8 Quantitative amino acid analysis

Quantitative amino acid analysis provides useful information about the accurate protein concentration and the molar ratio of amino acids present. One of the standard methods for measuring the relative amounts of amino acids in protein hydrolysates includes ion-exchange chromatographic separation of individual amino acids, followed by ninhydrin derivatisation. However, pre-column modification of amino acids and subsequent high resolution of their derivatives by reverse-phase high-performance liquid chromatography (RP-HPLC) is now the preferred method for quantitative amino acid analysis. The derivatisation step incorporates covalently bound chromophores, allowing for photometric or fluorometric detection.

2.8.1 Sample

A fresh preparation of Nfs1/Isd11 in 4 mM HEPES, pH 7.0, 40 mM NaCl, 0.2 mM DTT, 0.2 mM EDTA, and 1% (v/v) glycerol was used as sample for quantitative amino acid analysis.

2.8.2 Procedure

The protein sample was sent to the Protein and Nucleic Acid Chemistry Facility at the University of Cambridge for standard analysis of protein hydrolysates by ion-exchange chromatography and post-column ninhydrin derivatisation.

2.9 UV-visible absorbance spectrophotometry

The use of the absorption, emission, or scattering of electromagnetic radiation by matter (atoms, molecules, ions, or solids) to qualitatively or quantitatively investigate the matter or physical processes is called spectroscopy. The interaction of electromagnetic radiation with matter results in redirection of radiation and/or transitions between the energy levels of the atoms or molecules. The method of UV-visible absorbance spectrophotometry can be used for the qualitative and quantitative estimation of proteins. This method is based on the Beer–Lambert law, and the instrument is known as a UV-visible absorbance spectrophotometer. The UV-visible absorbance spectrophotometer measures the amount of light that a sample absorbs in the UV and visible regions of the electromagnetic spectrum (i.e., from 200 nm to 750 nm). A certain part of the molecule that independently contributes to individual regions of an absorption spectrum is termed a chromophore.

2.9.1 Materials

Reagents

- Purified proteins: Nfs1Δ1–34 and the Nfs1Δ1–34/Isd11Δ1–10 complex
- L-cysteine (Sigma-Aldrich)

Equipment and instruments

- UVettes, 220–1,600 nm (Eppendorf)
- U-3010 absorbance spectrophotometer (Hitachi)

2.9.2 Spectrophotometric determination of protein concentration

Quantitative estimation of proteins in solution can be performed by making use of the fact that the three chromophores in proteins (tryptophan, tyrosine and cystine) absorb at 280 nm. Beer–Lambert law states that the absorbance (A) is proportional to both the concentration of the absorber and the thickness of the layer, as

$$A = \varepsilon \times c \times l$$

where ε is the molar absorbance (or extinction) coefficient for the absorber in M^{-1} cm^{-1}, c is the concentration of the absorber in M, and l is the pathlength through the solution in cm (1 cm for standard cuvettes). For conveniency, ε is replaced by the absorbance value for a 0.1% solution measured in a 1-cm cuvette ($A_{280}^{0.1\%}$). This way of expressing the extinction coefficient allows one to report the protein concentration in mg ml^{-1}.

Based upon primary sequence analysis using the ProtParam tool (http://expasy.org/tools/protparam.html), the $A_{280}^{0.1\%}$ values were computed to be 0.707 for Nfs1Δ1–34, 0.772 for Nfs1Δ1–98, and 0.685 for Nfs1Δ1–34/Isd11Δ1–10.

2.9.3 Obtaining substrate binding spectra

Substrate binding spectra can be used to investigate the degree of interaction between an enzyme and its substrate. Many cofactors of enzymes absorb light in the UV-visible region of the electromagnetic spectrum. For instance, the PLP cofactor of cysteine desulphurases absorbs at 420 nm when it is covalently bound to the enzyme through a Schiff base. The binding of free cysteine to the enzyme perturbs the spectrum by displacing PLP. Therefore, the activities of cysteine desulphurases can be measured spectrophotometrically by following the decrease in A_{420} as a function of time.

Absorbance spectra of Nfs1Δ1–34 and the Nfs1Δ1–34/Isd11Δ1–10 complex, each in the SEC equilibration/elution buffer at a final concentration of 3.65 mg ml^{-1}, were recorded at room temperature both in the absence and presence of 10 mM free cysteine (incubation at 4 °C) with the following settings:

Scan range	260–500 nm
Scan speed	1,200 nm min^{-1}
Sampling interval	2 nm
Slit width	2 nm

2.10 Fluorescence spectrophotometry

Fluorescence is an emission process that involves the transition from a higher to a lower energy state within a given molecule. It is measured by detecting this emitted radiation rather than absorption. The instrument is known as a fluorescence spectrophotometer or a spectrofluorimeter. Because the emission intensity is proportional to the concentration of the emitter at low concentrations, fluorescence spectrophotometry can be used to quantify the emitting species of the molecule (fluorophore). Tryptophan and a few cofactors exhibit this emission phenomenon, and their presence allows intrinsic fluorescence to be measured in proteins. The binding and release of ligands, at sites close to the fluorophore, give rise to alterations in the related fluorescence spectra. Thus, useful information about conformational changes and unfolding can be gained.

2.10.1 Materials

Reagents

- Purified proteins: Nfs1Δ1–34 and the Nfs1Δ1–34/Isd11Δ1–10 complex

Equipment and instruments

- Fluorescence cuvettes (Kartell)
- F-2500 fluorescence spectrophotometer (Hitachi)

2.10.2 Data collection

Emission spectra of Nfs1Δ1–34 and the Nfs1Δ1–34/Isd11Δ1–10 complex, each in the SEC equilibration/elution buffer at a final concentration of 3.65 mg ml^{-1}, were recorded at room temperature with the following settings:

Excitation wavelength	295 nm
Emission wavelength range	315–400 nm
Scan speed	1,500 nm min^{-1}
Excitation slit width	10 nm
Emission slit width	10 nm

2.11 Far-UV circular dichroism spectroscopy

Circular dichroism (CD) spectroscopy is a technique that measures the difference between the molar extinction coefficients for left-handed (L) and right-handed (R) circularly polarised light, as

$$\Delta\varepsilon = \varepsilon_{\mathrm{L}} - \varepsilon_{\mathrm{R}} \quad (\text{units are } M^{-1}\ cm^{-1})$$

ε can be replaced by $\Delta\varepsilon$ in the Beer–Lambert equation to derive the difference in absorption between L and R components (ΔA), as

$$\Delta A = \Delta\varepsilon \times c \times l$$

Much of the literature makes use of the ellipticity (θ), which is related to ΔA by the equation

$$\theta = 32{,}980 \times \Delta A \quad (\text{units are mdeg})$$

The circular dichroism is observed only for chromophores that are in, or closely associated with, an optically asymmetric environment. Near-UV CD spectroscopy relies upon the atomic environment and closeness of packing of aromatic residues and provides useful information about tertiary structure. Alternatively, the far-UV CD signals arise from the transitions of the peptide bond and reflect different types of secondary structural features (α-helix, β-sheet, and random coil) present. The near- and far-UV CD spectra are measured by a spectropolarimeter.

2.11.1 Materials

Reagents

- Purified proteins: Nfs1Δ1–34 and the Nfs1Δ1–34/Isd11Δ1–10 complex

Equipment and instruments

- Quartz cuvettes, 1-mm pathlength
- Chirascan spectropolarimeter (Applied Photophysics)

2.11.2 Data collection

Solutions of protein (0.02–0.2 mg ml^{-1}) were made in an appropriate buffer. The instrument was prepared according to the manufacturer's instructions, setting the CD parameters as follows:

Time per point	2 s
Wavelength range	185/200–260 nm
Step size	0.5 nm
Band width	1 nm
Repeats	3 times

First, a spectrum for the buffer was acquired at 25 °C. This was followed by collecting CD spectroscopic data 3 times for the protein sample at 25 °C. The spectra of the buffer and sample (cumulative average of the 3 repeat scans) were smoothed using the software installed on the spectropolarimeter. The smoothed baseline was subtracted from the smoothed protein spectrum, yielding the actual spectrum to be analysed.

2.11.3 Data analysis and interpretation

Although a simple inspection of the far-UV CD spectra may help to compare changes in the secondary structure of the individual proteins when they are associated in the intact complex, deconvolution of the CD signals using online analysis programs at DichroWeb (http://dichroweb.cryst.bbk.ac.uk/html/home.shtml) allows for the estimation of the secondary structure content of the proteins.

2.12 Homology modelling

Homology modelling predicts the three-dimensional (3D) structure for a protein of known sequence (the target sequence) by modelling it on the known 3D structure of a protein of related sequence (the template sequence). Usually, this approach is only

feasible above approximately 30% similarity. Homology models allow for identification of binding sites and provide useful information about molecular function, provided the residues of the conserved pocket are intact.

2.12.1 Template selection

Based on the primary sequence of Nfs1Δ1–98, proteins with homology and whose structures have been solved were identified by performing a BLASTP search against NCBI's Protein Data Bank proteins database (http://blast.ncbi.nlm.nih.gov/Blast.cgi).

2.12.2 Target–template alignment

Once the template sequence was selected, a multiple sequence alignment of the target and template sequences was produced using the ClustalW algorithm (http://www.ebi.ac.uk/Tools/clustalw2/index.html), which allowed for manipulation of parameters (e.g., gap penalties) to ensure that errors were avoided.

2.12.3 Model building and inspection

Model building was achieved using the semi-automated MODELLER program (http://www.salilab.org/modeller/), which employs the satisfaction-of-spatial-restraints method. The quality of the model was checked and confirmed by superimposing the model structure on the template structure on PyMol and manually inspecting the active site.

2.13 Protein crystallisation screening

X-ray crystallography currently is perceived as the most robust tool for determining the 3D structure of proteins and protein complexes. The major challenge in the X-ray crystallography of proteins remains the preparation of appropriate crystalline samples

and, more specifically, the search for optimum crystallisation conditions. A reasonable place to start is with a concentrated protein sample (5–20 mg ml^{-1}) and a commercially available screening kit containing about 50 different crystallisation reagents. Screening kits provide likely precipitants for protein crystallisation and can be applied manually or with the automated precision of a liquid-handling robot.

2.13.1 Materials

Reagents

- Purified proteins: Nfs1Δ1–34, Nfs1Δ1–98, and the Nfs1Δ1–34/Isd11Δ1–10 complex
- Crystallisation buffer: 10 mM HEPES, 100 mM NaCl, 0.5 mM DTT, 0.5 mM EDTA, 2.5% (v/v) glycerol, 100 μM PLP (pH 7.0)
- Crystallisation screening kits: Crystal Screen, Crystal Screen 2, PEG/Ion Screen (all Hampton Research); Structure Screen 1, Structure Screen 2 (both Molecular Dimensions)

Equipment and instruments

- Plates: 24-well plates or 96-well microplates
- Covers: siliconised 22-mm-diameter square cover slides or 96-well format crystallisation sheets
- 20-ml polypropylene syringe
- Vacuum grease
- 8-channel pipette

- Constant-temperature incubator
- Microcentrifuge
- Mosquito Crystal nanoliter liquid handler (TTP LabTech)
- Light microscope

2.13.2 Sample preparation

Proteins, which were pre-purified by sequential steps of affinity and size-exclusion chromatographies, were buffer-exchanged into the crystallisation buffer and concentrated to 10–20 mg ml^{-1} using Vivaspin 20 concentrators (10,000 MWCO) (see **Section 2.4.4** for details). Protein concentrations were determined spectrophotometrically (see **Section 2.9.2** for details). Any amorphous or particulate material was removed by centrifuging at 13,000 rpm for 10 min at 4 °C.

2.13.3 Screening strategies

For manual screening of crystallisation conditions, a thin bead of vacuum grease was applied with the aid of a syringe to the upper edge of each of the 24 reservoirs. 600 µl of each reagent from a commercial screen (Crystal Screen, Crystal Screen 2, or PEG/Ion Screen) was transferred to multiple 24-well plates, avoiding reagent contamination and carry over. 1 µl of the protein sample (Nfs1Δ1–34, Nfs1Δ1–98, or the Nfs1Δ1–34/Isd11Δ1–10 complex) was pipetted onto the centre of a clean cover slide and subsequently mixed by pipetting up and down with 1 µl of the corresponding crystallisation reagent. Working quickly to minimise evaporation, the cover slide was inverted over and sealed onto the corresponding reservoir. The crystallisation plates were incubated at 18 °C for at least 1 week, and the drops were examined under a light microscope.

For automated screening of crystallisation conditions, crystal trays were prepared by transferring 60 µl of each well solution from a commercial screen (Structure Screen 1 or Structure Screen 2) to a 96-well microplate using a multi-channel pipette. The nanolitre liquid-handling robot was initialised and programmed according to the manufacturer's instructions. When the robot finished the pipetting programme, the crystallisation sheet was applied to the microplate, centering the drop(s) over the corresponding reservoir. The protective backing was removed from the cover sheet. The microplate was incubated at 18 °C for at least three days, and the drops were examined under a light microscope.

Chapter 3: *In silico* analysis and production of yeast Isd11

3.1 Bioinformatic studies suggest that Isd11 is a eukaryote-specific mitochondrial protein with a high α-helical propensity

In an attempt to understand and predict structural and functional features of Isd11 as well as to develop new experimental strategies, several web-based bioinformatic tools were applied. The amino acid sequence of yeast Isd11 retrieved from the *Saccharomyces* Genome Database (SGD) was used in a Position-Specific Iterated BLAST (PSI-BLAST) search (Altschul *et al.*, 2005) against NCBI's non-redundant protein sequence database to identify putative/established homologues. Different from BLASTP, PSI-BLAST greatly increases sensitivity to weak but biologically relevant sequence similarities. Homologues of yeast Isd11 were detected in fungi, plants, and animals, but no prokaryotic homologues were found, supporting the previous reports on the eukaryotic addition of Isd11 to the prokaryote-derived ISC-assembly machinery (Adam *et al.*, 2006; Wiedemann *et al.*, 2006; Richards & van der Giezen, 2006). Selected homologous sequences were aligned and compared using ClustalW (Larkin *et al.*, 2007). Primary structural conservation is not restricted to a particular segment of Isd11; it extends from N- to C-terminus (Figure 3.1).

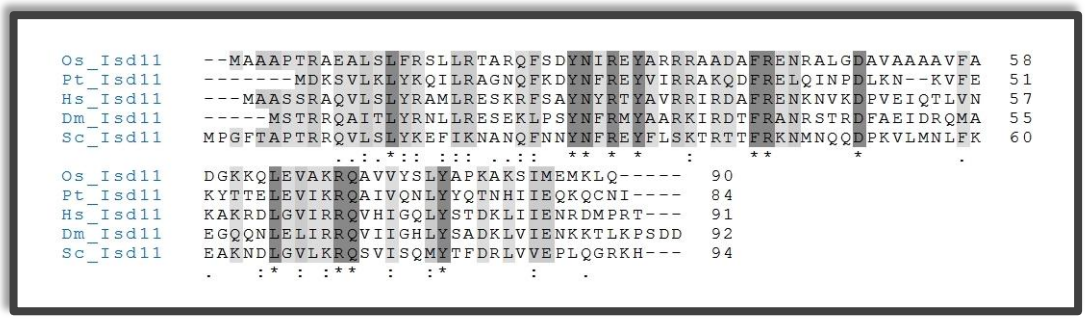

Figure 3.1 Multiple alignment of deduced amino acid sequences of Isd11 proteins from taxonomically diverse organisms. Identical residues are indicated by an asterisk, and conservative and semi-conservative substitutions are indicated by a colon and a dot, respectively. (Os for *Orzya sativa*; Pt for *Paramecium tetraurelia*; Hs for *Homo sapiens*; Dm for *Drosophila melanogaster*; Sc for *Saccharomyces cerevisiae*)

MitoProt II (Claros & Vincens, 1996), a dedicated software for calculating the N-terminal protein region supporting a mitochondrial targeting sequence and the associated cleavage site, inferred that the first 10 amino acids form a basic amphipathic helix containing the mitochondrial targeting information. The inferred mature Isd11 protein itself was also predicted to be composed of three α-helices (Figure 3.2) by using Porter, a reliable server for protein secondary structure prediction (Pollastri & McLysaght, 2005).

In addition to the amino acid sequence, the nucleotide sequence of yeast *isd11* retrieved from SGD was also analysed to determine the occurrence and distribution of rare *E. coli* codons. Rare codons are those codons that are rarely found in highly expressed genes of a given host and include AGG (which encodes Arg), AGA (Arg), AUA (Ile), CUA (Leu), CGA (Arg), CGG (Arg), and CCC (Pro) in *E. coli* (Kane, 1995). The presence of rare codon clusters or a large number of single rare codons in the cloned *isd11* gene could introduce translational problems in *E. coli*. A search of the nucleotide sequence for rare codons revealed that the inferred mature Isd11

protein contains 6 Arg and 1 Leu codons that *E. coli* does not normally encounter (Figure 3.2).

Figure 3.2 Predictive analysis of the primary sequence of yeast Isd11 based on bioinformatic tools. 10-residue block in red represents the putative mitochondrial targeting sequence, with the cleavage site indicated by a triangle. 3-residue block in green represents the LYR (LYK) motif. Residues in blue represent the amino acids encoded by rare *E. coli* codons. Black bars show the predicted consensus secondary structure of the protein.

Given the fact that Isd11 is a novel protein with no structurally characterised homologues, *ab initio* protein modelling was applied to predict its 3D structure. The process involves developing libraries of short segments, which, in turn, are used for building bigger structures. The primary sequence of the predicted mature form of Isd11 was used to feed Robetta, a server that provides automated tools for protein structure prediction and analysis (Kim *et al.*, 2004). The Robetta server generated five models that represent the centres of the five largest clusters of conformations (Figure 3.3).

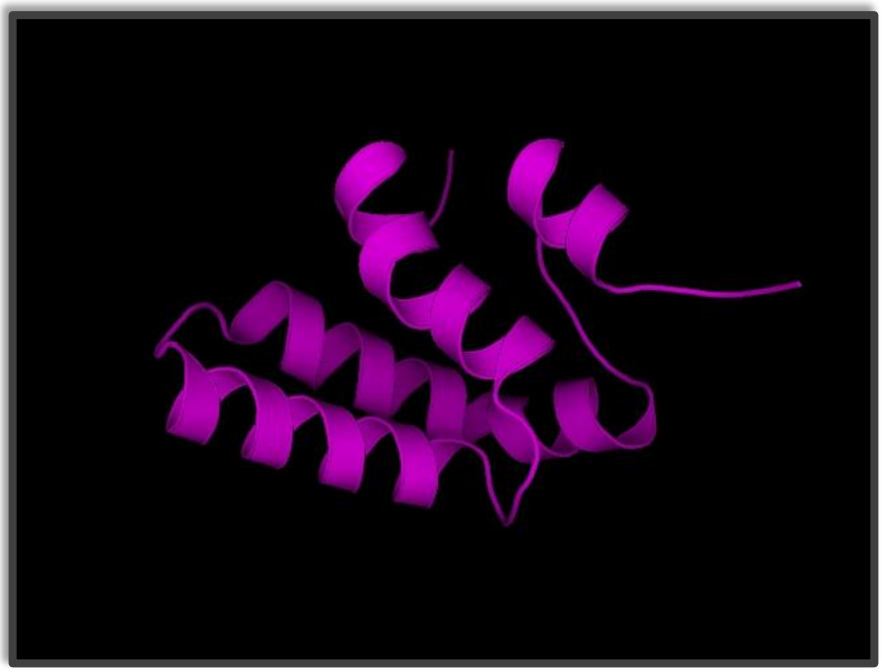

Figure 3.3 Top-scoring (energy rank = 1) *ab-initio* model of yeast Isd11. The image was generated using PyMOL (http://www.pymol.org).

Although protein fold recognition by threading proved to be inconclusive, the compact all-helical fold of Isd11 resembles a nucleic-acid-binding motif.

3.2 The DNA fragment encoding the predicted mature form of Isd11 can be overexpressed in the *E. coli* system

The DNA fragment encoding the predicted mature form of Isd11, Isd11Δ1–10, was amplified directly from the genomic DNA of yeast (Figure 3.4). To minimise the likelihood of mutations introduced by standard PCR, high-fidelity PCR using the proofreading *PfuUltra* DNA polymerase was used. Following double digestion with restriction enzymes, the PCR product was directionally cloned into the pET-14b vector with compatible DNA ends. The resulting construct, designated pKT1, was confirmed by DNA sequencing.

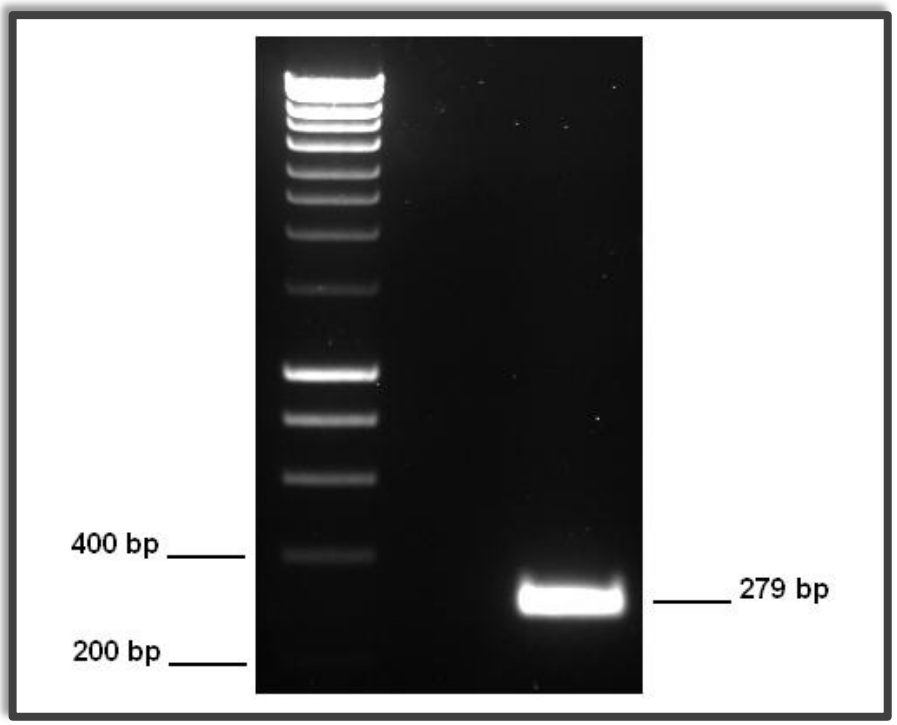

Figure 3.4 Agarose gel electrophoretic analysis of PCR-amplified *isd11*Δ1–30. The wide-range DNA ladder is shown on the left. The size of relevant reference DNA fragments and the amplicon are indicated next to each band.

To enhance the expression of the Isd11Δ1–10-encoding insert, the rare-codon-optimiser strain RosettaBlue(DE3)pLysS was selected as the expression host. Besides compensating for the rare codons encoding Arg and Leu, RosettaBlue(DE3)pLysS cells produce T7 lysozyme to repress low-level transcription from the T7 RNA polymerase promoter before IPTG induction, stabilising inserts encoding potentially toxic proteins. Analytical-scale expression screening revealed that yeast Isd11 could be expressed at high levels using the IPTG-inducible pET-14b/RosettaBlue(DE3)pLysS protein production system (Figure 3.5).

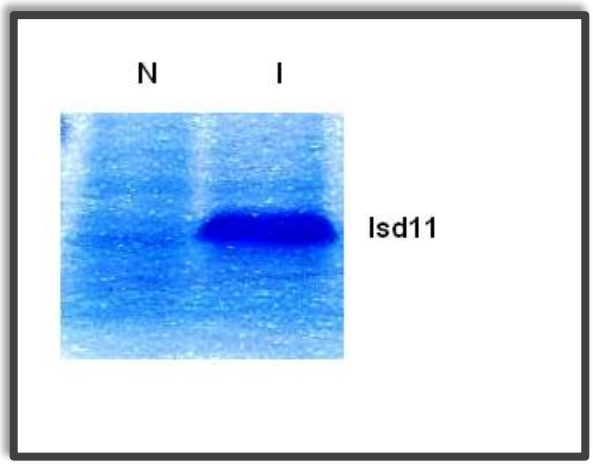

Figure 3.5 SDS–polyacrylamide gel electrophoretic analysis of Isd11Δ1–10 overproduced on an analytical scale. N for non-induced total cell protein; I for induced total cell protein.

3.3 Recombinantly produced Isd11 is deposited as inclusion bodies in the cytoplasm of host cells

Preparative-scale expression experiments performed at various IPTG concentrations (0.4 mM, 0.2 mM or 0.1 mM) and induction temperatures (37 °C, 25 °C or 18 °C) for various incubation times (2 h, 4 h or 14 h) yielded no soluble Isd11 as revealed by the protein's absence in cleared lysates. Hence, it was concluded that recombinant Isd11 has an absolute tendency to form insoluble aggregates called inclusion bodies. Inclusion bodies arise by deposition of partially folded or misfolded proteins through the exposition of hydrophobic patches and the resultant non-covalent intermolecular attractions (Villaverde & Carrió, 2003). Knowing that Isd11 was deposited as inclusion bodies, the original purification protocol described for Nfs1 was modified so as to include urea as the denaturant. Immobilised Ni^{2+}-affinity chromatography under denaturing conditions yielded a single band corresponding to the deduced molecular mass of His_6-tagged Isd11Δ1–10 (12.4 kDa) as detected by SDS–PAGE (Figure 3.6).

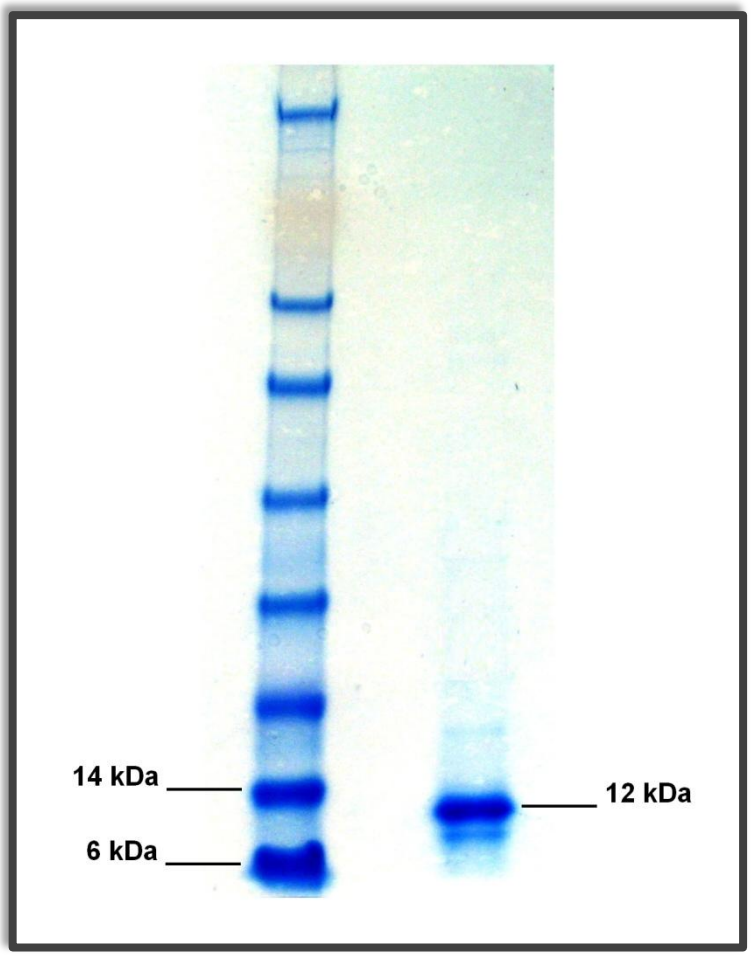

Figure 3.6 SDS–polyacrylamide gel electrophoretic analysis of Isd11Δ1–10 produced on a preparative scale and purified by affinity chromatography under denaturing conditions. The pre-stained protein ladder is shown on the left. The apparent molecular mass of relevant reference proteins and the deduced molecular mass of Isd11 are indicated next to each band.

3.4 Denatured Isd11 cannot be readily refolded *in vitro* into its native state

A considerable effort went into the recovery of Isd11 by refolding *in vitro*. Following inclusion body isolation, protein solubilisation with urea, and immobilised Ni^{2+}-affinity chromatography under denaturing conditions, Isd11Δ1–10 was subjected to refolding by: (i) immobilising the denatured protein onto a 5-ml HisTrap HP affinity column and gradually eliminating excess urea (also called on-column refolding), (ii)

diluting the denatured protein into a renaturation buffer supplemented with non-detergent sulfobetaines, or (iii) diluting the denatured protein into a renaturation buffer containing the amphipathic carbohydrate-based polymer NV10 from Expedeon. Only the third approach was partially successful in recovering Isd11. The costly NV10 polymer, when used at the minimum recommended concentration, yielded very limited amounts of renatured Isd11 as revealed by the protein's presence in the cleared and concentrated renaturation buffer.

3.5 Summary

The novel fold of Isd11 made it difficult to infer precise molecular function solely on the basis of its primary structure, highlighting the necessity of experimental evidence. On the other hand, it was clear that Isd11 could not be easily prepared from *E. coli* cells in a soluble form in the quantities needed for biophysical characterisation. Perhaps Nfs1 could be used to solubilise Isd11 or the two proteins, Nfs1 and Isd11, could be co-expressed, allowing further characterisation of the role of Isd11. The production of Nfs1 and of the complex of Nfs1 and Isd11 are discussed in **Chapter 4** and **Chapter 5**.

Chapter 4: Production and characterisation of yeast Nfs1

4.1 Bioinformatic studies of Nfs1 assist in the development of new experimental strategies

In order to predict certain structural and functional aspects of Nfs1 as well as to drive new experiments, several publicly available *in silico* tools were employed. The amino acid sequence of yeast Nfs1 retrieved from the *Saccharomyces* Genome Database (SGD) was used in a Protein–Protein BLAST (BLASTP) search (Altschul *et al.*, 2005) against NCBI's Protein Data Bank protein database to identify structurally characterised homologues. The top hit was *E. coli* IscS, which was followed by *T. maritima* NifS, rat and human selenocysteine lyases, and *E. coli* SufS respectively. Selected homologous sequences were aligned and compared (Figure 4.1**)** using ClustalW (Larkin *et al.*, 2007).

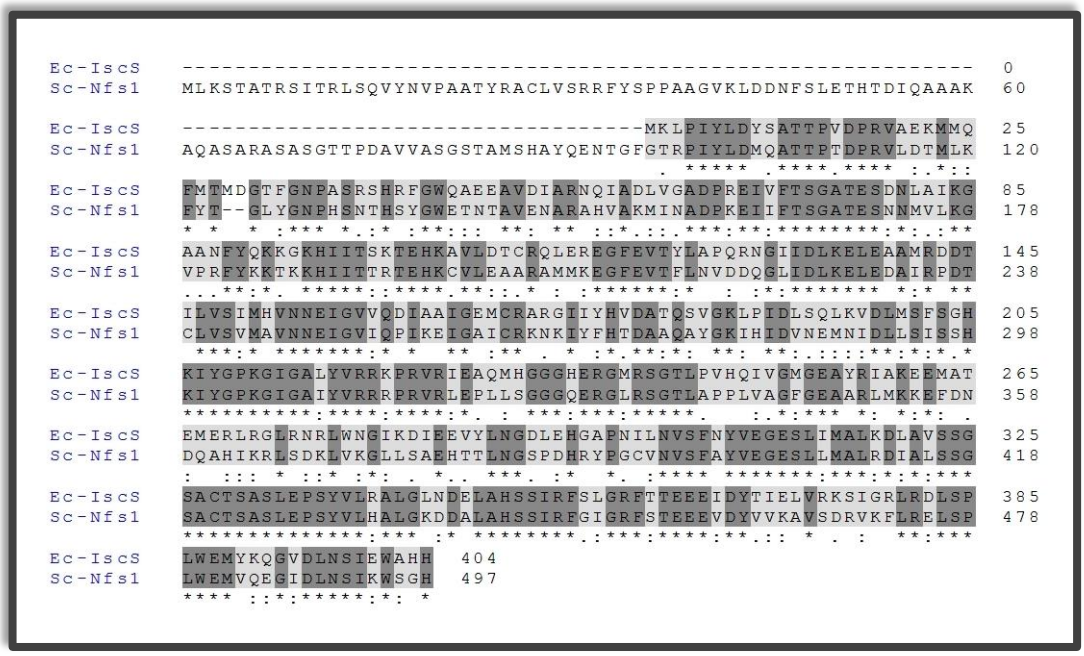

Figure 4.1 Alignment of deduced amino acid sequences of *E. coli* (Ec) IscS and *S. cerevisiae* (Sc) Nfs1. Identical residues are indicated by an asterisk, and conservative and semi-conservative substitutions are indicated by a colon and a dot, respectively. The two proteins share 56% similarity.

MitoProt II (Claros & Vincens, 1996) predicted that the first 34 amino acid residues form a basic amphipathic helix containing the mitochondrial targeting information. A search of the nucleotide sequence for rare codons revealed that the predicted mature Nfs1 protein contains 20 Arg, 7 Leu, 4 Ile, and 3 Pro codons that *E. coli* does not normally encounter (Kane, 1995). Three of the Arg codons form a cluster that resides in the mid-region of the protein.

4.2 Yeast Nfs1 constructs can be successfully overexpressed in *E. coli*

The DNA fragments encoding the predicted mature form of Nfs1, Nfs1Δ1–34, and the truncated form of Nfs1, Nfs1Δ1–98, were amplified directly from the genomic DNA of yeast (Figure 4.2). To minimise the likelihood of mutations introduced by standard PCR, high-fidelity PCR using the proofreading *PfuUltra* DNA polymerase was used. Following double digestion with restriction enzymes, the PCR products were directionally cloned into the pET-14b vector with compatible DNA ends. pET-14b encodes a cleavable N-terminal His_6 tag that facilitates the affinity purification of Nfs1. The resulting constructs, designated pKT2 and pKT3, were validated by DNA sequencing.

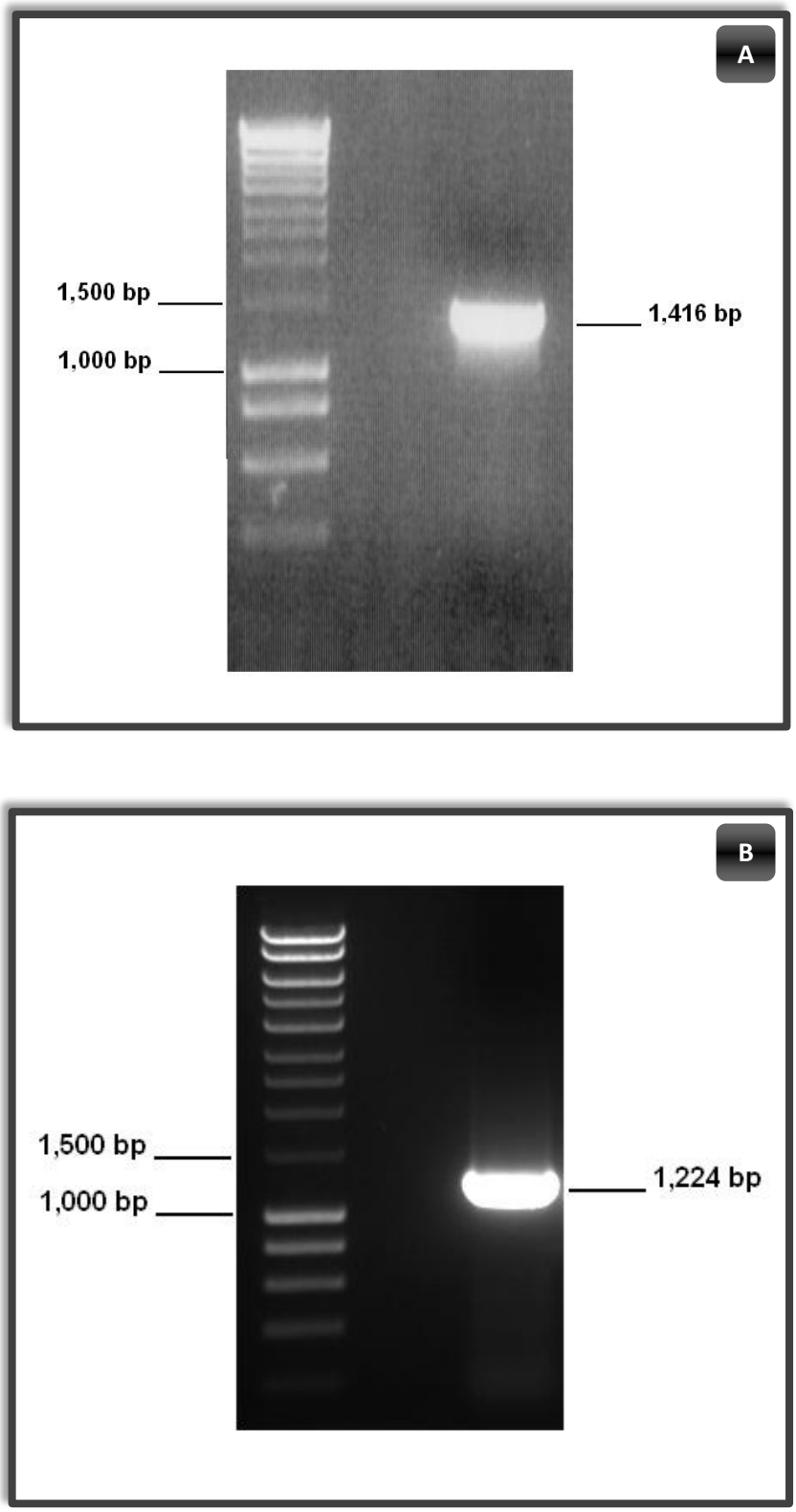

Figure 4.2 Agarose gel electrophoretic analysis of PCR-amplified (**A**) *nfs1*Δ1–102 and (**B**) *nfs1*Δ1–294. The wide-range DNA ladder is shown on the left side of the PCR product of interest. The size of relevant reference DNA fragments and individual PCR products are indicated next to each band.

Analytical-scale expression screening showed that both Nfs1Δ1–34 and Nfs1Δ1–98 can be expressed at high levels using the IPTG-inducible pET-14b/ RosettaBlue(DE3)pLysS protein production system (data not shown).

4.3 Recombinantly produced Nfs1 is a soluble protein with a bright yellow colour attributable to PLP

Overnight induction of preparative-scale *E. coli* cultures harbouring either pKT2 or pKT3 with 0.4 mM IPTG at 25 °C resulted in high levels of soluble Nfs1, indicating that a combination of the strong T7 RNA polymerase promoter and the rare-codon-optimiser strain RosettaBlue(DE3)pLysS provides a very useful platform for soluble Nfs1 production. To purify Nfs1, the soluble cell fraction was first loaded onto a 5-ml HisTrap HP affinity column. Nfs1 exhibited a bright yellow colour in accordance with the presence of protein-bound PLP. This characteristic colour allowed downstream purification and concentration steps to be easily tracked (Figure 4.3).

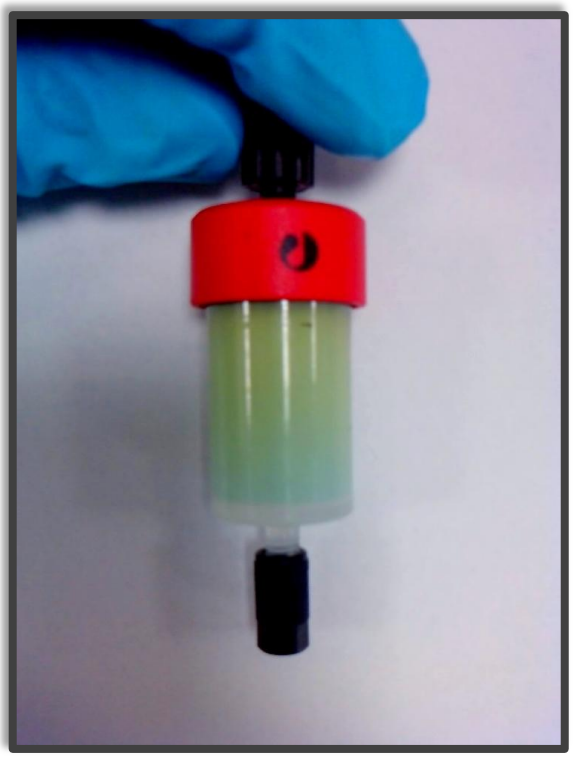

Figure 4.3 Sample of Nfs1Δ1–34 captured on a HisTrap HP affinity column. The protein is bright yellow in colour, a characteristic attributable to bound PLP.

Following immobilised Ni^{2+}-affinity chromatography, the protein was loaded onto a 120-ml HiPrep Sephacryl S-200 HR size-exclusion column for further purification at the preparative scale. The elution profiles of both Nfs1Δ1–34 and Nfs1Δ1–98 showed a large symmetrical peak with a small leading shoulder (Figure 4.4). The peak fractions were collected and pooled accordingly.

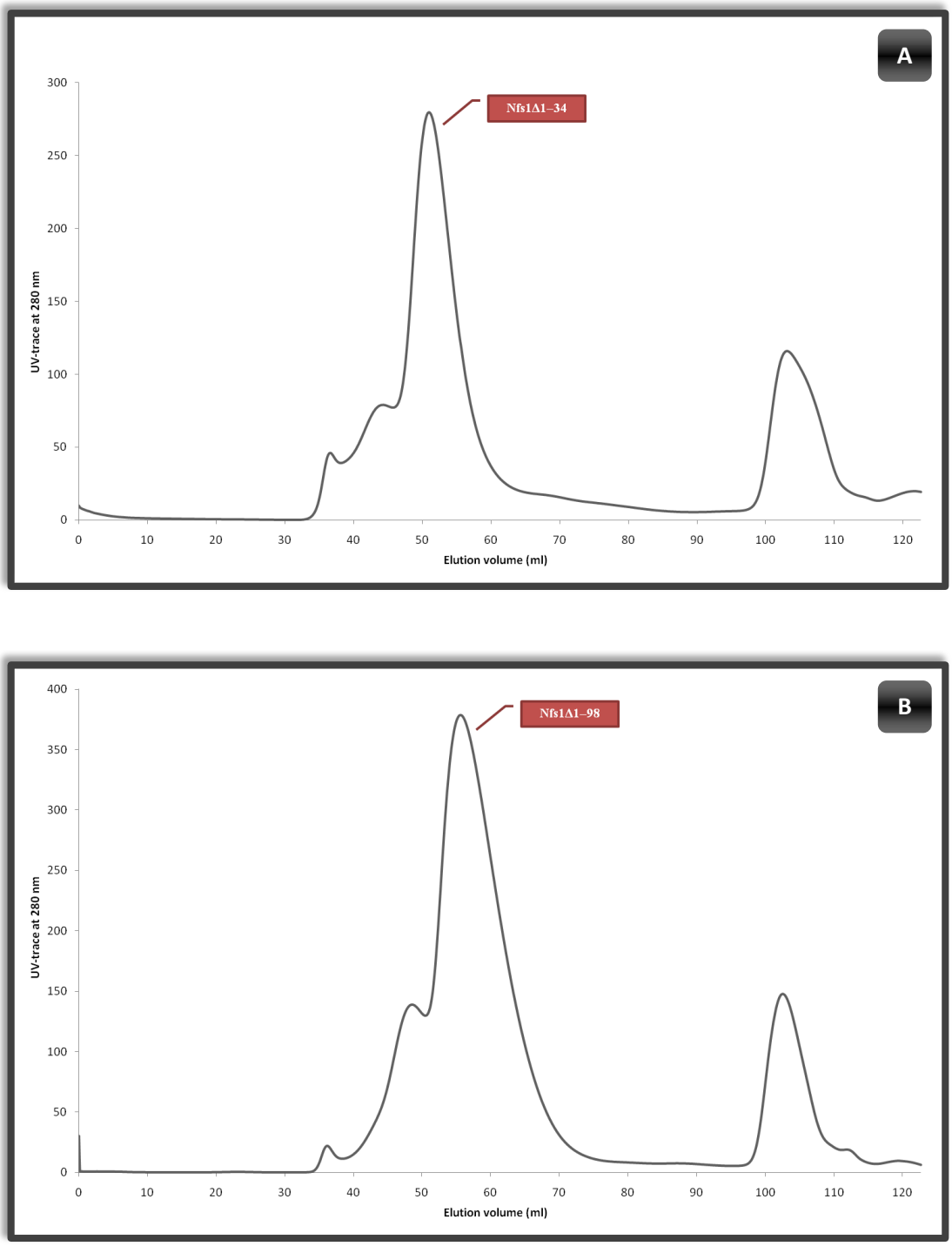

Figure 4.4 Elution profiles of (**A**) and Nfs1Δ1–34 and (**B**) Nfs1Δ1–98 from the HiPrep Sephacryl S-200 HR size-exclusion column. The peaks containing the target protein are labelled.

Protein homogeneity was verified by SDS–PAGE under reducing conditions, which yielded a single band corresponding to the calculated molecular mass of His_6-tagged

Nfs1 (52.9 kDa for Nfs1Δ1–34; 46.5 kDa for Nfs1Δ1–98) (Figure 4.5). The protein, at 2 mg ml^{-1}, could be stored at 4 °C for 8 weeks with no visible precipitation.

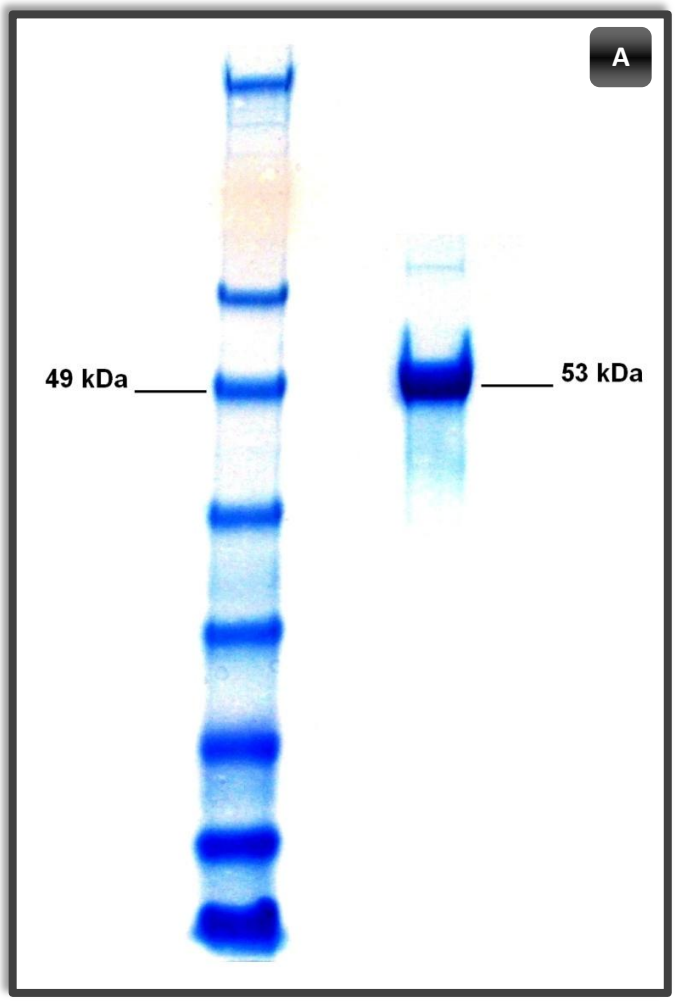

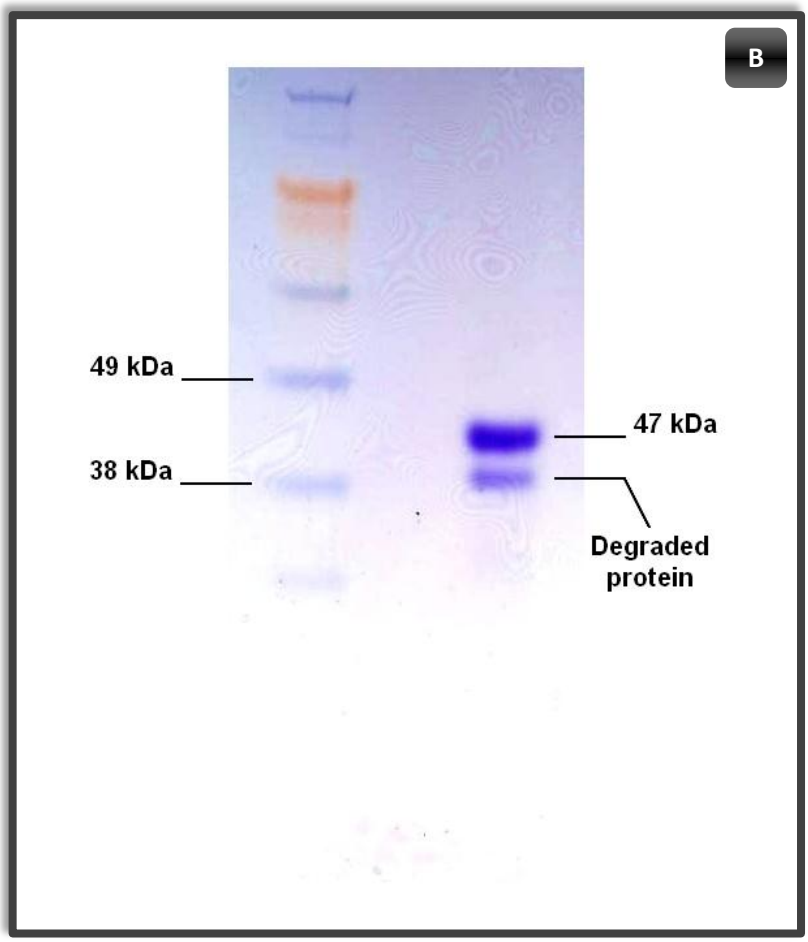

Figure 4.5 SDS–polyacrylamide gel electrophoretic analysis of (**A**) Nfs1Δ1–34 and (**B**) Nfs1Δ1–34, both produced on a preparative scale and purified by subsequent steps of affinity and size-exclusion chromatographies. The pre-stained protein ladder is shown on the left side of the protein of interest. The apparent molecular mass of relevant reference proteins and the deduced molecular mass of Nfs1 isoforms are indicated next to each band.

4.4 Size-exclusion chromatography indicates that recombinant Nfs1 exists as a homodimer in solution

In an attempt to estimate the apparent molecular mass of Nfs1 at the analytical scale, a 24-ml Superdex 200 10/300 GL size-exclusion column, which was previously calibrated with globular proteins of known molecular mass, was used. The apparent molecular mass of the Nfs1Δ1–34 was calculated from the calibration curve represented by the equation

$$K_{av} = -0.2087 \ln(M_r) + 2.7653$$

where K_{av} is the fraction of the stationary gel volume that is accessible to Nfs1Δ1–34 and M_r is the relative molecular mass of Nfs1Δ1–34 in kDa. Recombinant Nfs1 has an apparent molecular mass of approximately 100 kDa, which corresponds to the mass of a homodimer. This finding is consistent with the previous studies on the characterisation of the oligomeric state of cysteine desulphurases (Zheng *et al.*, 1993; Flint *et al.*, 1996; Kaiser *et al.*, 2000; Cupp-Vickery *et al.*, 2003; Mühlenhoff *et al.*, 2004).

4.5 UV-visible absorbance spectrophotometry confirms the presence of PLP and shows that recombinant Nfs1 is active towards L-cysteine

UV-visible absorbance spectrophotometry, scanning wavelengths from 260 nm to 500 nm, was used to characterise the bound chromophore. The spectrum was recorded at room temperature for purified Nfs1Δ1–34 (at a concentration of 3.65 mg ml^{-1} in the SEC equilibration/elution buffer). Nfs1 displayed the typical UV-visible absorbance spectrum of PLP-containing enzymes, giving two intense absorbance bands at 270 nm and 420 nm (Figure 4.6). The former is assigned to the aromatic residues tryptophan and tyrosine, and the latter is assigned to the protonated internal aldimine (Behshad & Bollinger, 2009).

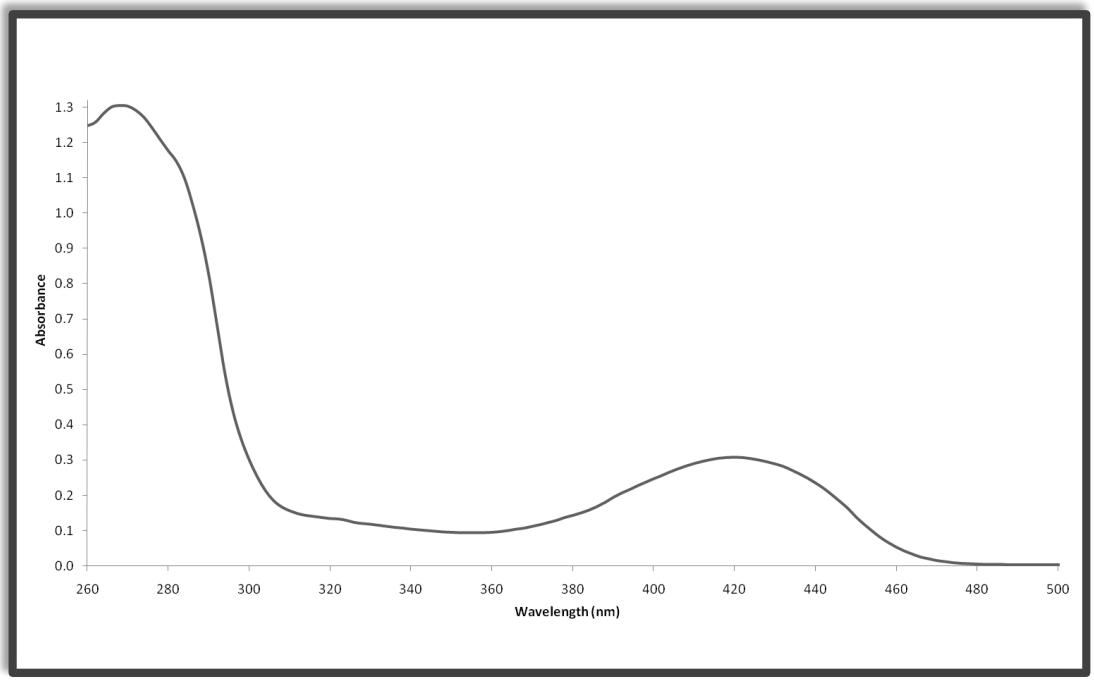

Figure 4.6 UV-visible absorbance spectrum of Nfs1Δ1–34. The peaks at 270 nm and 420 nm correspond to the aromatic residues and the enzyme-bound PLP co-factor, respectively.

The activity of recombinantly produced Nfs1Δ1–34 was assessed by incubating the protein with 10 mM free L-cysteine, with the reaction followed spectrophotometrically. The reaction was carried out at 4 °C in the SEC equilibration/elution buffer. DTT in the buffer reacts with the enzyme-bound persulphide, regenerating the active-site Cys residue and liberating sulphur in the S^{2-} redox state (Fontecave & Ollagnier-de-Choudens, 2008). This is the reason why Nfs1 was assayed *in vitro* in the absence of a specific sulphur-acceptor protein but in the presence of DTT, using L-cysteine as substrate. Measurements were taken at 5-minute intervals over 20 minutes on a Hitachi U-3010 spectrophotometer maintained at room temperature. Because the substrate was used in high molar excess, the system displayed absorption bands corresponding to all long-living species (Figure 4.7).

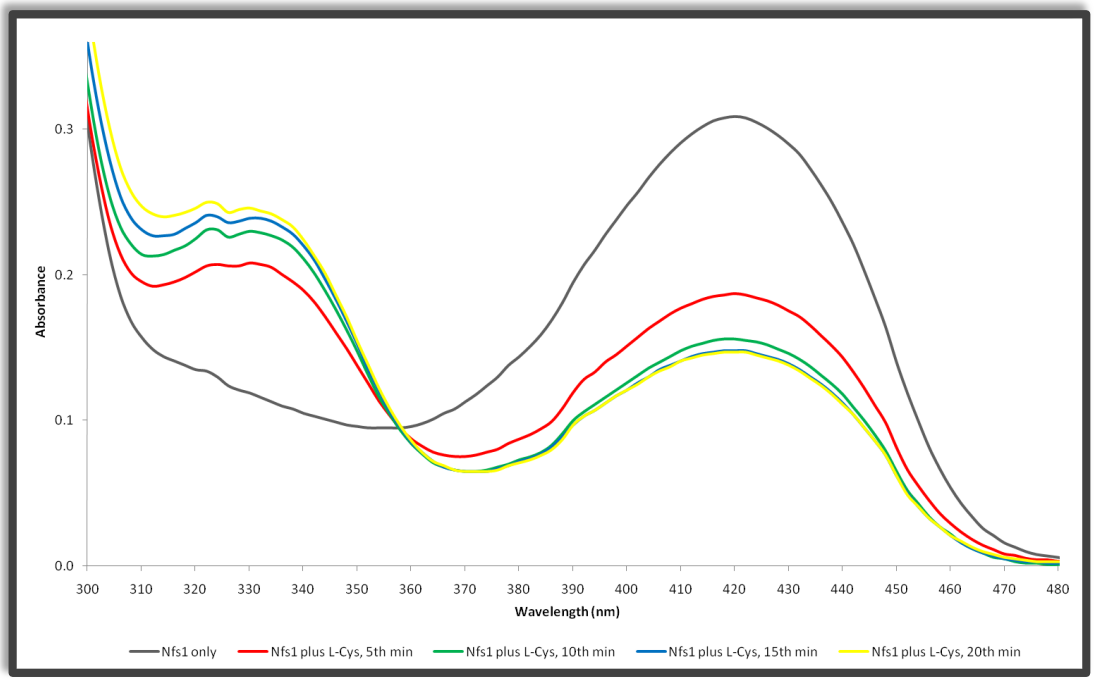

Figure 4.7 Time-dependent spectral analysis of L-cysteine binding to Nfs1Δ1–34. Addition of free cysteine leads to a loss of absorption at 420 nm. At the same time, a second reaction intermediate absorbing at 330 nm is populated.

Upon addition of L-cysteine, the intensity of the absorption band at 420 nm, assigned to the protonated internal aldimine, decreases with a concomitant increase of absorbance at 330 nm. The newly formed absorbing species represents the ketimine intermediate (Behshad & Bollinger, 2009). These results suggest that Nfs1 follows the same reaction scheme as its bacterial homologues (Figure 1.4). The change in absorbance at 420 nm (or 330 nm) is considerable for the first 5-minute interval, but then in subsequent 5-minute intervals the activity reduces. Clearly, the Nfs1–PLP adduct is not being regenerated, or else the peak at 420 nm would persist, so it is plausible that only a single turnover is being monitored. It may be that the high concentration of the free cysteine added (10 mM) competes with the catalytic cysteine, the sulphur acceptor, leading to a trapped substrate–PLP ketimine adduct. Alternatively, the 10 mM L-cysteine could form a disulphide with the cysteine on the flexible loop of Nfs1 preventing it from accepting the sulphur, again trapping the

ketimine. In either case it is clear that the enzyme-bound PLP is reacting with the free cysteine and forming the ketimine, revealing that the active centre of the recombinant enzyme is correctly formed. Nfs1 precipitated after overnight incubation with cysteine at 4 °C. This may be because the resting enzyme (Nfs1–SH) is more soluble than the persulphide compound (Nfs1–S–SH).

4.6 Far-UV CD spectroscopy reveals that recombinant Nfs1 has an extensive α-helical content

In an attempt to obtain reliable estimates of regular secondary structural features (α-helices, β-sheets, and turns) present in Nfs1, CD spectroscopy was applied in the region of peptide bond absorption (far-UV, from 185 nm to 260 nm). Nfs1Δ1–34 (at a concentration of 0.025 mg ml^{-1} in 10 mM potassium phosphate, pH 7.5, supplemented with 1 mM PLP) was used for the CD measurements. The far-UV CD spectrum (Figure 4.8), which represents a baseline-corrected cumulative average of three repeat scans, was measured at 25 °C on a Chirascan spectropolarimeter (Applied Photophysics), using a cell pathlength of 1 mm and a bandwith setting of 1 nm. Data were normalised by scaling to molar concentrations of the repeating unit of the protein. For the far-UV CD spectroscopy, the repeating unit is the peptide bond, and each residue in the protein is associated with a peptide bond. Therefore, data are expressed in terms of the mean residue weight (115 Da for most proteins). The mean residue ellipticity ($[\theta]_{mrw}$) of Nfs1 at a given wavelength was calculated from the equation

$$[\theta]_{\mathrm{mrw}} = \frac{\theta \times mrw}{c \times l}$$

where c is the Nfs1 concentration in mg ml^{-1}, l is the cell pathlength in mm, mrw is the mean residue weight in Da, and θ is the ellipticity in millidegrees (mdeg). $[\theta]_{mrw}$ has the units deg cm^2 $dmol^{-1}$.

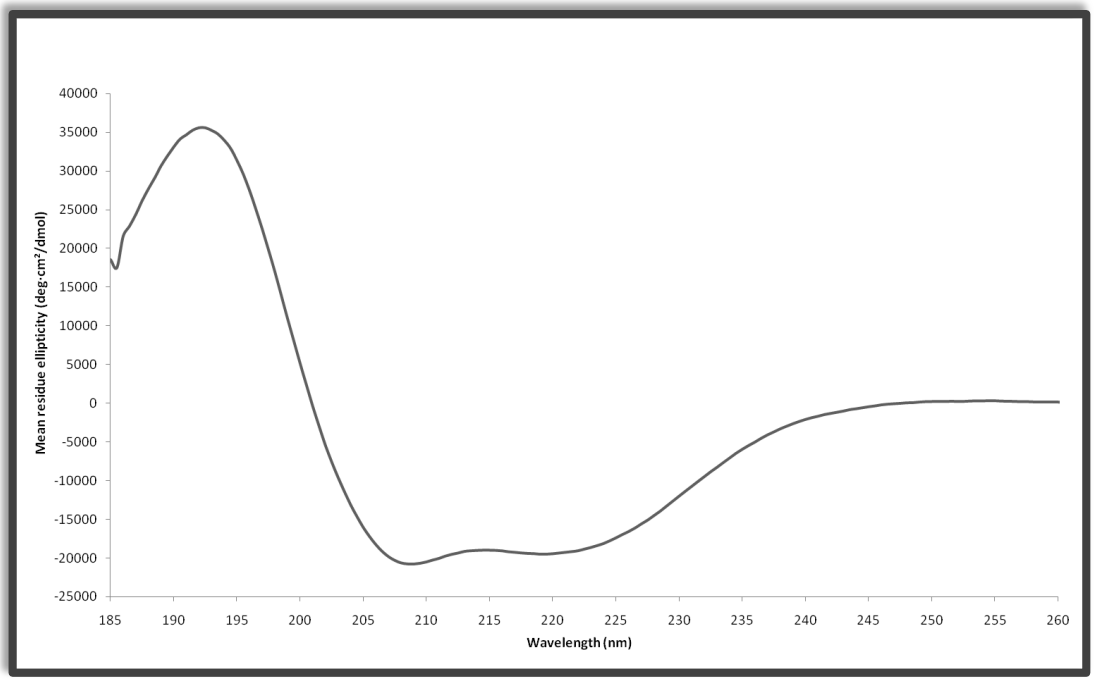

Figure 4.8 Far-UV CD spectrum of Nfs1Δ1–34. The bands at 208 and 222 nm are characteristic of a high content of α-helix.

The spectrum of Nfs1 displayed two strong negative bands at 208 nm and 222 nm, coupled with a strong positive band at 190 nm. These signals indicate that the recombinantly produced protein is extensively α-helical. For a more detailed analysis of the far-UV CD data, the spectrum was deconvoluted via DichroWeb, a dedicated online server hosted by Birkbeck College, University of London (Whitmore & Wallace, 2004). DichroWeb makes use of a range of algorithms and reference databases to estimate the percentages of regular secondary structural elements. Use of the CDSSTR algorithm and the SP175 reference set (Lees *et al.*, 2006) yielded the smallest (0.006) normalised root mean square deviation (NRMSD) value for the spectrum of Nfs1. NRMSD reflects the goodness-of-fit parameter and values of

equal to or less than 0.05 are considered to be ideal. NRMSD analysis, thus, suggests a nearly perfect fit between the calculated CD spectrum (which is derived from the reference proteins) and the spectrum of Nfs1 over the entire wavelength range used (190–240 nm for the SP175 reference set). Regular secondary structural elements were quantified accordingly, confirming the high helical propensity of the amide backbone (Table 4.1).

Table 4.1 Calculated fractions of the regular secondary structural features of Nfs1Δ1–34. Predictions confirm the high α-helical propensity of Nfs1 and provide an insight into its β-sheet content.

α-Helix	β-Strand	Turn	Unstructured
54.5%	7.9%	10.9%	26.7%

Far-UV CD spectroscopy results are in agreement with those obtained from the X-ray crystallographic studies of *E. coli* IscS, which contains a greater percentage of residues in α-helical conformation (40.1%) than β-stranded conformation (13.8%) (Cupp-Vickery *et al.*, 2003). Although far-UV CD spectroscopy proved to be a very useful technique in describing the overall secondary structural elements of Nfs1, only X-ray crystallography could locate where these elements exist within the protein.

4.7 Homology modelling provides insights into the structural organisation of Nfs1 and the integrity of its active site

A considerable effort went into the crystallisation of Nfs1, using both Nfs1Δ1–34 and Nfs1Δ1–98 (see **Section 2.13** for details), but these crystallisation trials were unsuccessful. 50–70% of the drops contained precipitates, while the rest were clear at various protein concentrations tested (5–20 mg ml^{-1}) (data not shown). Therefore,

homology or comparative modelling was employed to obtain a useful 3D model for the protein. The program MODELLER, which implements homology modelling through satisfaction of spatial restraints (Sali & Blundell, 1993; Fiser *et al.*, 2000), was used to make a plausible model of the protein. Among all available molecular structures representing NifS-like proteins, *E. coli* IscS (PDB entry 1P3W) was identified as the best structural template for modelling yeast Nfs1Δ1–98. *E. coli* IscS shares 56% sequence identity with the Nfs1 target. The Nfs1 sequence was aligned with the IscS sequence using ClustalW (Larkin *et al.*, 2007), and this alignment was used to feed MODELLER along with the atomic coordinates of IscS. The resulting model was inspected visually .

Both IscS and Nfs1Δ1–98 have virtually the same overall topology with nearly identical secondary structural elements (Figure 4.9).

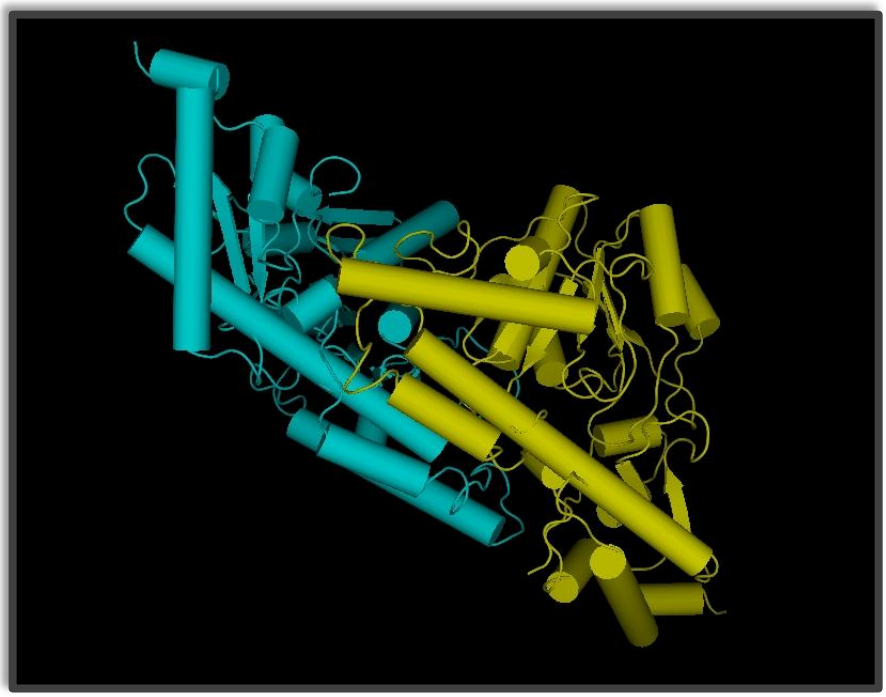

Figure 4.9 Modelled overall structure of Nfs1Δ1–98. The two subunits are colour-coded cyan or yellow. α-helices are shown as cylinders. The image was generated using PyMOL (http://www.pymol.org).

The PLP cofactor is anchored in the active site of Nfs1 via formation of an internal aldimine Schiff base with Lys299 as well as a number of hydrogen bonds (Figure 4.10). Asp239 and Gln242 help stabilise the position of the pyridine ring of PLP, while Thr135, Ser262 and His264 help stabilise the position of its phosphate group in the active site.

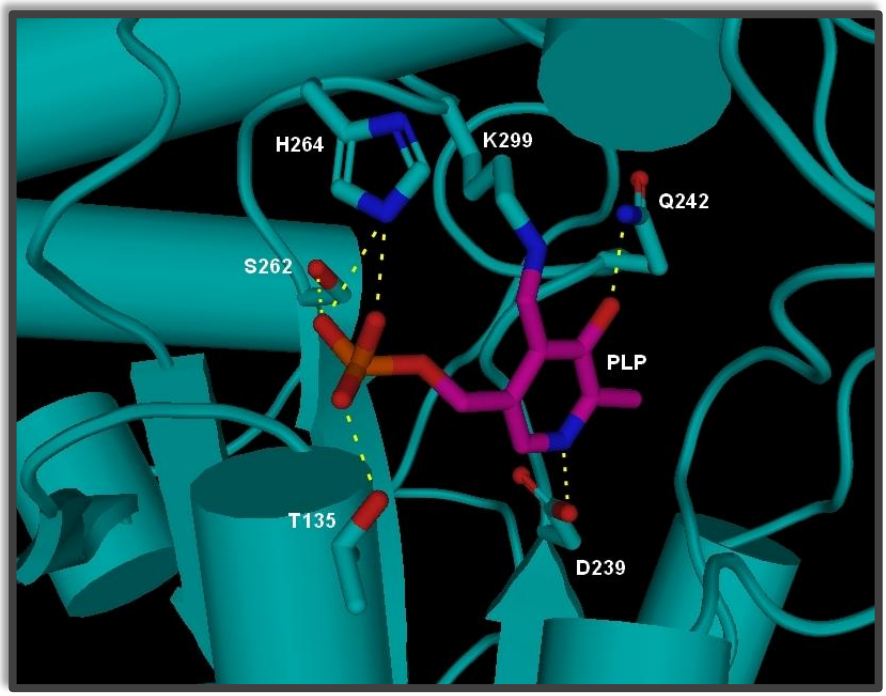

Figure 4.10 Cartoon representation of the active site of Nfs1Δ1–98, with PLP and the PLP-binding residues shown in stick representation. The PLP co-factor is shown in magenta making a covalent link to Lys299. Polar interactions stabilising the position of PLP in the active site are indicated by yellow dashed lines. The image was rendered using PyMOL (http://www.pymol.org).

The catalytic cysteinyl residue (Cys328) of IscS is located in the middle of a 10-residue-long flexible loop (GSA**C**TSASLE), which is directed away from the active site (Cupp-Vickery *et al.*, 2003). This residue corresponds to Cys421 in Nfs1 and is proposed to act as a nucleophile to attack the sulfhydryl group of the PLP-bound L-cysteine substrate, forming a protein-bound cysteinyl persulfide intermediate (Zheng *et al.*, 1994). As Cys328 is missing from the crystal structure of IscS, no attempt was

made to model this flexible loop, though it is clearly within reach of the active centre.

4.8 Summary

Yeast Nsf1 was successfully overproduced in *E. coli*, making pKT2 and pKT3 among the first constructs shown to yield soluble Nfs1 upon expression under the T7 RNA polymerase promoter in a prokaryotic host. Both the sequence identity and biophysical data support the view that Nfs1 has the same architecture as bacterial IscS and, like the bacterial enzyme, is a homodimer in solution. There is clear evidence of PLP binding to Nfs1 and its active centre closely resembles that of IscS, suggesting conservation of the catalytic mechanism.

Chapter 5: Production of the yeast Nfs1/Isd11 protein complex and studies of the Nfs1–Isd11 interaction

5.1 Co-expression of the two target DNA fragments in *E. coli* allows formation of the Nfs1/Isd11 protein complex

The DNA fragments encoding the predicted mature forms of Isd11 and Nfs1, Isd11Δ1–10 and Nfs1Δ1–34 respectively, were amplified directly from the genomic DNA of yeast. PCR primers were engineered so as to introduce a non-cleavable His_6 tag to the N-terminus of Nfs1 upon translation. To minimise the likelihood of mutations introduced by standard PCR, high-fidelity PCR using the proofreading *PfuUltra* DNA polymerase was used. Following double digestion with the appropriate restriction enzymes, the PCR products were sequentially inserted into the two separate multiple cloning sites of the same pCDFDuet-1 vector, which introduced a second non-cleavable His_6 tag to the N-terminus of Isd11 upon translation, using a ligation-dependent cloning strategy to generate the co-expression construct designated pKT4. The integrity of pKT4 was confirmed by DNA sequencing.

Unlike pET-14b carrying a plain T7 promoter, pCDFDuet-1 carries two T7*lac* promoters (which involve T7 RNA polymerase promoters followed by *lac* operators) that provide tighter regulation over basal expression. Since the use of a plasmid carrying a T7*lac* promoter in combination with a host strain bearing a pLysS plasmid is not recommended by the manufacturer, the former RosettaBlue(DE)pLysS strain was replaced with the similar RosettaBlue(DE3) strain. Overnight induction of preparative-scale bacterial cultures bearing pKT4 with 1 mM IPTG at 25 °C resulted

in high levels of soluble Nfs1/Isd11, suggesting that a combination of the dual T7*lac* promoters and the rare-codon-optimiser strain RosettaBlue(DE3) provides a very useful platform for the co-expression of the DNA fragments encoding Nfs1 and Isd11.

To purify Nfs1/Isd11, the soluble cell fraction was first loaded onto a 5-ml HisTrap HP affinity column. Following immobilised Ni^{2+}-affinity chromatography, the protein was loaded onto a 120-ml HiPrep Sephacryl S-200 HR size-exclusion column for further purification at the preparative scale. The elution profile of Nfs1/Isd11 showed a large symmetrical peak with a small trailing shoulder (Figure 5.1). The peak fractions containing the Nfs1/Isd11 complex were collected and pooled accordingly.

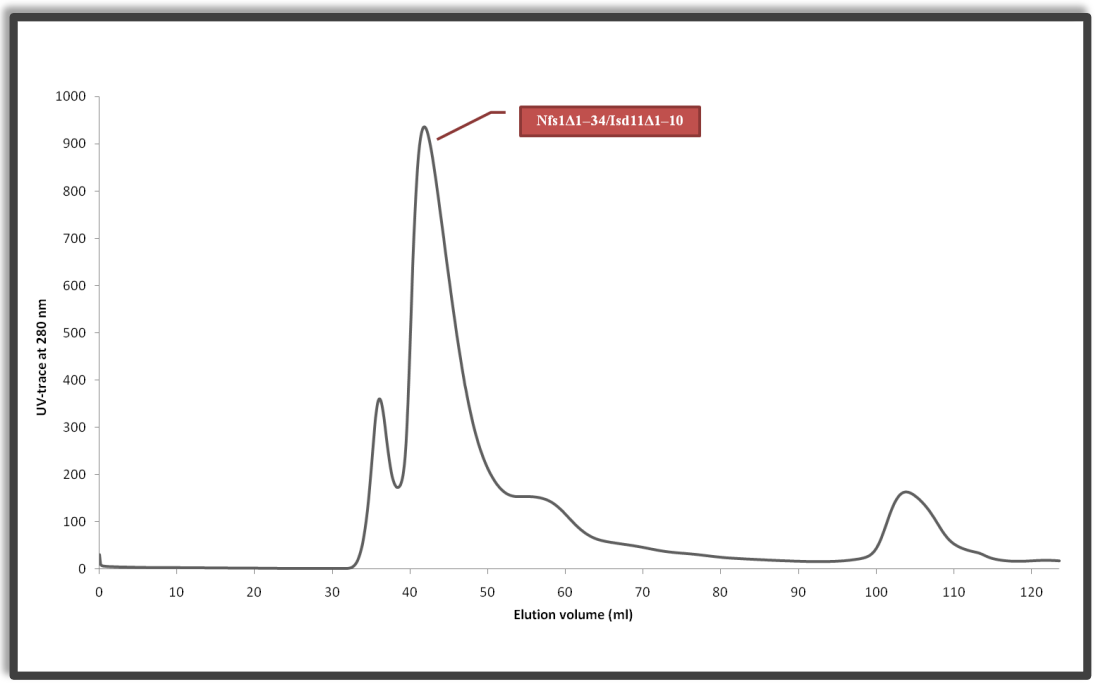

Figure 5.1 Elution profile of the Nfs1/Isd11 complex from the HiPrep Sephacryl S-200 size-exclusion column. The peak containing the complex is labelled.

Protein homogeneity was confirmed by reducing SDS–PAGE, which yielded two bands corresponding to the computed molecular mass of His_6-tagged Nfs1Δ1–34 (51.5 kDa) and His_6-tagged Isd11Δ1–10 (11.8 kDa) (Figure 5.2). The protein, at 2 mg ml^{-1}, could be stored at 4 °C for more than 8 weeks with no visible precipitation.

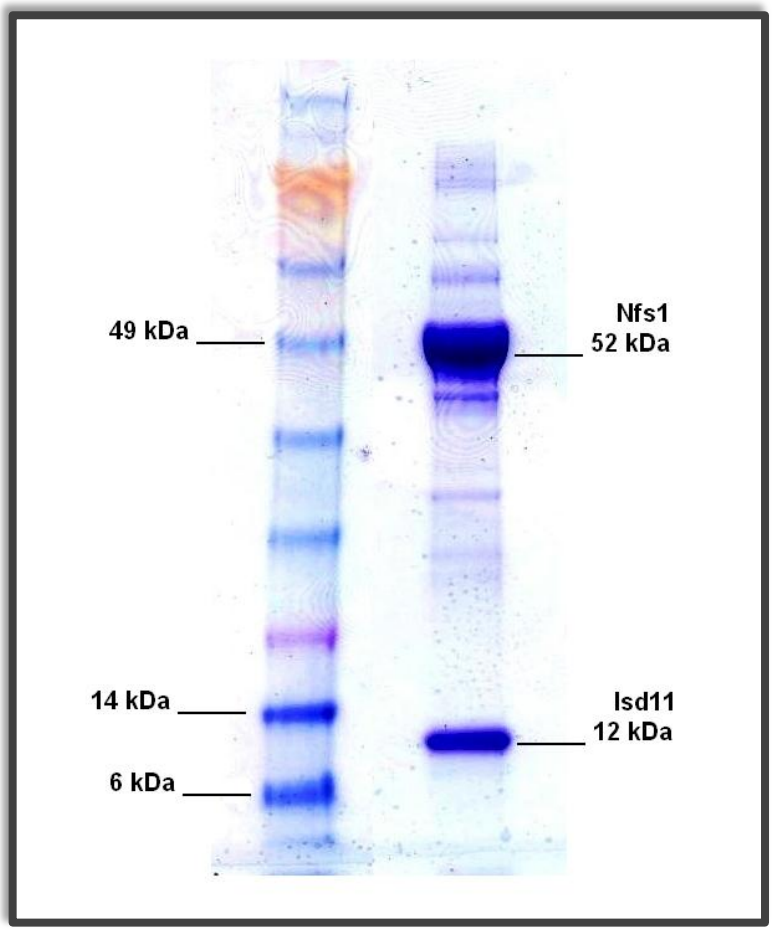

Figure 5.2 SDS-PAGE analysis of the purified and concentrated Nfs1/Isd11 complex, showing the dissociated subunits Nfs1 and Isd11. The pre-stained protein ladder is shown on the left.

5.2 Size-exclusion chromatography estimates that the Nfs1/Isd11 complex has a native mass nearly twice that of the Nfs1 homodimer

In an attempt to estimate the apparent molecular mass of Nfs1/Isd11 at the analytical scale, a 24-ml Superdex 200 10/300 GL size-exclusion column, which was previously calibrated with globular proteins of known molecular mass, was used. The molecular mass of the Nfs1/Isd11 complex was calculated from the calibration curve represented by the equation

$$K_{\mathrm{av}} = -0.2087 \ln(M_{\mathrm{r}}) + 2.7653$$

where K_{av} is the fraction of the stationary gel volume that is accessible to Nfs1/Isd11 and M_{r} is the relative molecular mass of Nfs1/Isd11 in kDa. Recombinantly produced Nfs1/Isd11 has an apparent molecular mass of approximately 190 kDa, suggesting that Nfs1 adopts a higher oligomeric state upon complexation.

5.3 UV-visible absorbance spectrophotometry reveals that recombinantly produced Nfs1/Isd11 retains its activity towards L-cysteine and that Isd11 helps stabilise Nfs1 during and/or after the catalytic desulphuration of L-cysteine

The UV-visible absorbance spectrum of the complex was recorded at room temperature for purified Nfs1Δ1–34/Isd11Δ1–10 (at 3.65 mg ml^{-1} in the SEC equilibration/elution buffer). Nfs1/Isd11 showed almost the same spectral profile as Nfs1, giving two intense absorbance bands at 280 nm and 420 nm (Figure 5.3). The

former is attributed to the aromatic residues tryptophan and tyrosine, and the latter is attributed to the protonated internal aldimine (Behshad & Bollinger, 2009).

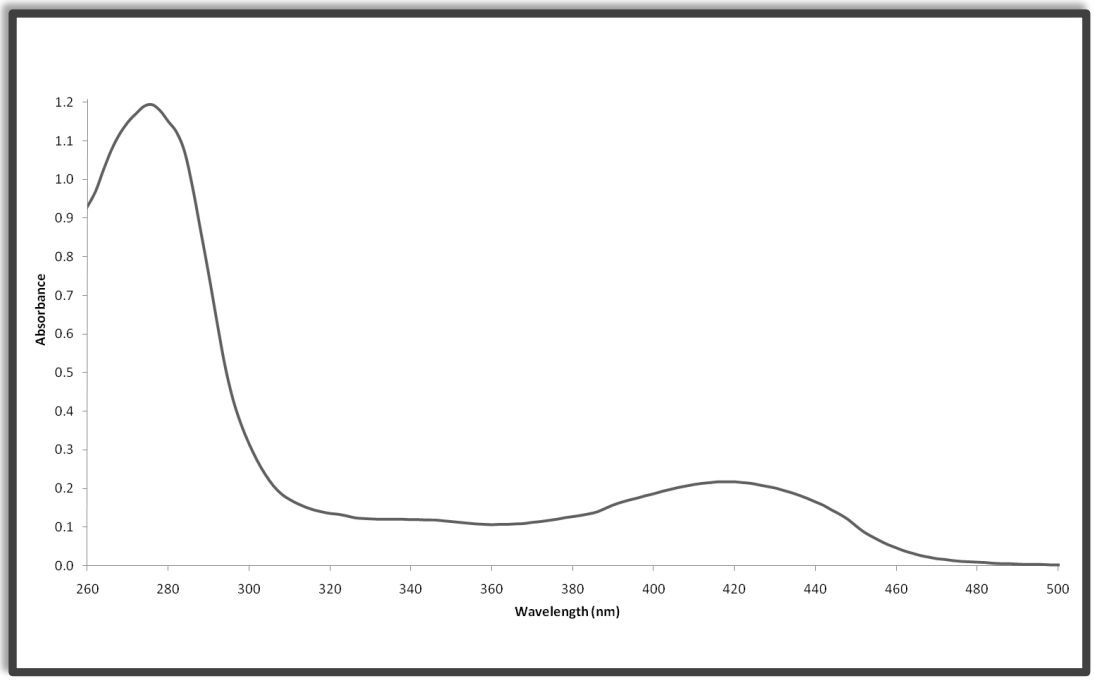

Figure 5.3 UV-visible absorbance spectrum of Nfs1/Isd11. The peaks at 280 nm and 420 nm correspond to the aromatic residues and the enzyme-bound PLP co-factor, respectively.

The activity of recombinant Nfs1/Isd11 was assayed by incubating the protein complex with 10 mM free L-cysteine, with the reaction monitored spectrophotometrically. The reaction was conducted at 4 °C in the SEC equilibration/elution buffer. Measurements were taken at 5-minute intervals over 20 minutes on a Hitachi U-3010 spectrophotometer maintained at room temperature. Because the substrate was used in high molar excess, the system displayed absorption bands corresponding to all long-living species (Figure 5.4).

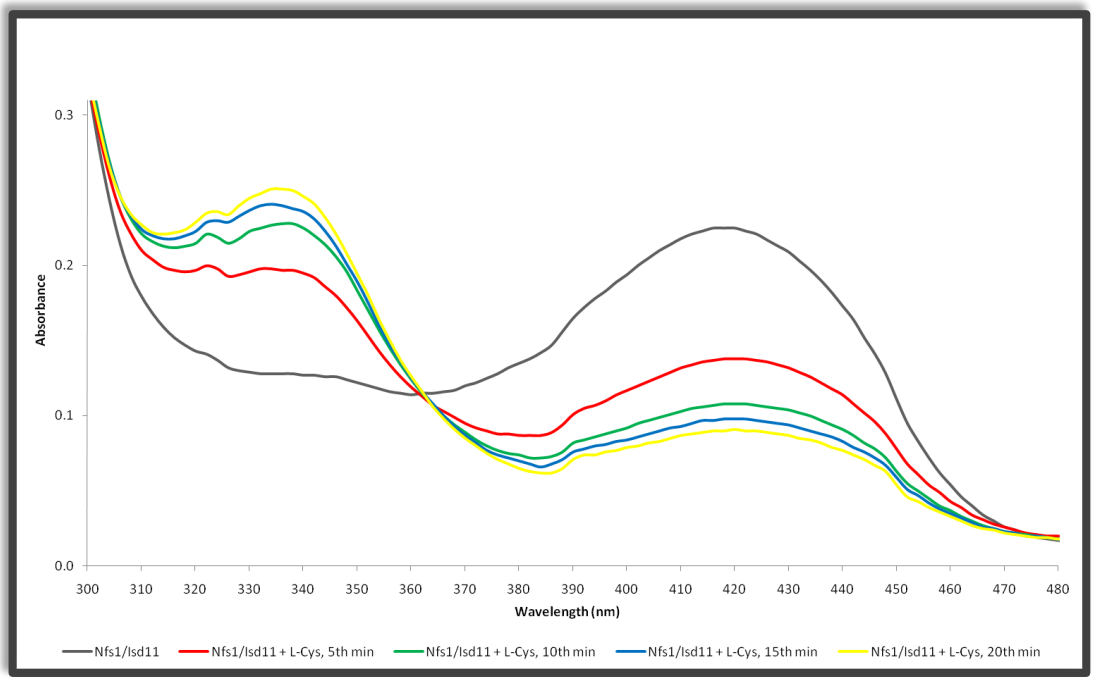

Figure 5.4 Time-dependent spectral analysis of L-cysteine binding to Nfs1/Isd11. Addition of free cysteine leads to a loss of absorption at 420 nm. Simultaneously, a second reaction intermediate absorbing at 336 nm is populated.

With L-cysteine added, the intensity of the absorption band at 420 nm, attributed to the protonated internal aldimine, decreases with a concomitant increase of absorbance at 336 nm. The newly formed absorbing species represents the ketimine adduct of PLP and the L-cysteine substrate (Behshad & Bollinger, 2009). These results indicate that the active centre of recombinantly produced Nfs1/Isd11 is correctly formed and that the complex follows the same reaction scheme as Nfs1 and its bacterial homologues, raising the question of what the specific function of bound Isd11 is. One explanation is that Isd11 may act as an adaptor protein, linking multiple copies of the Nfs1 monomer. This would increase the effective concentration of the desulphurase enzyme. Alternatively, Isd11 may facilitate the onward transfer of elemental sulphur released from L-cysteine.

As in the case of Nfs1, only a single turnover is observed here. The change in absorbance at 420 nm (or 336 nm) is considerable for the first 5-minute interval, but then in subsequent 5-minute intervals the activity reduces. However, the spectral pattern of Nfs1/Isd11 is different from that of Nfs1 in such a way that the spectra corresponding to the 15^{th} and the 20^{th} minutes can still be distinguished from each other, suggesting that the complex maintains its activity for a longer period of time compared to Nfs1. Unlike Nfs1, Nfs1/Isd11 showed no signs of precipitation following overnight incubation with cysteine at 4 °C. Isd11, therefore, seems to stabilise Nfs1 during and/or after the L-cysteine desulphuration reaction.

5.4 Quantitative amino acid analysis of Nfs1/Isd11 suggests that Nfs1 interacts with Isd11 in a 1:1 ratio

A considerable effort was devoted to determining the relative ratio of subunits in the Nfs1/Isd11 protein complex. Quantitative Western blot analysis of purified Nfs1/Isd11, using the Odyssey Infrared Imaging System, was adopted as the first choice for quantifying His_6-tagged subunits (see **Section 2.7** for details). This method, however, failed to provide useful information due to impaired transfer of Isd11 onto the PVDF membrane. In this second approach, a sample of Nfs1/Isd11 in 4 mM HEPES, pH 7.0, 40 mM NaCl, 0.2 mM DTT, 0.2 mM EDTA, and 1% (v/v) glycerol was sent to the Protein and Nucleic Acid Chemistry Facility at the University of Cambridge for quantitative amino acid analysis. Standard analysis of protein hydrolysates was performed by ion-exchange chromatographic separation of individual amino acids, monitored by ninhydrin reaction. One run identified all hydrolysate amino acids except tryptophan and cysteine. Asparagine and glutamine

were hydrolysed to aspartate and glutamate, respectively, during the protocol. (Table 5.1).

Table 5.1 Quantitative amino acid analysis of Nfs1/Isd11. The amino acid compositions (number of each residue per monomer) of Nfs1 and Isd11 are given in the top two columns. The added contribution of hydrolysed Asn residues to the total number of Asp residues is indicated by Asx.

	Nfs1	Isd11
Ala	46	2
Arg	24	6
Asn	19	9
Asp	26	4
Cys	5	0
Gln	10	8
Glu	29	4
Gly	35	3
His	22	7
Ile	28	2
Leu	39	9
Lys	28	9
Met	13	4
Phe	14	7
Pro	20	3
Ser	36	7
Thr	29	4
Trp	3	0
Tyr	14	4
Val	30	6

	$Nfs1_2$–Isd11			**Nfs1–Isd11**			**Nfs1–$Isd11_2$**		
	Expected	Found	Variance	Expected	Found	Variance	Expected	Found	Variance
Ala	94	99.64	0.34	48	54.57	0.90	50	64.06	3.95
Arg	54	52.33	0.05	30	28.66	0.06	36	33.64	0.15
Asx	103	100.21	0.08	58	54.88	0.17	71	64.43	0.61
Gly	73	73.26	0.00	38	40.12	0.12	41	47.1	0.91
His	51	38.12	3.25	29	20.88	2.27	36	24.51	3.67
Ile	58	56.72	0.03	30	31.06	0.04	32	36.46	0.62
Leu	87	96.77	1.10	48	53	0.52	57	62.22	0.48
Lys	65	60.51	0.31	37	33.14	0.40	46	38.9	1.10
Phe	35	32.61	0.16	21	17.86	0.47	28	20.97	1.77
Pro	43	40.89	0.10	23	22.39	0.02	26	26.29	0.00
Thr	62	62.57	0.01	33	34.27	0.05	37	40.23	0.28
Tyr	32	25.51	1.32	18	13.97	0.90	22	16.4	1.43
Val	66	72.83	0.71	36	39.88	0.42	42	46.82	0.55
			Avg. 0.57			*Avg.* 0.49			*Avg.* 1.19

From comparison of the average variance contributions of reliable amino acids for each of the three possible repeating units ($Nfs1_2$–Isd11, Nfs1–Isd11 and Nfs1–$Isd11_2$), Nfs1 is most likely to interact with Isd11 in a molar ratio of 1:1.

5.5 Analytical ultracentrifugation suggests that Nfs1 and Isd11 associate to form the $(Nfs1/Isd11)_3$ heterohexamer

To precisely characterise the oligomeric architecture of the Nfs1/Isd11 protein complex, analytical ultracentrifugation (AUC) was performed by my colleague, Dr Rebecca Beavil, from King's College London. The sedimentation-equilibrium AUC experiment was set up with three different concentrations (A_{280} = 0.8, A_{280} = 0.6 and A_{280} = 0.4) of the Nfs1/Isd11 complex loaded in three different analytical cells of an Optima XL-A analytical ultracentrifuge (Beckman Coulter) at the same time. The samples were run at three different rotor speeds (7,000 rpm, 8,500 rpm and 10,000 rpm) at 4 °C. The AUC data from three different protein concentrations at a given speed were fitted simultaneously to a range of models. The best fit was obtained for a non-interacting two-species model which makes use of a modified version of the equation given in **Section 2.6**. This model suggested that the sample was a mixture of mostly the $(Nfs1/Isd11)_3$ heterohexamer with some non-interacting material of fixed molecular mass (approximately one-third the size of the $(Nfs1/Isd11)_3$ heterohexamer), which could be a degradation product, a broken complex or a contaminating protein (Figure 5.5).

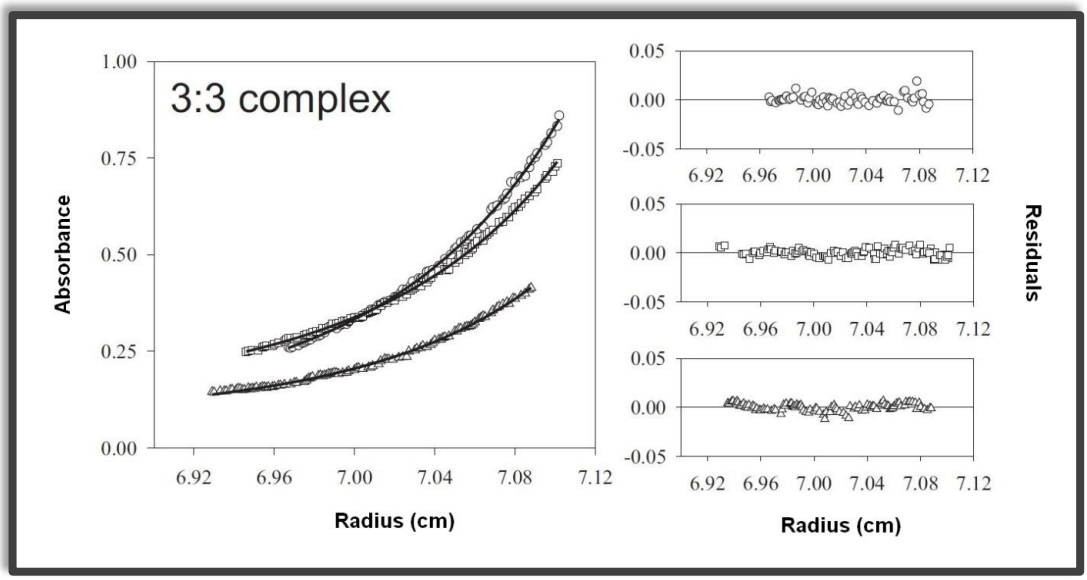

Figure 5.5 Sedimentation equilibrium profile at 280 nm, and the corresponding residuals, for the Nfs1/Isd11 complex run at 8,500 rpm. The model comprising $(Nfs1/Isd11)_3$ and a smaller non-interacting component describes the experimental data best. Loading concentrations are shown in different symbols, as: A_{280} of 0.8 is indicated by circles; A_{280} of 0.6 is indicated by squares; A_{280} of 0.4 is indicated by triangles.

The accuracy of each fit was judged by the residuals and statistics. Unlike the $(Nfs1/Isd11)_3$ heterohexamer model, which produced a random distribution of residuals around zero, the $(Nfs1/Isd11)_2$ heterotetramer and the $(Nfs1/Isd11)_4$ heterooctamer models yielded poor fits of the curves to the sedimentation equilibrium data (Figure 5.6).

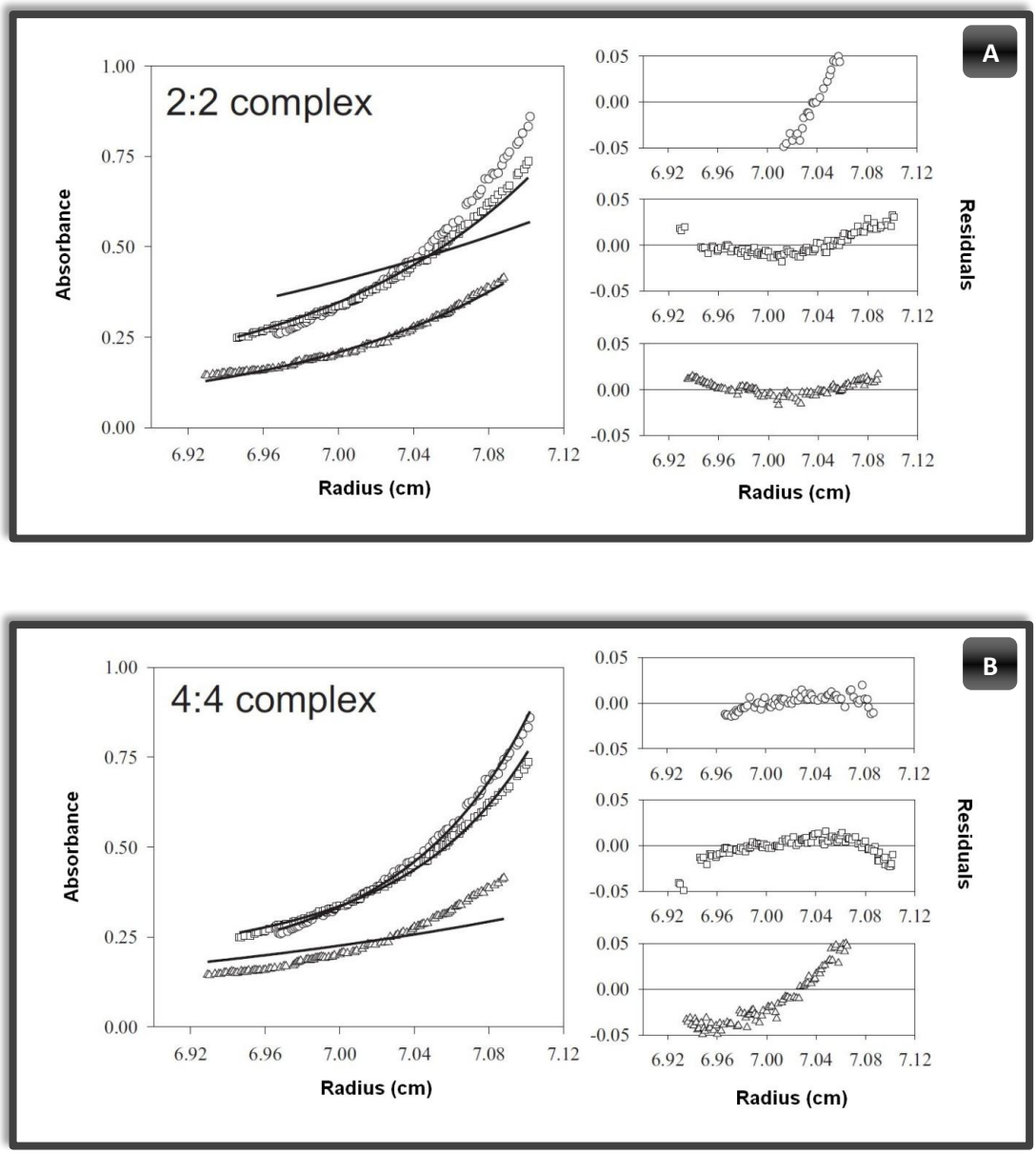

Figure 5.6 Sedimentation equilibrium profile at 280 nm, and the corresponding residuals, for the Nfs1/Isd11 complex run at 8,500 rpm. Poor fits of the curves to the experimental data are obtained with (**A**) $(Nfs1/Isd11)_2$ and (**B**) $(Nfs1/Isd11)_4$ models. These poor-fits are accompanied by the unevenly distributed residuals. Loading concentrations are shown in different symbols, as: A_{280} of 0.8 is indicated by circles; A_{280} of 0.6 is indicated by squares; A_{280} of 0.4 is indicated by triangles.

5.6 Intrinsic tryptophan fluorescence measurements indicate a conformational change in Nfs1 upon Isd11 binding

In contrast to Isd11, which lacks tryptophans, Nfs1 contains three tryptophanyl residues at positions 138, 480 and 494. In an attempt to obtain information regarding the accessibility and microenvironment of these intrinsic fluorophores, the emission spectra of Nfs1Δ1–34 both alone and in complex with Isd11Δ1–10 were recorded (Figure 5.7). Protein (at 0.12 mg ml^{-1} in the SEC elution buffer) was used for the fluorescence measurements, which were performed on a Hitachi F-2500 fluorescence spectrophotometer maintained at room temperature. The excitation wavelength was set at 295 nm to minimise interference from tyrosinyl residues, and the emission scans were acquired from 315 nm to 400 nm, using excitation and emission slit widths of 10 nm. Data were reported without subtracting the buffer signal as it did not contribute significantly to the fluorescence intensity of the proteins.

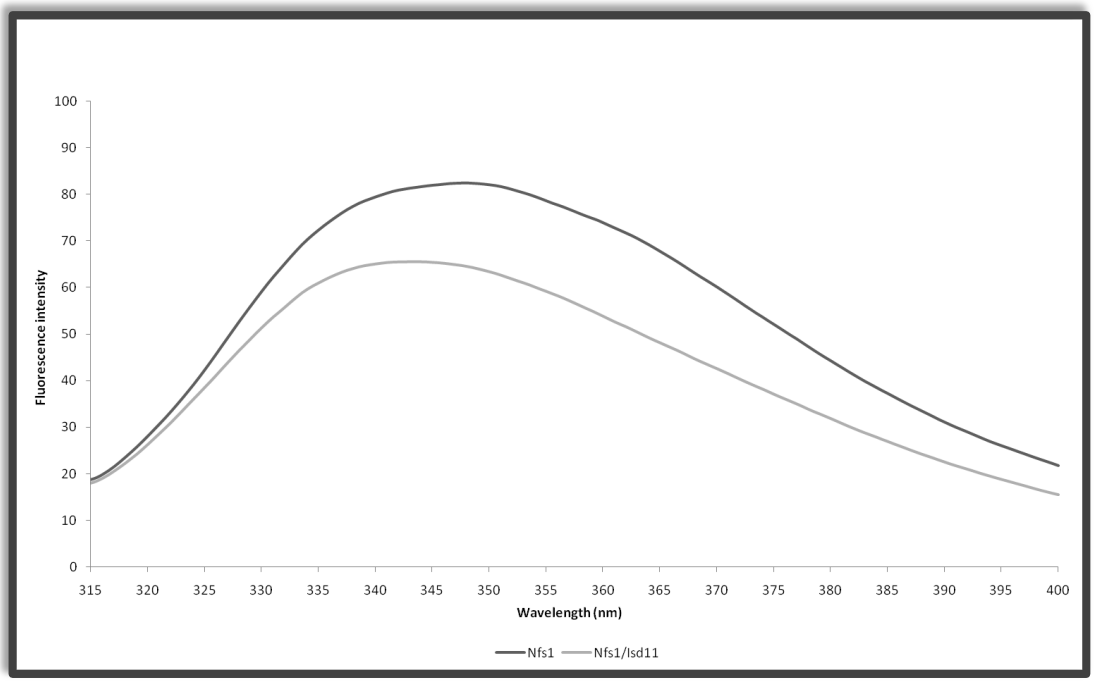

Figure 5.7 Comparison of the emission spectra of Nfs1 and the Nfs1/Isd11 complex. Upon complex formation, the intensity of Nfs1 fluorescence quenches and the emission band shifts to a lower wavelength.

From inspection of the emission spectra of Nfs1 and Nfs1/Isd11, it is clear that Nfs1 adopts a conformation different to that in free form when it is in complex with Isd11. Upon Isd11 binding, the emission maximum for Nfs1 shifts from 348 nm to 343 nm, suggesting that one or more tryptophans become less exposed to the aqueous buffer. With Isd11 bound, intrinsic tryptophan fluorescence also quenches by 21%, which is possibly due to the varying interaction of tryptophans with peptide bonds and a number of amino acid side-chains within the complex structure. There are two plausible explanations for these findings: (i) the buried tryptophan is normally situated in the Nfs1–Isd11 binding site; (ii) the binding of Isd11 induces a conformational change in Nfs1 in such a way that the tryptophan becomes more buried. On the basis of the limited data available from this experiment, it is difficult to assign tryptophans.

5.7 Far-UV CD spectroscopy supports the earlier indication that Nfs1 undergoes a conformational rearrangement upon complex formation

In addition to fluorescence spectrophotometry, CD spectroscopy can also be employed to characterise protein–protein interactions in structural terms. Measurement of an alteration in the far-UV CD spectroscopic signal of Nfs1 upon complex formation made it possible to structurally investigate the interaction between Nfs1 and Isd11. CD spectra of Nfs1Δ1–34 and Nfs1Δ1–34/Isd11Δ1–10 in the region 200–260 nm (Figure 5.8), both representing a baseline-corrected cumulative average of three repeat scans, were obtained at 25 °C on a Chirascan spectropolarimeter (Applied Photophysics), using a cell pathlength of 1 mm and a bandwith setting of 1 nm. Both proteins were used at a concentration of 0.12 mg ml^{-1} in 2.5 mM HEPES, pH 7.0, supplemented with 25 mM NaCl. Data were normalised by calculating the mean residue ellipticity, $[\theta]_{mrw}$. This allowed spectra in the far-UV region to be directly compared for Nfs1 and the Nfs1/Isd11 complex.

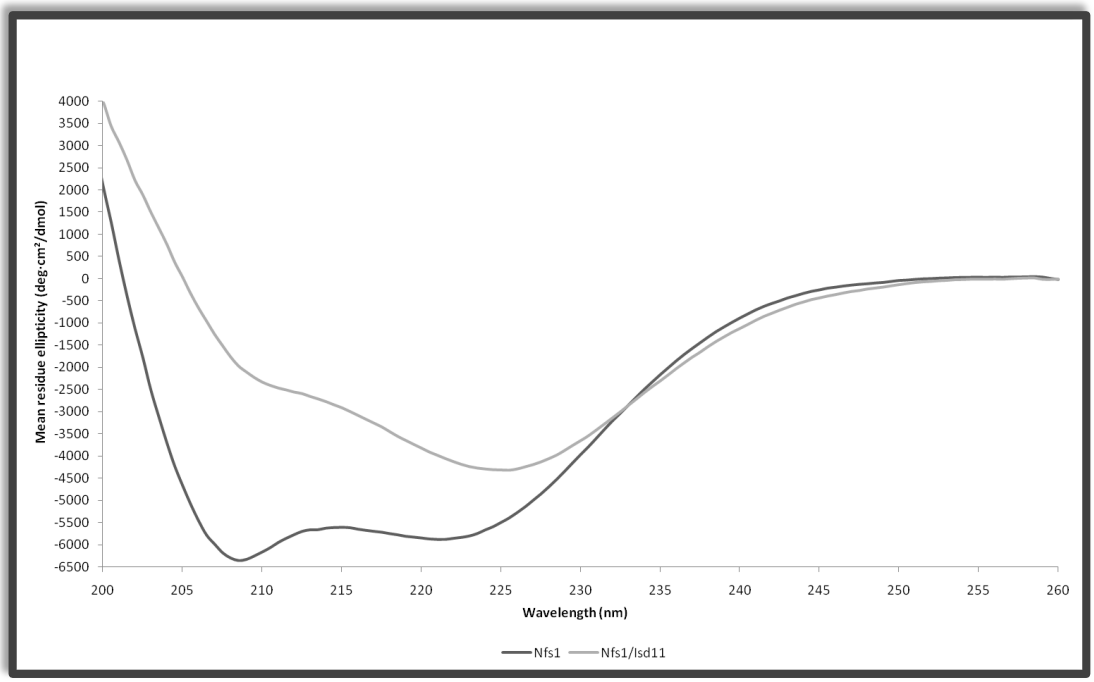

Figure 5.8 Comparison of the far-UV CD spectra of Nfs1 and Nfs1/Isd11. Binding of Isd11 leads to a considerable loss of the CD signal at 208 nm, with a moderate loss at 222 nm.

The binding of Isd11 was monitored by changes in the ellipticity at 208 nm and 222 nm. It is evident that there is a relatively greater change in the former signal (69% compared to 29%). Although secondary-structure prediction tools point to the predominantly α-helical nature of Isd11, far-UV CD spectroscopy suggests a decrease in the helical content of Nfs1 in complex with Isd11. This phenomenon can be explained by the fact that complex formation sometimes results in a considerable alteration in the spectroscopic signal even when the estimated contents of secondary structural elements remain essentially the same (Kelly & Price, 2006). Therefore, changes in the far-UV CD spectrum of the Nfs1/Isd11 protein complex may show alterations in the orientation of helices with respect to each other rather than the actual content of helices, supporting the intrinsic tryptophan fluorescence studies. Although the possibility exists that Isd11 may adopt a conformation other than the

α-helical type (i.e., β-sheet or random coil), its contribution to the signal must be small compared with that of Nfs1, which is roughly five times the size of Isd11.

5.8 Summary

The experimental evidence clearly shows that the Nfs1/Isd11 complex is more massive than the Nfs1 homodimer, suggesting that Isd11 adds on to the Nfs1 homodimer or brings homodimers together. Quantitative amino acid analysis supports a 1:1 ratio of Nfs1 to Isd11, placing an important constraint on the composition of the complex, which must comprise an equal number of Isd11 and Nfs1 subunits. Size-exclusion chromatography and the more precise ultracentrifugation measurements both suggest that the complex comprises $Nfs1_3$–$Isd11_3$, giving a mass of approximately 190 kDa. This is quite surprising due to the fact that Nfs1 alone is a homodimer. If Isd11 promoted oligomerisation of the Nfs1 homodimer, then the simplest oligomeric state would be a dimer of dimers, with composition $Nfs1_4$–$Isd11_4$. This would have a mass of approximately 250 kDa. It is the analytical ultracentrifugation result that cannot be ignored; the size-exclusion column is imprecise and errors could account for the discrepancy in measured size. However, one is left with the analytical ultracentrifugation result, which indicates that a considerable rearrangement of Nfs1 subunits occurs in the complex. Clearly, such an unexpected result requires more corroborating evidence to confirm.

One source of such corroborating evidence comes from the far-UV CD measurements, which show changes in the structure of Nfs1 in the complex compared with Nfs1 alone. However, one should be cautious about such indirect measurements. What is needed is the application of a battery of other techniques to support or refute the existence of the $(Nfs1/Isd11)_3$ heterohexamer. Such studies

would include small-angle X-ray and neutron scattering as well as the ultimate arbitrator in many instances, direct visualisation of the complex in the crystal lattice revealing its oligomeric state. During the course of this project, no crystals of the Nfs1/Isd11 protein complex could be grown. For all the protein concentrations tested (5–20 mg ml^{-1}), about 30–50% clear and 50–70% precipitate-containing drops were observed in manual and automated crystal screens (data not shown).

Chapter 6: Conclusion and future prospects

The primary ISC assembly machinery of eukaryotes, which is responsible for the maturation of mitochondrial Fe–S proteins, is found in mitochondria or in mitochondrial remnants called mitosomes and hydrogenosomes in some parasites. This conservation of the ISC assembly machinery in mitosomes and hydrogenosomes obviously reflects the critical contribution of these organelles to parasite physiology. The maturation of cytosolic and nuclear Fe–S proteins requires several more extramitochondrial components that belong to the CIA machinery. Fe–S proteins are quite evidently among the key players for virtually all organisms in cellular events. The essential pathway of Fe–S cluster formation, therefore, presents an opportunity for researchers to develop novel antiparasitic drugs, in particular when the Fe–S cluster assembly proteins are significantly divergent from their mammalian counterparts.

Although a large subset of the Fe–S cluster assembly proteins have now been characterised, there is little understanding of how different proteins of this biosynthetic pathway interact together (either stably or transiently) in a complex functional network to assemble Fe–S clusters from scratch. Biochemical, biophysical and structural studies of the multiprotein complexes involved in Fe–S cluster assembly and delivery to recipient apoproteins will provide insight into the *in vivo* mechanism for Fe–S protein maturation and allow for the replication of the process *in vitro*. Such knowledge represents an important prerequisite to developing future diagnostic and therapeutic approaches for the prevention and treatment of human diseases linked to Fe–S cluster assembly.

Yeast Isd11, which is a recently identified component of the ISC assembly apparatus, is a small (11 kDa) protein carrying an overall basic charge (theoretical pI 10.3). It is assigned to the LYR family (Pfam entry PF05347), which is characterised by the presence of a conserved LYR (or LYK) tripeptide motif near the N-termini of its protein members. Other LYR-motif-containing proteins include the 14-kDa and 22-kDa subunits, B14 and B22 respectively, of mitochondrial complex I (which is absent in *S. cerevisiae*) and the 13-kDa assembly factor, SDHAF1, of mitochondrial complex II. Given that both complex I and complex II contain multiple Fe–S clusters, all these data raise the question of whether the LYR motif is a signature of relatively small, mitochondrial proteins involved in the formation, insertion and/or retention of Fe–S clusters (Ghezzi *et al.*, 2009). In this Thesis, I show that co-expression of *isd11* and *nfs1* in *E. coli* aids in recovering Isd11 from inclusion bodies, in the form of a soluble two-protein complex (Nfs1/Isd11). However, it was not possible to produce soluble Isd11 in isolation in reasonable quantities, which presented a major challenge to this project. Eukaryotic expression systems (e.g., *Saccharomyces* and *Pichia*), cell-free translation systems (e.g., wheat germ) or chemical synthesis might hold promise in this regard. Had it been possible to produce Isd11 in the absence of Nfs1, then the conformation could have been probed by NMR spectroscopy using isotropically enriched (^{15}N and ^{13}C) protein. Changes in conformation on complexation with Nfs1 could also have been monitored by following changes in the chemical shifts. Titration of Isd11 into Nfs1 could also have been followed thermodynamically (e.g., by isothermal titration calorimetry) as well as spectroscopically (e.g., by NMR and fluorescence spectrophotometry) allowing the stoichiometry of this complex and affinity of its constituting proteins towards each other to be determined precisely.

Interestingly, *E. coli* possesses a small (8 kDa) protein called IscX, which forms a tight complex with IscS (Tokumoto *et al.*, 2002). IscX carries an overall acidic charge (theoretical pI 4.0) and is encoded by the last gene in the *isc* operon. The NMR structure of IscX has revealed that the protein exists as a monomer in solution and adopts a compact three-helix fold bearing close resemblance to that of DNA-binding proteins (Pastore *et al.*, 2006). IscX has no primary sequence similarity to Isd11, though both proteins appear to have a compact all-helical fold which may be a key aspect of their recognition by cysteine desulphurases. If eukaryotes lost IscX from the mitochondrial endosymbiont but maintained IscS (Nfs1), then they had to invent a novel functional analogue, which could be Isd11. A useful experiment would be to investigate if there is an interaction between IscX and Nfs1 by complementing a yeast Isd11 knock-out strain with *E. coli* IscX. Although IscX is proposed to be an adaptor of IscS, genetic studies have shown that IscX is not essential for Fe–S cluster assembly (Tokumoto & Takahashi, 2001).

Unlike Isd11, Nfs1 is a well-known component of the mitochondrial ISC assembly machinery. It is a PLP-dependent enzyme that catalyses the conversion of L-cysteine to L-alanine and elemental sulphur. The latter product is bound to a conserved cysteinyl residue, in the form of a persulphide intermediate, and, subsequently, transferred to a recipient protein. Here, I report the production of the predicted mature form of yeast Nfs1 (Nfs1Δ1–34) and a further truncated version of the same protein (Nfs1Δ1–98) for the first time in *E. coli*. I propose that Nfs1Δ1–98 is more suitable than Nfs1Δ1–34 for crystallisation experiments because it corresponds to the crystallisable fold of *E. coli* IscS. UV–visible absorbance spectophotometry proved to be an excellent tool for following the cysteine desulphuration reaction as the reaction intermediates have distinct absorbance characteristics in the region

330–510 nm. Stopped-flow UV–visible absorbance spectrophotometry could be used to identify all of the accumulating intermediates, tentatively map them onto the proposed mechanism (Figure 1.4) and determine the kinetic parameters of each step.

Selenocysteine lyases, which are also PLP-dependent enzymes, catalyse the degradation of L-selenocysteine to yield L-alanine and selenium. Although selenocysteine lyases share several common features with cysteine desulphurases (such as the PLP-binding lysine, active-site cysteine and acid/base catalyst histidine), there is only a limited degree of sequence identity between the two groups of enzymes. Recently, selenocysteine lyase (SCL) from *T. brucei* has been characterised (Poliak *et al.*, 2009). When compared with Nfs1 from the same organism, SCL lacks the C-terminal region consisting of a short α-helix and a trailing flexible segment, as revealed by the crystal structure of IscS (Figure 6.1). What is more, although Nfs1 co-purifies with its functional partner Isd11, SCL seems not to interact stably with any other protein. Taken together, these findings imply that Isd11 is likely to bind to the C-terminus of Nfs1, stabilising the flexible flanking residues in an appropriate conformation. Two of the three tryptophanyl residues of yeast Nfs1 reside in this C-terminal region, which is absent in *T. brucei* SCL, possibly explaining the occurrence of a blue-shift of the emission maximum upon Isd11 binding (see **Section 5.6**). This hypothesis could be tested by mutating one or more of the conserved amino acids residing in the C-terminus of Nfs1 and, subsequently, observing the effect of this on the Nfs1–Isd11 interaction.

Figure 6.1 Alignment of deduced amino acid sequences of selenocysteine lyase (SCL) and the predicted mature form (Smíd *et al.*, 2006) of cysteine desulphurase (Nfs1) both from *T. brucei*. The C-terminal region of Nfs1, which is absent in SCL, may be critical in Isd11 binding. The 6-residue-long α-helix is underlined in red, and the 12-residue-long mobile segment is underlined in green. Identical residues are indicated by an asterisk, and conservative and semi-conservative substitutions are indicated by a colon and a dot, respectively.

The present study makes use of a wide range of biophysical techniques, ranging from far-UV CD spectroscopy to fluorescence spectrophotometry, to indirectly measure the interaction between Nfs1 and Isd11. The most direct means of structurally dissecting the Nfs1/Isd11 protein complex would be X-ray crystallography or cryo-electron microscopy. Small-angle X-ray/neutron scattering could also provide low-resolution structural information and monitor conformational changes upon complex formation. In addition, each of these direct methods would either support or refute

the existence of the $(Nfs1/Isd11)_3$ heterohexamer, which is suggested by size-exclusion chromatography and analytical ultracentrifugation in this study.

References

Adam, A. C., Bornhövd, C., Prokisch, H., Neupert, W. & Hell, K. (2006). The Nfs1 interacting protein Isd11 has an essential role in Fe/S cluster biogenesis in mitochondria. *EMBO Journal*, **25**, 174–183.

Ali, V., Shigeta, Y., Tokumoto, U., Takahashi, Y. & Nozaki, T. (2004). An intestinal parasitic protist, *Entamoeba histolytica*, possesses a non-redundant nitrogen fixation-like system for iron–sulfur cluster assembly under anaerobic conditions. *Journal of Biological Chemistry*, **279**, 16863–16874.

Altschul, S. F., Wootton, J. C., Gertz, E. M., Agarwala, R., Morgulis, A., Schäffer, A. A. & Yu, Y. K. (2005). Protein database searches using compositionally adjusted substitution matrices. *FEBS Journal*, **272**, 5101–5109.

Behshad, E. & Bollinger, J. M. (2009). Kinetic analysis of cysteine desulfurase CD0387 from *Synechocystis* sp. PCC 6803: formation of the persulfide intermediate. *Biochemistry*, **48**, 12014–12023.

Beinert, H., Holm, R. H. & Münck, E. (1997). Iron–sulfur clusters: nature's modular, multipurpose structures. *Science*, **277**, 653–659.

Beinert, H. (2000). Iron–sulfur proteins: ancient structures, still full of surprises. *Journal of Biological Inorganic Chemistry*, **5**, 2–15.

Claros, M. G. & Vincens, P. (1996). Computational method to predict mitochondrially imported proteins and their targeting sequences. *European Journal of Biochemistry*, **241**, 779–786.

Cupp-Vickery, J. R., Urbina, H. & Vickery, L. E. (2003). Crystal structure of IscS, a cysteine desulfurase from *Escherichia coli*. *Journal of Molecular Biology*, **330**, 1049–1059.

Fiser, A., Do, R. K. & Sali, A. (2000). Modeling of loops in protein structures. *Protein Science*, **9**, 1753–1773.

Flint, D. H. (1996). *Escherichia coli* contains a protein that is homologous in function and N-terminal sequence to the protein encoded by the nifS gene of Azotobacter vinelandii and that can participate in the synthesis of Fe–S cluster of dihydroxy-acid dehydratase. *Journal of Biological Chemistry*, **271**, 16068–16074.

Fontecave, M. & Ollagnier-de-Choudens, S. (2008). Iron–sulfur cluster biosynthesis in bacteria: mechanisms of cluster assembly and transfer. *Archives of Biochemistry and Biophysics*, **474**, 226–237.

Ghezzi, D., Goffrini, P., Uziel, G., Horvath, R., Klopstock, T., Lochmüller, H., D'Adamo, P., Gasparini, P., Strom, T. M., Prokisch, H., Invernizzi, F., Ferrero, I. & Zeviani, M. (2009). *SDHAF1*, encoding a LYR complex-II specific assembly factor, is mutated in SDH-defective infantile leukoencephalopathy. *Nature Genetics*, **41**, 654–656.

Gill, E. E., Diaz-Triviño, S., Barberà, M. J., Silberman, J. D., Stechmann, A., Gaston, D., Tamas, I. & Roger, A. J. (2007). Novel mitochondrion-related organelles in the anaerobic amoeba *Mastigamoeba balamuthi*. *Molecular Microbiology*, **66**, 1306–1320.

Goffeau, A., Barrell, B. G., Bussey, H, Davis, R. W., Dujon, B., Feldmann, H., Galibert, F., Hoheisel, J. D., Jacq, C., Johnston, M., Louis, E. J., Mewes,

H. W., Murakami, Y., Philippsen, P., Tettelin, H. & Oliver, S. G. (1996). *Science*, **274**, 546–567.

Goldberg, A. V., Molik, S., Tsaousis, A. D., Neumann, K., Kuhnke, G., Delbac, F., Vivares, C. P., Hirt, R. P., Lill, R. & Embley, T. M. (2008). Localization and functionality of microsporidian iron–sulphur cluster assembly proteins. *Nature*, **452**, 624–629.

Johnson, D. C., Dean, D. R., Smith, A. D. & Johnson, M. K. (2005a). Structure, function, and formation of biological iron–sulfur clusters. *Annual Review of Biochemistry*, **74**, 247–281.

Johnson, D. C., Dos Santos, P. C. & Dean, D. R. (2005b). NifU and NifS are required for the maturation of nitrogenase and cannot replace the function of isc-gene products in *Azotobacter vinelandii*. *Biochemical Society Transactions*, **33**, 90–93.

Kaiser, J. T., Clausen, T., Bourenkow, G. P., Bartunik, H. D., Steinbacher, S. & Huber, R. (2000). Crystal structure of a NifS-like protein from *Thermotaga maritima*: implications for iron sulphur cluster assembly. *Journal of Molecular Biology*, **297**, 451–464.

Kane, J. F. (1995). Effects of rare codon clusters on high-level expression of heterologous proteins in *Escherichia coli*. *Current Opinion in Biotechnology*, **6**, 494–500.

Kelly, S. M. & Price, N. C. (2006). Circular dichroism to study protein interactions. *Current Protocols in Protein Science*, **Chapter 20**, 20.10.1–20.10.18.

Kim, D. E., Chivian, D. & Baker, D. (2004). Protein structure prediction and analysis using the Robetta server. *Nucleic Acids Research*, **32**(suppl 2), W526–W531.

Kispal, G., Csere, P., Prohl, C. & Lill, R. (1999). The mitochondrial proteins Atm1p and Nfs1p are essential for biogenesis of cytosolic Fe/S proteins. *EMBO Journal*, **18**, 3981–3989.

Land, T. & Rouault, T. A. (1998). Targeting of a human iron–sulfur cluster assembly enzyme, nifs, to different subcellular compartments is regulated through alternative AUG utilization. *Molecular Cell*, **2**, 807–815.

Larkin, M. A., Blackshields, G., Brown, N. P., Chenna, R., McGettigan, P. A., McWilliam, H., Valentin, F., Wallace, I. M., Wilm, A., Lopez, R., Thompson, J. D., Gibson, T. J. & Higgins, D. G. (2007). Clustal W and Clustal X version 2.0. *Bioinformatics*, **23**, 2947–2948.

Lees, J. G., Miles, A. J., Wien, F. & Wallace, B. A (2006). A reference database for circular dichroism spectroscopy covering fold and secondary structure space. *Bioinformatics*, **22**, 1955–1962.

Li, J., Kogan, M, Knight, S. A. B., Pain, D. & Dancis, A. (1999). Yeast mitochondrial protein, Nfs1p, coordinately regulates iron–sulfur cluster proteins, cellular iron uptake, and iron distribution. *Journal of Biological Chemistry*, **274**, 33025–33034.

Li, H., Gakh, O., Smith IV, D. Y. & Isaya, G. (2009). Oligomeric yeast frataxin drives assembly of core machinery for mitochondrial iron–sulfur cluster synthesis. *Journal of Biological Chemistry*, **284**, 21971–21980.

Lill, R., Dutkiewicz, R., Elsässer, H. P., Hausmann, A., Netz, D. J. A., Pierik, A. J., Stehling, O., Urzica, E. & Mühlenhoff, U. (2006). Mechanisms of iron–sulfur protein maturation in mitochondria, cytosol and nucleus of eukaryotes. *Biochimica et Biophysica Acta*, **1763**, 652–667.

Lill, R. & Mühlenhoff, U. (2008). Maturation of iron–sulfur proteins in eukaryotes: mechanisms, connected processes, and diseases. *Annual Review of Biochemistry*, **77**, 669–700.

Lill, R. (2009). Function and biogenesis of iron–sulphur proteins. *Nature*, **460**, 831–838.

Marelja, Z., Stöcklein, W., Nimtz, M. & Leimkühler, S. (2008). A novel role for human Nfs1 in the cytoplasm. *Journal of Biological Chemistry*, **283**, 25178–25185.

Mühlenhoff, U., Balk, J., Richhardt, N., Kaiser, J. T., Sipos, K., Kispal, G. & Lill, R. (2004). Functional characterization of the eukaryotic cysteine desulfurase Nfs1p from *Saccharomyces cerevisiae*. *Journal of Biological Chemistry*, **279**, 36906–36915.

Naamati, A., Regev-Rudzki, N., Galperin, S., Lill, R. & Pines, O. (2009). Dual targeting of Nfs1 and discovery of its novel processing enzyme, Icp55. *Journal of Biological Chemistry*, **284**, 30200–30208.

Nakai, Y., Nakai, M., Hayashi, H. & Kagamiyama, H. (2001). Nuclear localization of yeast Nfs1p is required for cell survival. *Journal of Biological Chemistry*, **276**, 8314–8320.

Nakai, Y., Umeda, N., Suzuki, T., Nakai, M., Hayashi, H., Watanabe, K. & Kagamiyama, H. (2004). Yeast Nfs1p is involved in thio-modification of both mitochondrial and cytoplasmic tRNAs. *Journal of Biological Chemistry*, **279**, 12363–12368.

Oliver, S. G. *et al.* (1992). The complete DNA sequence of yeast chromosome III. *Nature*, **357**, 38–46.

Paris, Z., Changmai, P., Rubio, M. A. T., Zíkova, A., Stuart, K. D., Alfonzo, J. D. & Lukes, J. (2010). The Fe/S cluster assembly protein Isd11 is essential for tRNA thiolation in Trypanosoma brucei. *Journal of Biological Chemistry*, **285**, 22394–22402.

Pastore, C., Adinolfi, S., Huynen, M. A., Rybin, V., Martin, S., Mayer, M., Bukau, B. & Pastore, A. (2006). YfhJ, a molecular adaptor in iron–sulphur cluster formation or a frataxin-like protein? *Structure*, **14**, 857–867.

Poliak, P., Van Hoewyk, D., Oborník, M., Zíkova, A., Stuart, K. D., Tachezy, J., Pilon, M. & Lukeš, J. (2010). Functions and cellular localization of cysteine desulfurase and selenocysteine lyase in *Trypanosoma brucei*. *FEBS Journal*, **277**, 383–393.

Pollastri, G. & McLysaght, A. (2005). Porter: a new, accurate server for protein secondary structure prediction. *Bioinformatics*, **21**, 1719–1720.

Py, B. & Barras, F. (2010). Building Fe–S proteins: bacterial strategies. *Nature Reviews Microbiology*, **8**, 436–446.

Rees, D. C. & Howard, J. B. (2003). The interface between the biological and inorganic worlds: iron–sulfur metalloclusters. *Science*, **300**, 929–931.

Reinders, J., Zahedi, R. P., Pfanner, N., Meisinger, C. & Sickmann, A. (2006). Toward the complete yeast mitochondrial proteome: multidimensional separation techniques for mitochondrial proteomics. *Journal of Proteome Research*, **5**, 1543–1554.

Richards, T. A. & van der Giezen, M. (2006). Evolution of the Isd11–IscS complex reveals a single α-proteobacterial endosymbiosis for all eukaryotes. *Molecular Biology and Evolution*, **23**, 1341–1344.

Rouault, T. A. & Tong, W. H. (2008). Iron–sulfur cluster biogenesis and human disease. *Trends in Genetics*, **24**, 398–407.

Sali, A. & Blundell, T. L. (1993). Comparative protein modelling by satisfaction of spatial restraints. *Journal of Molecular Biology*, **234**, 779–815.

Shan, Y., Napoli, E. & Cortopassi, G. (2007). Mitochondrial frataxin interacts with ISD11 of the NFS1/ISCU complex and multiple mitochondrial chaperones. *Human Molecular Genetics*, **16**, 929–941.

Sheftel, A. D. & Lill, R. (2009). The power plant of the cell is also a smithy: the emerging role of mitochondria in cellular iron homeostasis. *Annals of Medicine*, **41**, 82–99.

Sheftel, A., Stehling, O. & Lill, R. (2010). Iron–sulfur proteins in health and disease. *Trends in Endocrinology and Metabolism*, **21**, 302–314.

Shi, Y., Ghosh, M. C., Tong, W. H. & Rouault, T. A. (2009). Human ISD11 is essential for both iron–sulfur cluster assembly and maintenance of normal cellular iron homeostasis. *Human Molecular Genetics*, **18**, 3014–3025.

Shi, R., Proteau, A., Villarroya, M., Moukadiri, I., Zhang, L., Trempe, J. F., Matte, A., Armengod, M. E. & Cygler, M. (2010). Structural basis for Fe–S cluster assembly and tRNA thiolation mediated by IscS protein–protein interactions. *PLOS Biology*, **8**.

Sickmann, A., Reinders, J., Wagner, Y., Joppich, C., Zahedi, R., Meyer, H. E., Schönfisch, B., Perschil, I., Chacinska, A., Guiard, B., Rehling, P., Pfanner, N. & Meisinger, C. (2003). The proteome of *Saccharomyces cerevisiae* mitochondria. *Proceedings of the National Academy of Sciences USA*, **100**, 13207–13212.

Smíd, O., Horáková, E., Vilímová, V., Hrdý, I., Cammack, R., Horváth, A., Lukeš, J. & Tachezy, J. (2006). Knock-downs of iron–sulfur cluster assembly proteins IscS and IscU down-regulate the active mitochondrion of procyclic *Trypanosoma brucei*. *Journal of Biological Chemistry*, **281**, 28679–28686.

Tokumoto, U. & Takahashi, Y. (2001). Genetic analysis of the *isc* operon in *Escherichia coli* involved in the biogenesis of cellular iron–sulfur proteins. *Journal of Biochemistry*, **130**, 63–71.

Tokumoto, U., Nomura, S., Minami, Y., Mihara, H., Kato, S., Kurihara, T., Esaki, N., Kanazawa, H., Matsubara, H. & Takahashi, Y. (2002). Network of protein–protein interactions among iron–sulfur cluster assembly proteins in *Escherichia coli*. *Journal of Biochemistry*, **131**, 713–719.

van der Giezen, M., Cox, S. & Tovar, J. (2004). The iron–sulfur cluster assembly genes *iscS* and *iscU* of Entamoeba histolytica were acquired by horizontal gene transfer. *BMC Evolutionary Biology*, **4**.

Villaverde, A. & Carrìo, M. M. (2003). Protein aggregation in recombinant bacteria: biological role of inclusion bodies. *Biotechnology Letters*, **25**, 1385–1395.

Whitmore, L. & Wallace, B. A. (2004). DICHROWEB, an online server for protein secondary structure analyses from circular dichroism spectroscopic data. *Nucleic Acids Research*, **32**(suppl 2), W668–W673.

Wiedemann, N., Urzica, E., Guiard, B., Müller, H., Lohaus, C., Meyer, H. E., Ryan, M. T., Meisinger, C., Mühlenhoff, U., Lill, R. & Pfanner, N. (2006). Essential role of Isd11 in mitochondrial iron–sulfur cluster synthesis on Isu scaffold proteins. *EMBO Journal*, **25**, 184–195.

Ye, H. & Rouault, T. A. (2010). Human iron–sulfur cluster assembly, cellular iron homeostasis, and disease. *Biochemistry*, **49**, 4945–4956.

Zheng, L., White, R. H., Cash, V. L., Jack, R. F. & Dean, D. R. (1993). Cysteine desulfurase activity indicates a role for NIFS in metallocluster biosynthesis. *Proceedings of the National Academy of Sciences USA*, **90**, 2754–2758.

Zheng, L., White, R. H., Cash, V. L. & Dean, D. R. (1994). Mechanism for the desulfurization of L-cysteine catalyzed by the *nifS* gene product. *Biochemistry*, **33**, 4714–4720.

Zhu, H., Bilgin, M., Bangham, R., Hall, D., Casamayor, A., Bertone, P., Lan, N., Jansen, R., Bidlingmaier, S., Houfek, T., Mitchell, T., Miller, P., Dean, R. A., Gerstein, M. & Snyder, M. (2001). Global analysis of protein activities using proteome chips. *Science*, **293**, 2101–2105.

Appendix

HyperLadder I (Bioline)

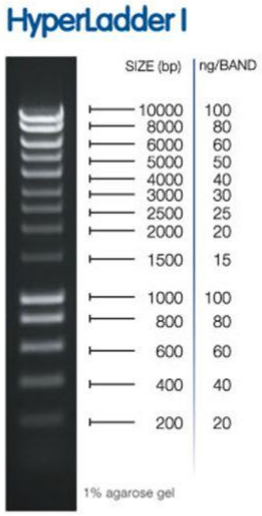

- Higher intensity bands: **1000bp and 10000bp**
- Supplied in a ready-to-use format
- Each lane (5µl) provides 720ng of DNA

SeeBlue Plus2 Pre-Stained Standard (Invitrogen)

Protein	Approximate Molecular Weights (kDa)				
	Tris-Glycine	Tricine	NuPAGE® MES	NuPAGE® MOPS	NuPAGE® Tris-Acetate
Myosin	250	210	188	191	210
Phosphorylase	148	105	98	97	111
BSA	98	78	62	64	71
Glutamic Dehydrogenase	64	55	49	51	55
Alcohol Dehydrogenase	50	45	38	39	41
Carbonic Anhydrase	36	34	28	28	n/a
Myoglobin Red	22	17	17	19	n/a
Lysozyme	16	16	14	14	n/a
Aprotinin	6	7	6	n/a	n/a
Insulin, B Chain	4	4	3	n/a	n/a

Cloning/expression region of pET-14b (Novagen)

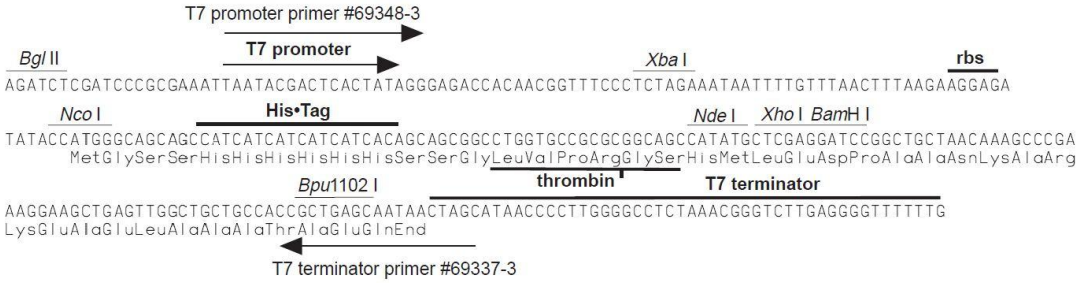

Cloning/expression region of pET-3a (Novagen)

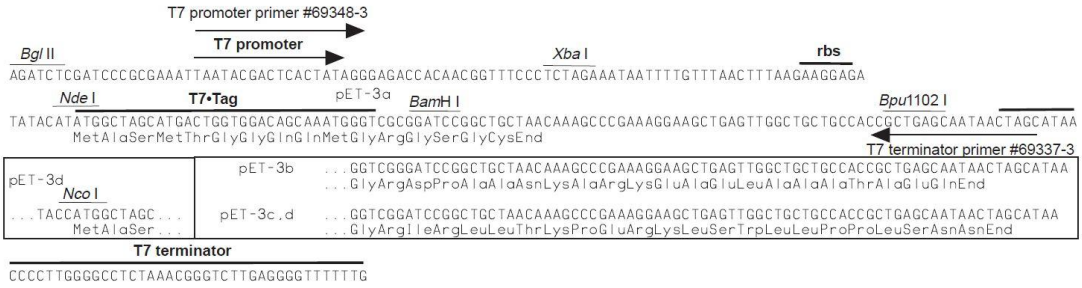

Cloning/expression regions of pCDFDuet-1 (Novagen)

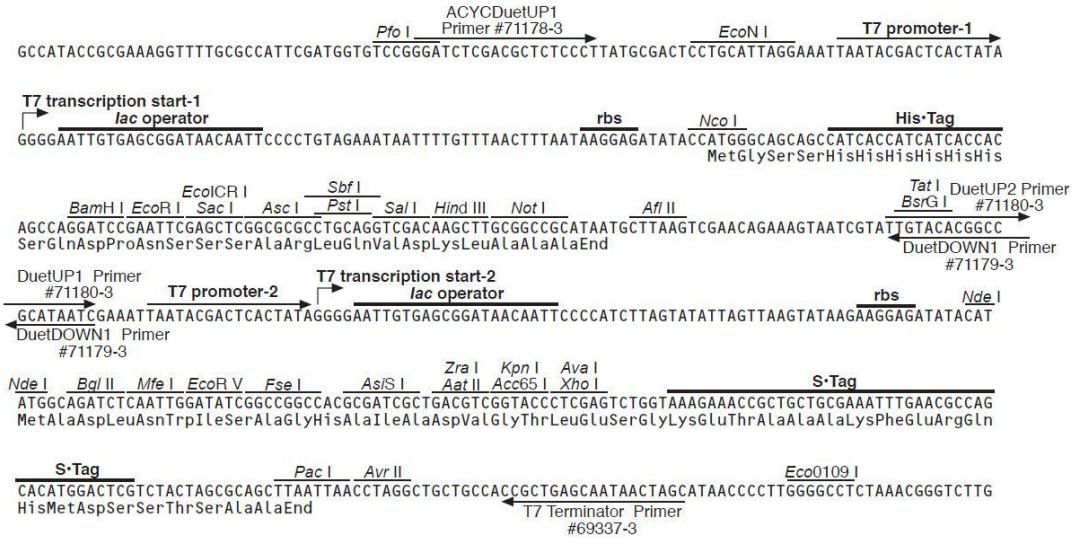

Genotype of α-Select Competent Cells (Bioline)

F^- *deo*R *end*A1 *rec*A1 *rel*A1 *gyr*A96 *hsd*R17(r_k^-, m_k^+) *sup*E44 *thi*-1 *pho*A Δ(*lac*ZYA-*arg*F)U169 Φ80*lac*ZΔM15 λ^-

Genotype of RosettaBlue(DE3) Competent Cells (Novagen)

endA1 hsdR17(r_{K12}^- m_{K12}^+) *supE44 thi-1 recA1 gyrA96 relA1 lac* (DE3) [F' *proA*$^+$*B*$^+$ *lacI*^{q} *ZΔM15* ::Tn*10*] pRARE^2 (Cam^R, Tet^R)

Genotype of RosettaBlue(DE3)pLysS Competent Cells (Novagen)

endA1 hsdR17(r_{K12}^- m_{K12}^+) *supE44 thi-1 recA1 gyrA96 relA1 lac* (DE3) [F' *proA*$^+$*B*$^+$ *lacI*^{q} *ZΔM15* ::Tn*10*] pLysSRARE^2 (Cam^R, Tet^R)

Deduced sequence of *S. cerevisiae* Nfs1 (UniProtKB entry P25374)

```
        10         20         30         40         50         60
MLKSTATRSI TRLSQVYNVP AATYRACLVS RRFYSPPAAG VKLDDNFSLE THTDIQAAAK

        70         80         90        100        110        120
AQASARASAS GTTPDAVVAS GSTAMSHAYQ ENTGFGTRPI YLDMQATTPT DPRVLDTMLK

       130        140        150        160        170        180
FYTGLYGNPH SNTHSYGWET NTAVENARAH VAKMINADPK EIIFTSGATE SNNMVLKGVP

       190        200        210        220        230        240
RFYKKTKKHI ITTRTEHKCV LEAARAMMKE GFEVTFLNVD DQGLIDLKEL EDAIRPDTCL

       250        260        270        280        290        300
VSVMAVNNEI GVIQPIKEIG AICRKNKIYF HTDAAQAYGK IHIDVNEMNI DLLSISSHKI

       310        320        330        340        350        360
YGPKGIGAIY VRRRPRVRLE PLLSGGGQER GLRSGTLAPP LVAGFGEAAR LMKKEFDNDQ

       370        380        390        400        410        420
AHIKRLSDKL VKGLLSAEHT TLNGSPDHRY PGCVNVSFAY VEGESLLMAL RDIALSSGSA

       430        440        450        460        470        480
CTSASLEPSY VLHALGKDDA LAHSSIRFGI GRFSTEEEVD YVVKAVSDRV KFLRELSPLW

       490
EMVQEGIDLN SIKWSGH
```

Deduced sequence of *S. cerevisiae* Isd11 (UniProtKB entry Q6Q560)

```
        10         20         30         40         50         60
MPGFTAPTRR QVLSLYKEFI KNANQFNNYN FREYFLSKTR TTFRKNMNQQ DPKVLMNLFK

        70         80         90
EAKNDLGVLK RQSVISQMYT FDRLVVEPLQ GRKH
```

Favourite quote

“Life is nothing but an electron looking for a place to rest.” (Nobel-prize-winning biochemist Albert Szent-Györgyi)